



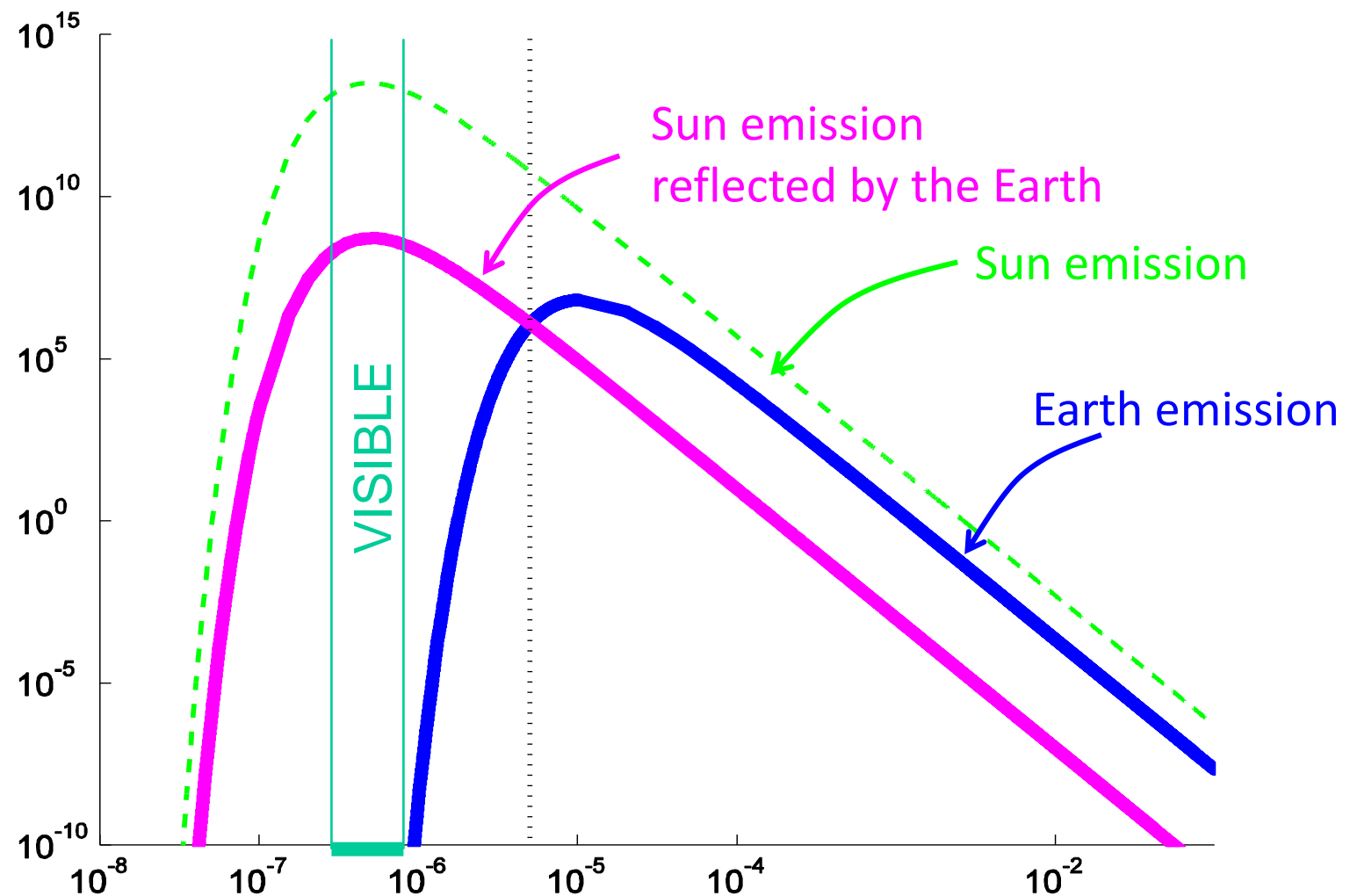
Radar remote sensing for the monitoring of land Surfaces

Pierre-Louis FRISON

pierre-louis.frison@u-pem.fr



Electromagnetic radiation coming from the Earth



Radar Fundamentals

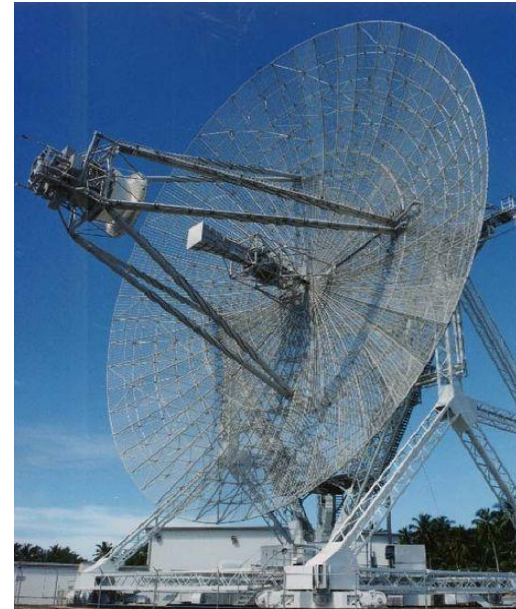
RADAR: RAdio Detection And Ranging

*Emission of emw
Reception backscattered echoes*



Road RADAR

(© US police)



US Army



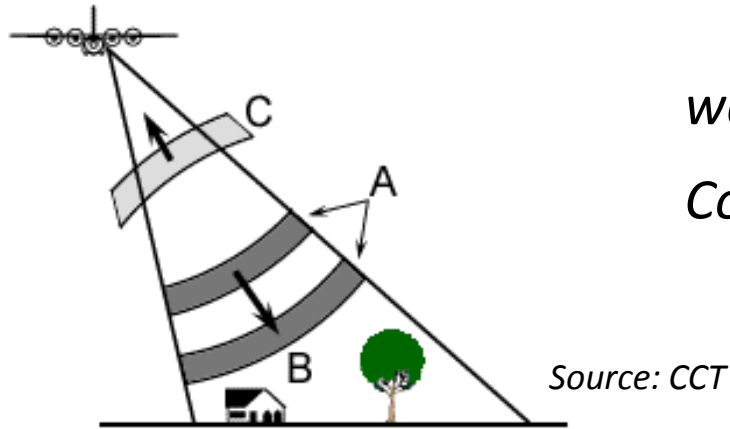
Imaging RADAR PALSAR
(© NASDA)

Radar remote sensing for land surfaces monitoring

Remote sensing:

Optical since 70's

Radar since 1991

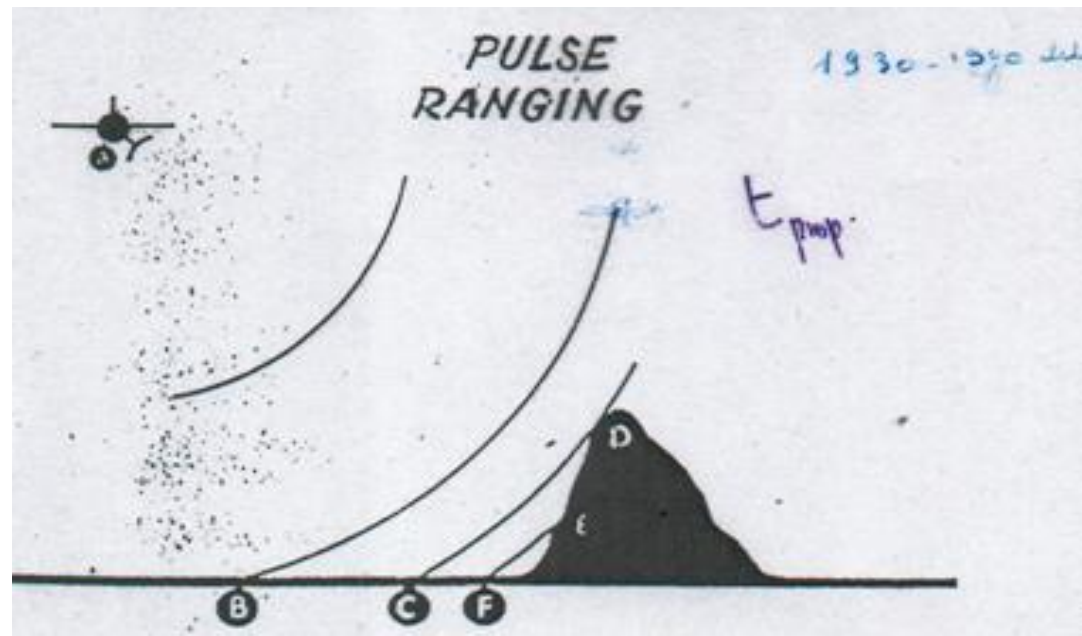


wavelength: $\lambda > 1\text{cm}$

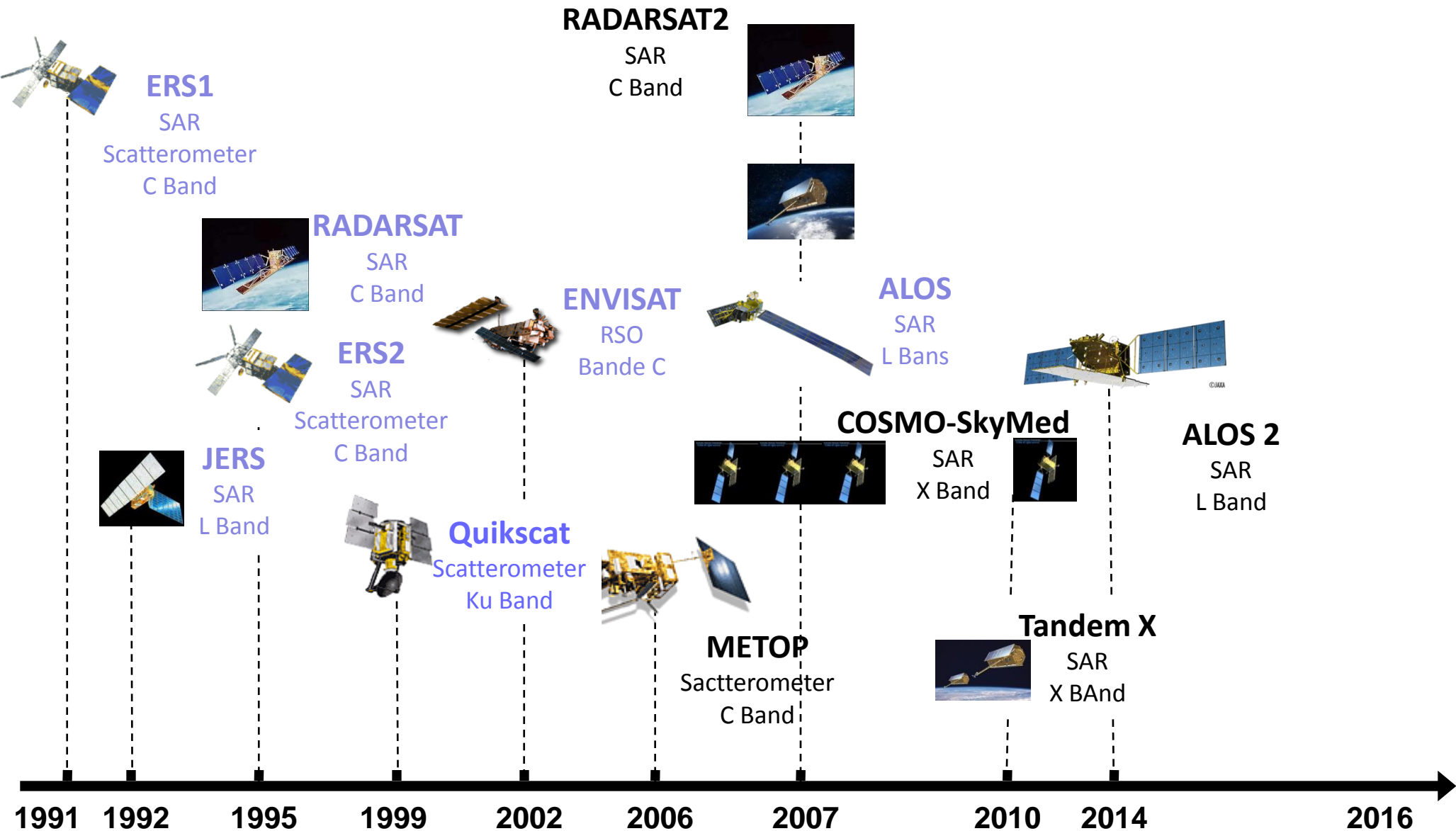
Coherent wave

RADAR: Radio Detection and Ranging

Echoes are ranged according to
Antenna – target distance

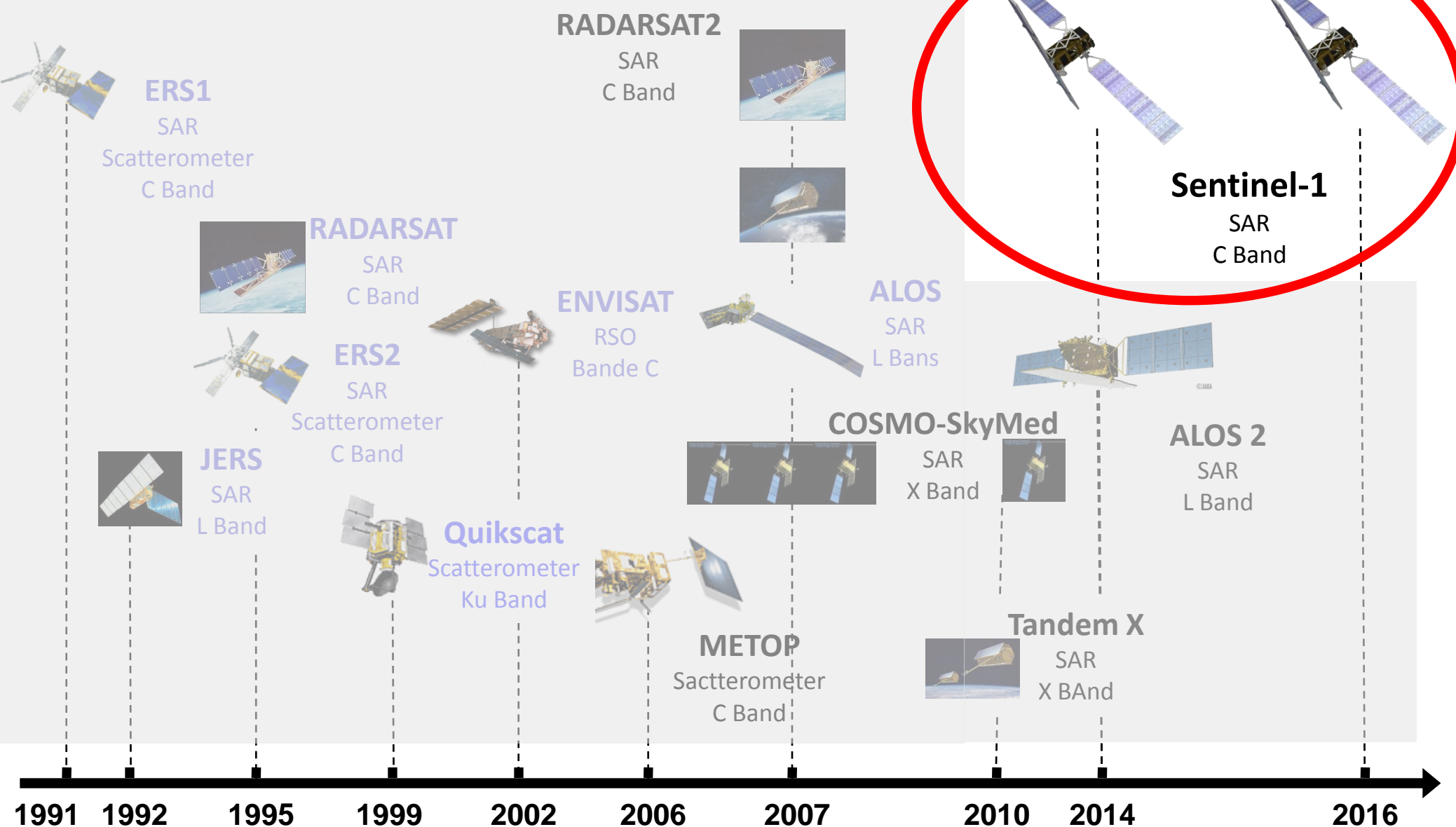


Spaceborne Radar sensors



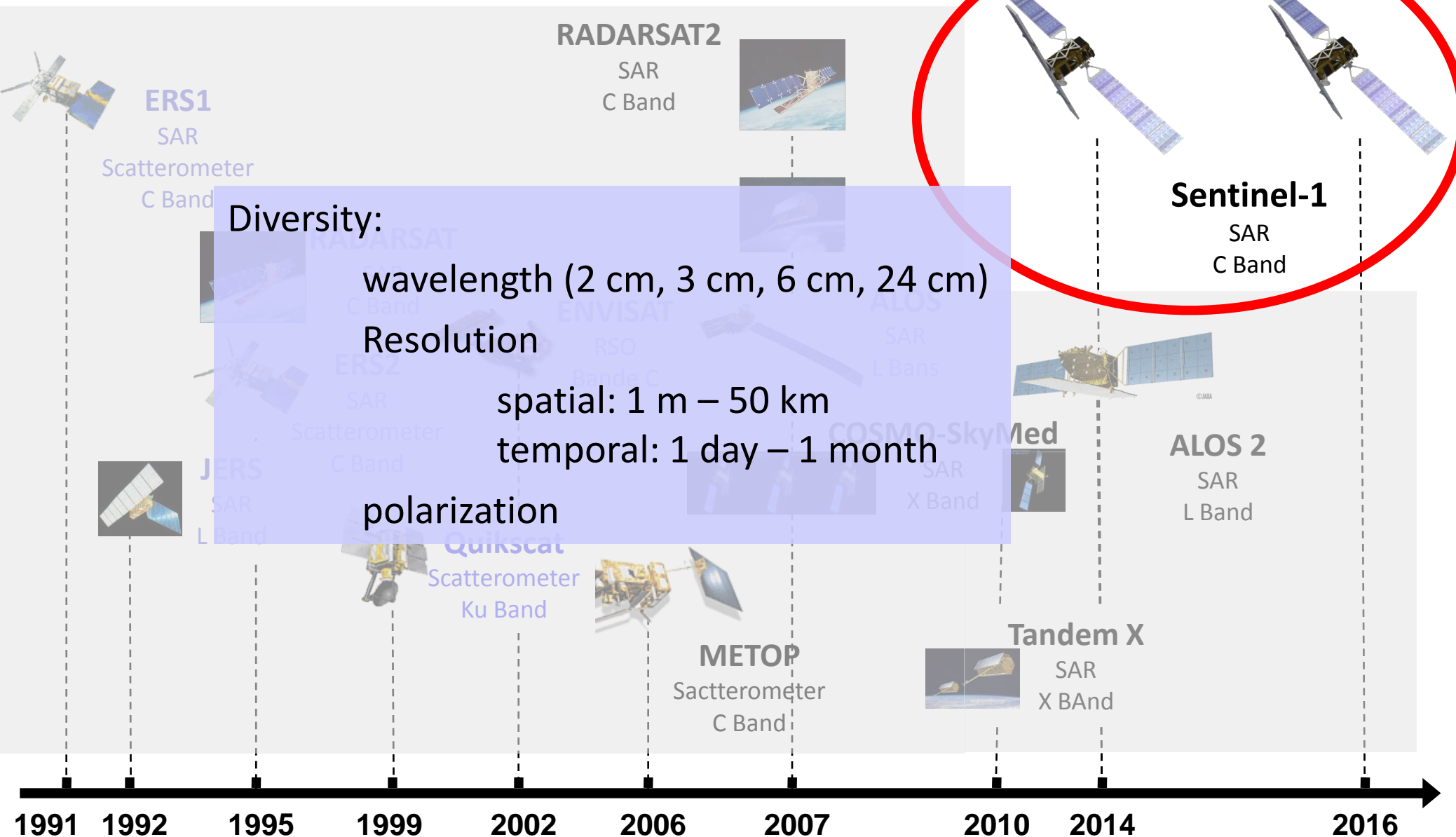
Spaceborne Radar sensors

COPERNICUS



Spaceborne Radar sensors

COPERNICUS



Radar remote sensing for land surfaces monitoring

Remote sensing:

Optical since 70's

Radar since 1991

Diversity:

wavelength (2 cm, 3 cm, 6 cm, 24 cm)

Resolution

spatial: 1 m – 50 km

temporal: 1 day – 1 month

polarization

Interest of Radar remote sensing:

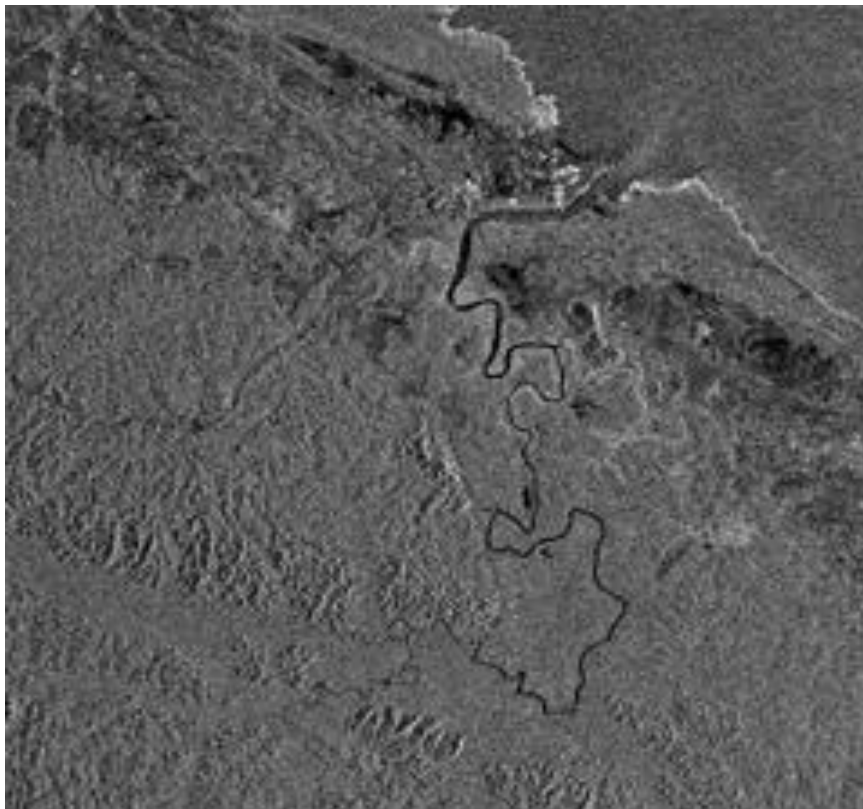
Complementary observations (vs Optical)

insensitive to the atmosphere and the presence of clouds

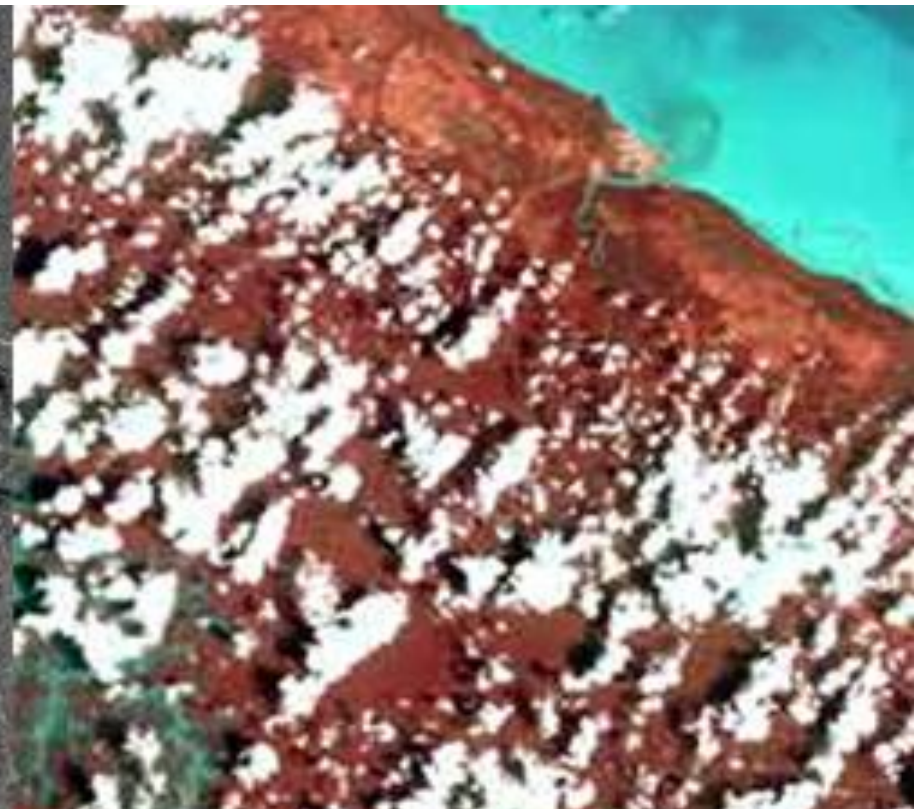
night/day observations

no problem with rain and cloudy conditions

Radar, ERS



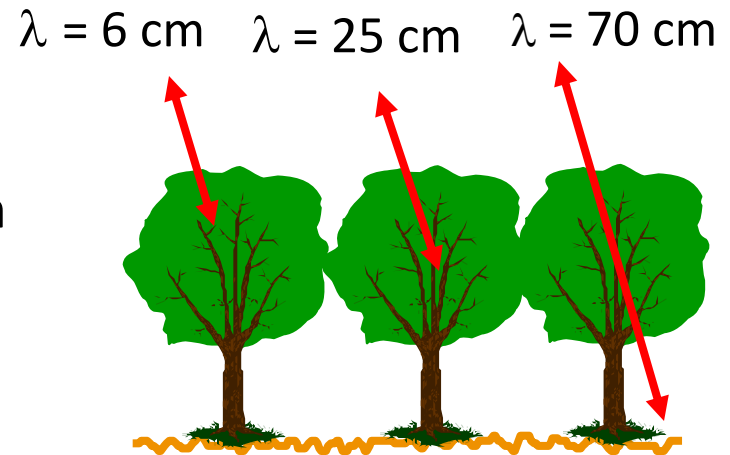
Optical, SPOT



Radar remote sensing for land surfaces monitoring

Radar sensitivity

- ☞ Biomass
- ☞ Structure and moisture of the vegetation
- ☞ soil roughness and moisture



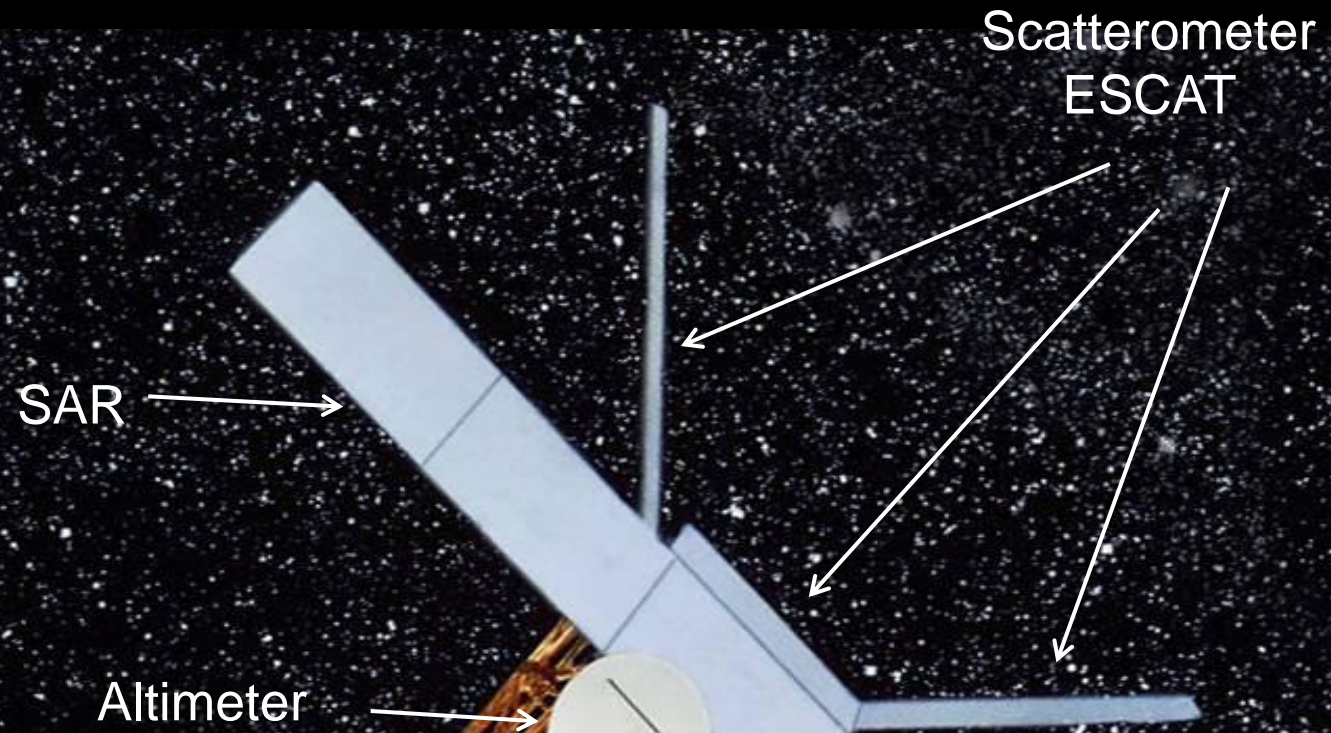
Access to key variables in ecosystems functioning

- ☞ vegetation discrimination (type, species, state,...)
- ☞ Net primary productivity
- ☞ Period of vegetation activity
- ☞ water state of vegetation cover (water potential, stress,)

ERS satellites

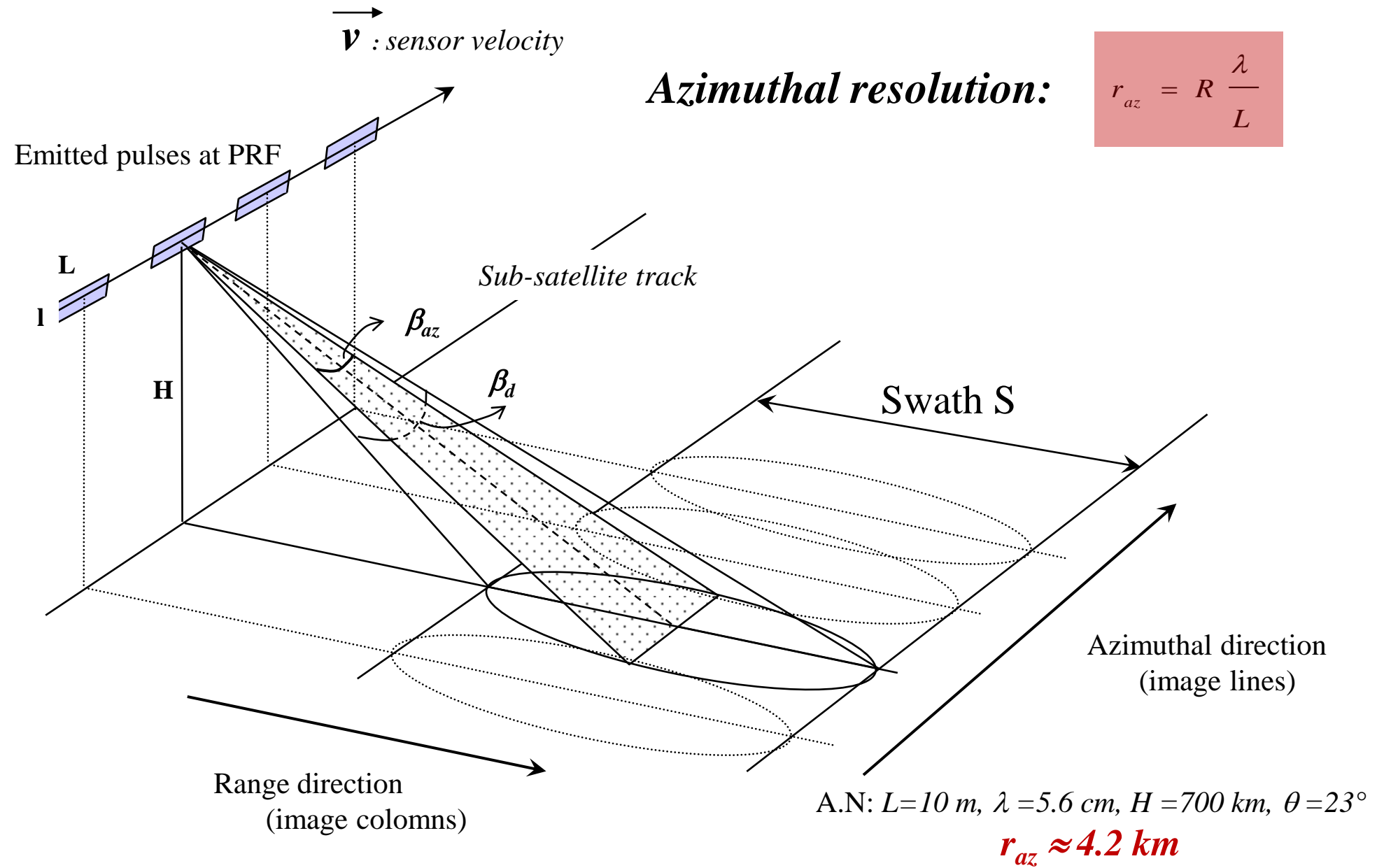
ERS-1: July1991

ERS-2: April1995



Scatterometer
ESCAT

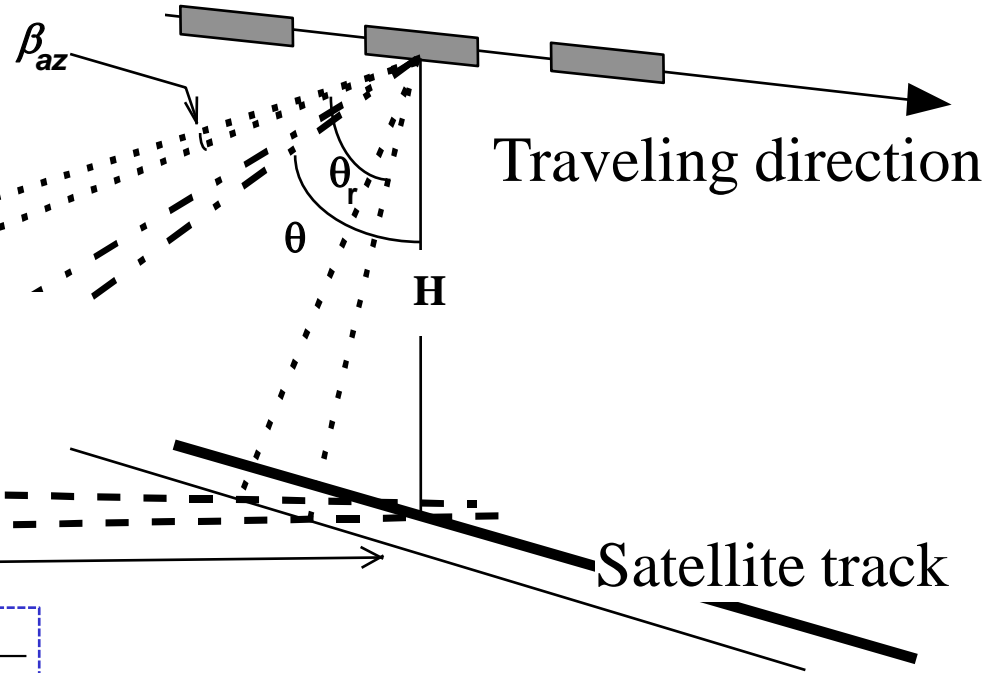
Side looking Radar sensor



Radar Imaging – spatial resolution

Range resolution

$$X_r = \frac{c \tau_p}{2} = \frac{c}{2B}$$



Ground range resolution

$$X_{r_sol} = \frac{c}{2B \sin \theta}$$

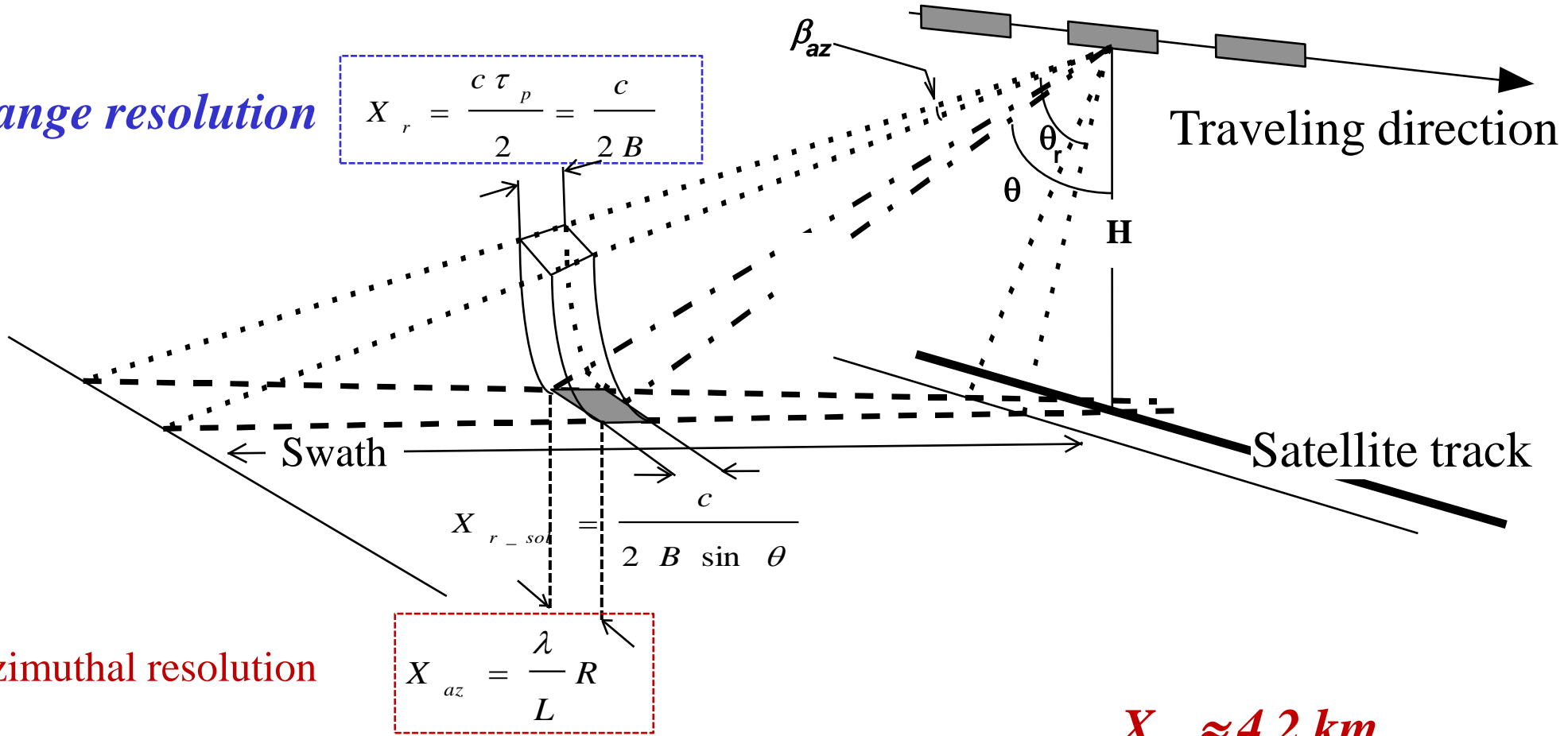
N. A.: Pulse Bandwidth: $B \approx 15 \text{ MHz}$

$\Rightarrow X_r \approx 10 \text{ m}$

Radar Imaging – spatial resolution

Range resolution

$$X_r = \frac{c \tau_p}{2} = \frac{c}{2B}$$



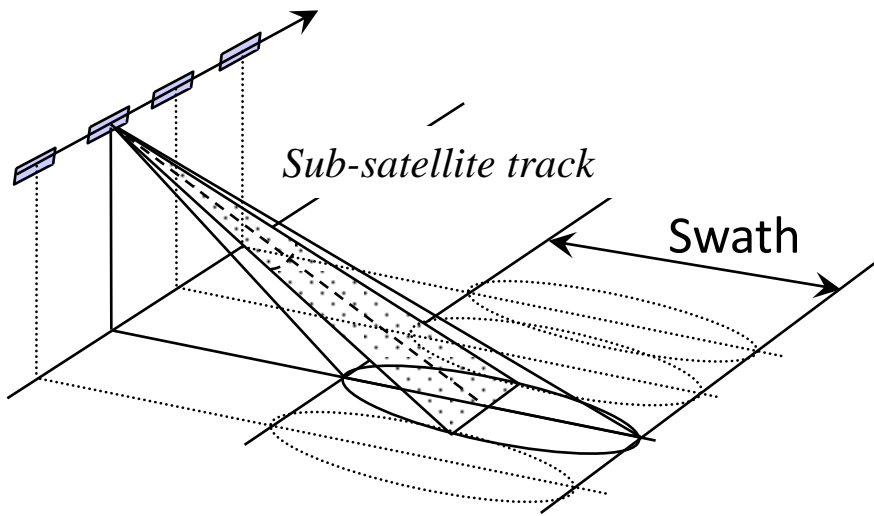
Azimuthal resolution

$$X_{az} = \frac{\lambda}{L} R$$

$$X_{az} \approx 4.2 \text{ km}$$

$$X_r \approx 10 \text{ m}$$

Side looking Radar sensor



Scatterometers

SAR

Raw echoes processing

Incoherent sum (I)

Coherent sum (A, ϕ)

Spatial resolution

low (10 – 50 km)

high (1 - 30 m)

Radiometric resolution

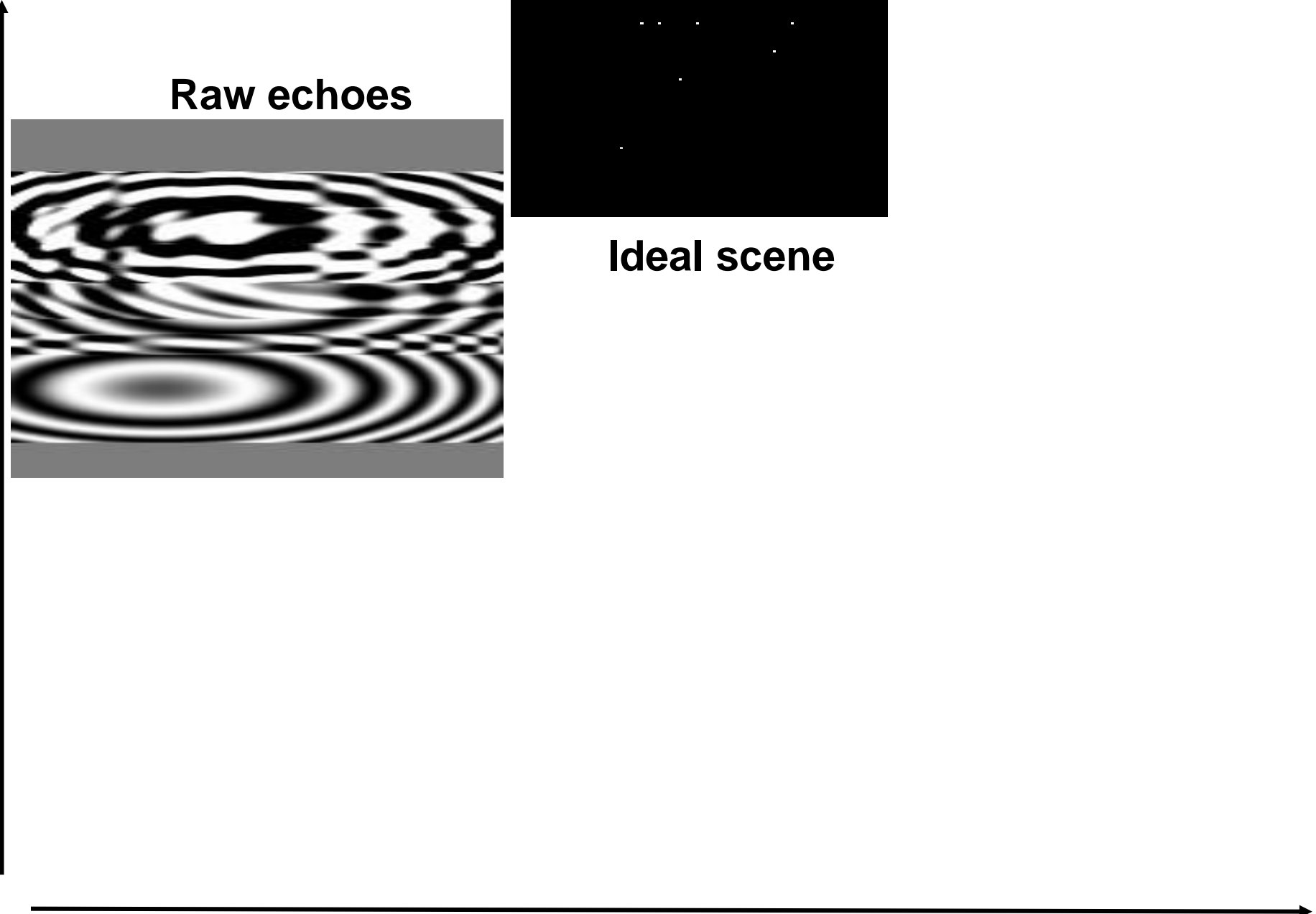
high (ELN ~ 400)

low (speckle)

Temporal period acquisitions

low (~ day)

High (~ month) ↗ up to 2015!



Scatterometers

SAR

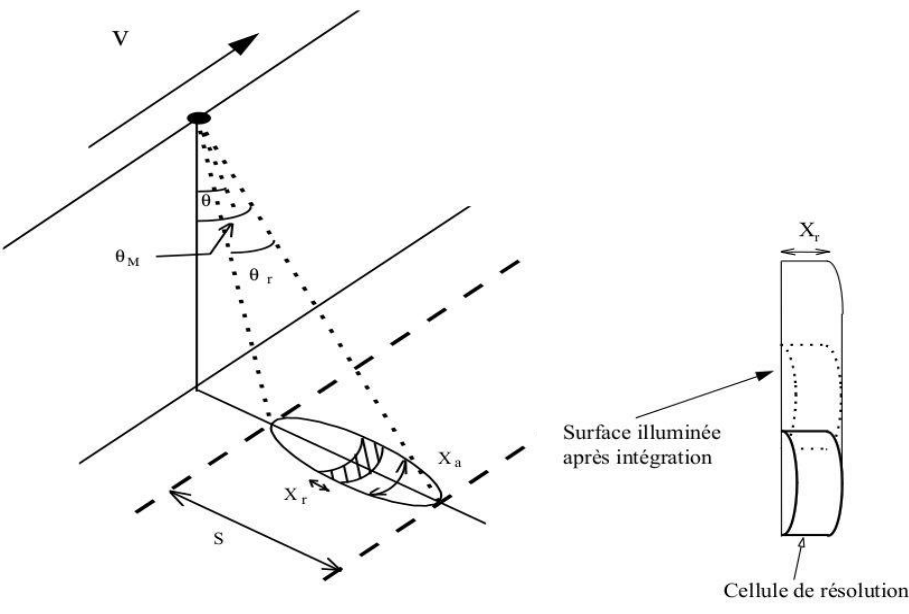
Raw echoes processing

Incoherent sum (I)

Low ($\sim 10 - 50$ km)

High (ENL ~ 400)

seas (winds)



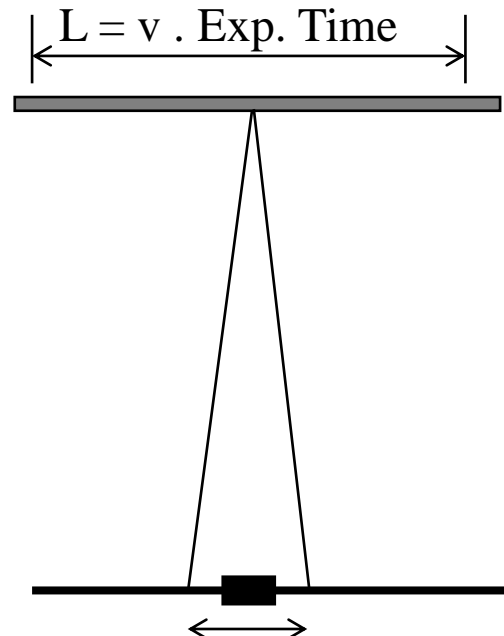
Spatial resolution

Coherent sum (A, ϕ)

Fine (1 - 30 m)

Low (speckle)

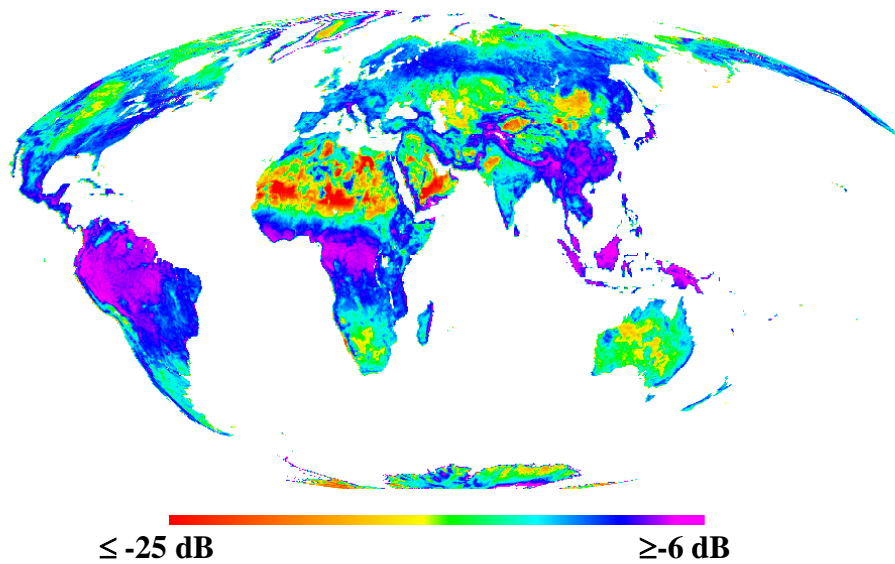
Land - seas



Side looking radar sensors

Scatterometers:

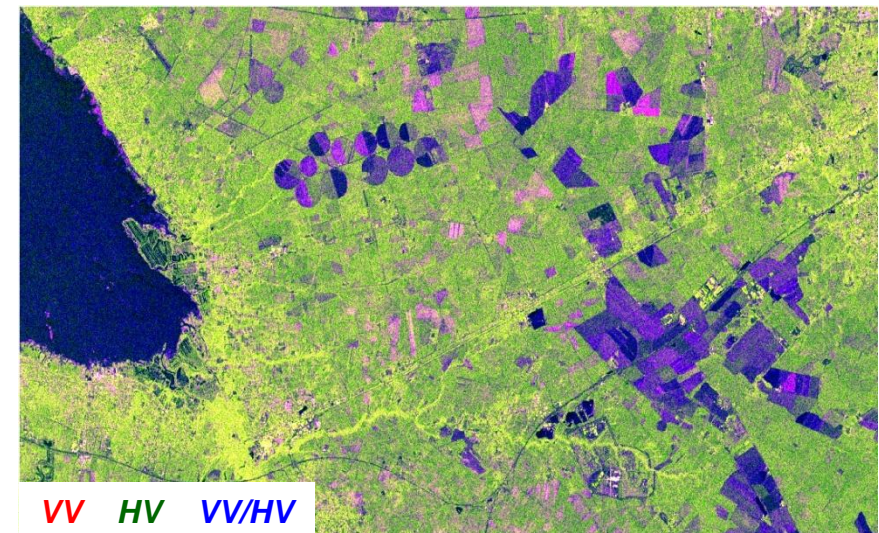
- ☛ Radar reflectivity estimation (σ^0)
- **low spatial resolution:** $\sim 10 - 50 \text{ km}$
- **high frequency of acquisitions (~ day)**



Scatt. ERS – May 1992

SAR:

- ☛ surface imaging
- **high spatial resolution:** $\sim 10 \text{ m}$
- **low frequency of acquisition (~ month)**



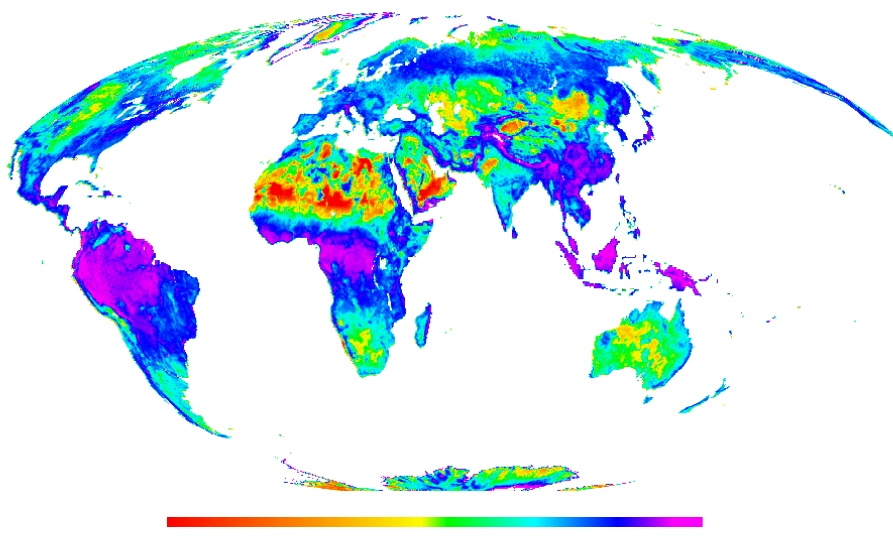
Sentinel-1
Les Landes – March 2015

Side looking radar sensors

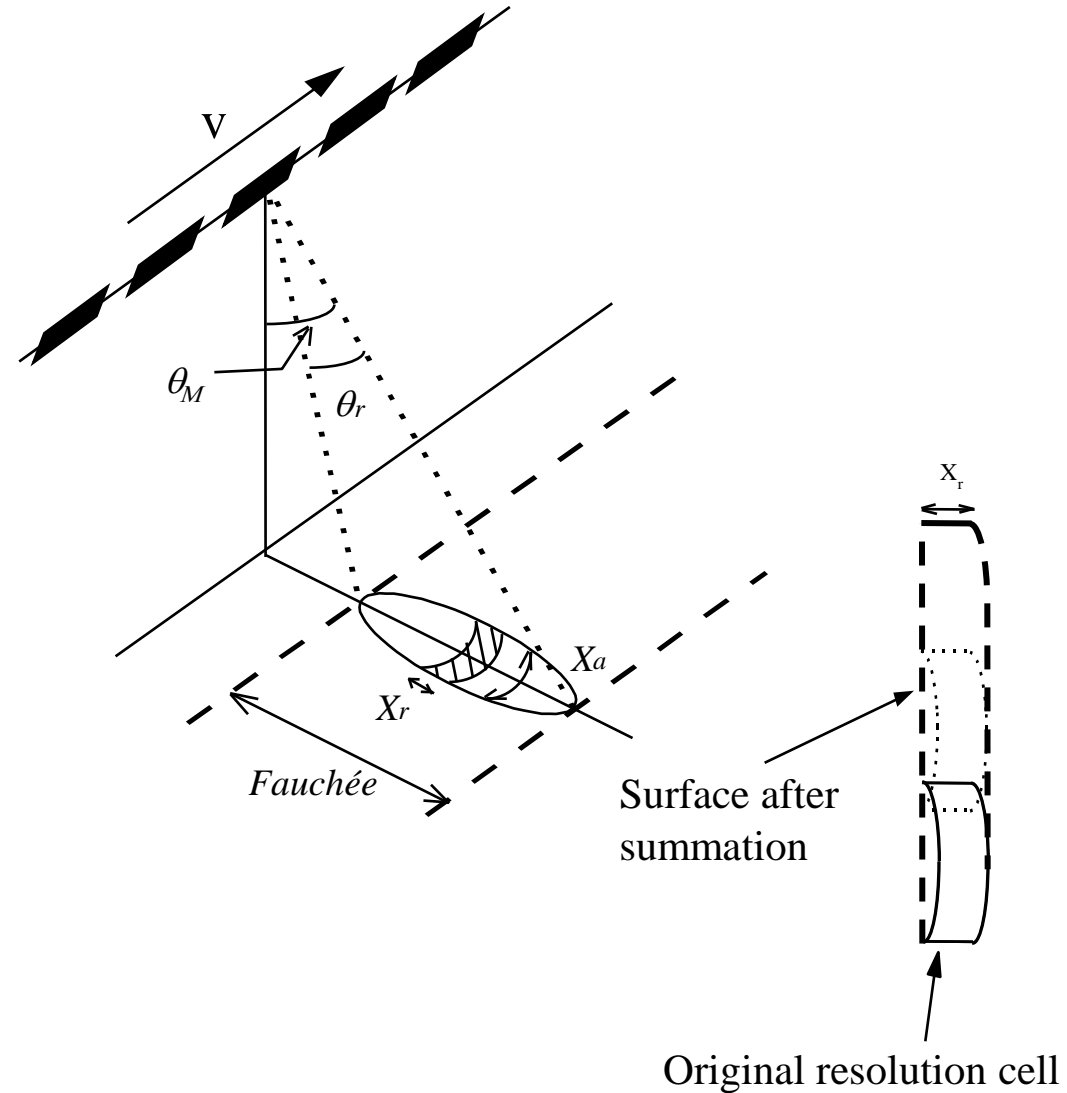
Scatterometers:

☛ Radar reflectivity estimation (σ°)

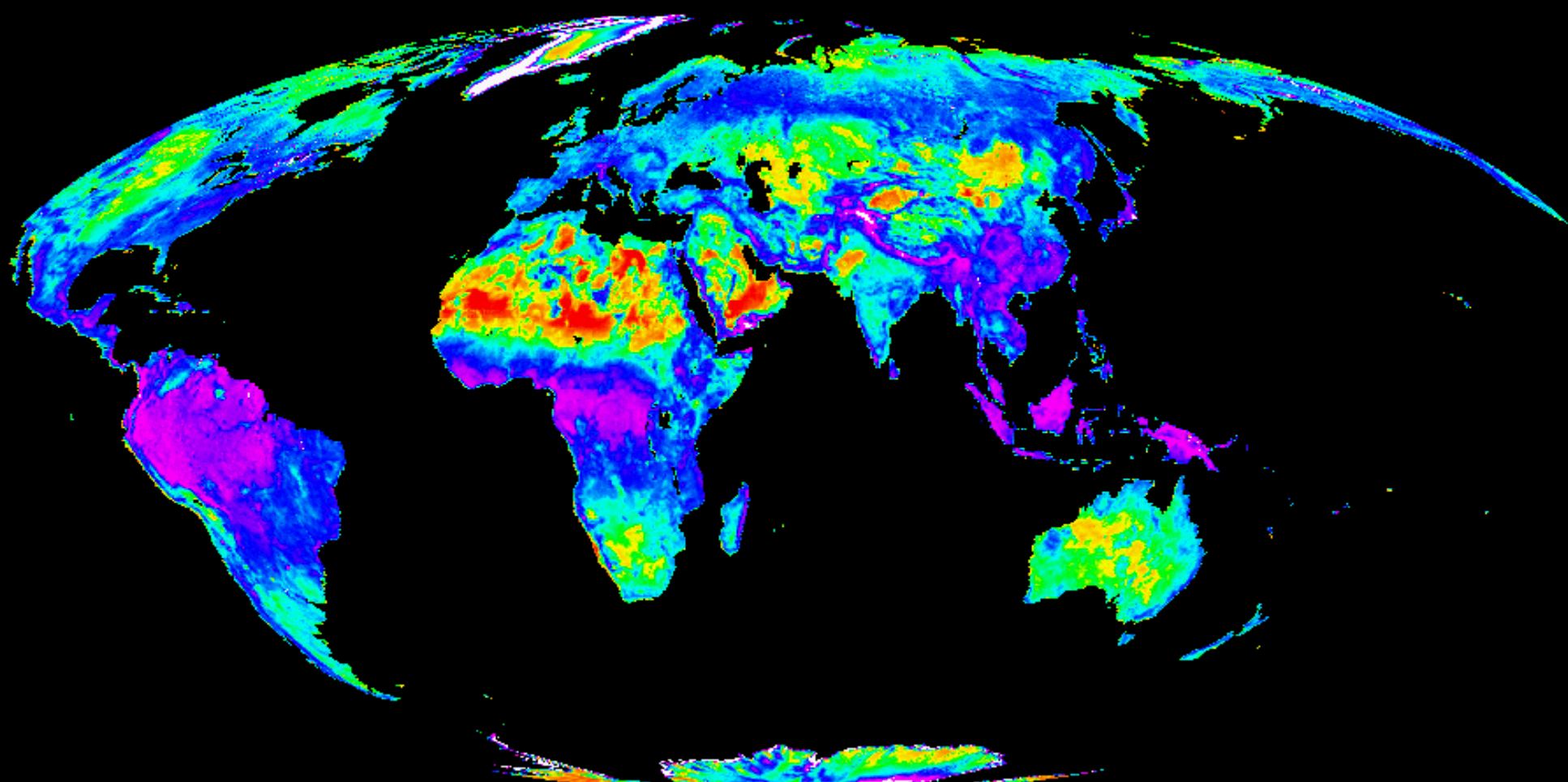
- **low spatial resolution:** $\sim 10 - 50 \text{ km}$
- **high frequency of acquisitions (~ day)**



Scatt. ERS – May 1992



ERS Scatterometer: global image of $\sigma^0(40^\circ)$

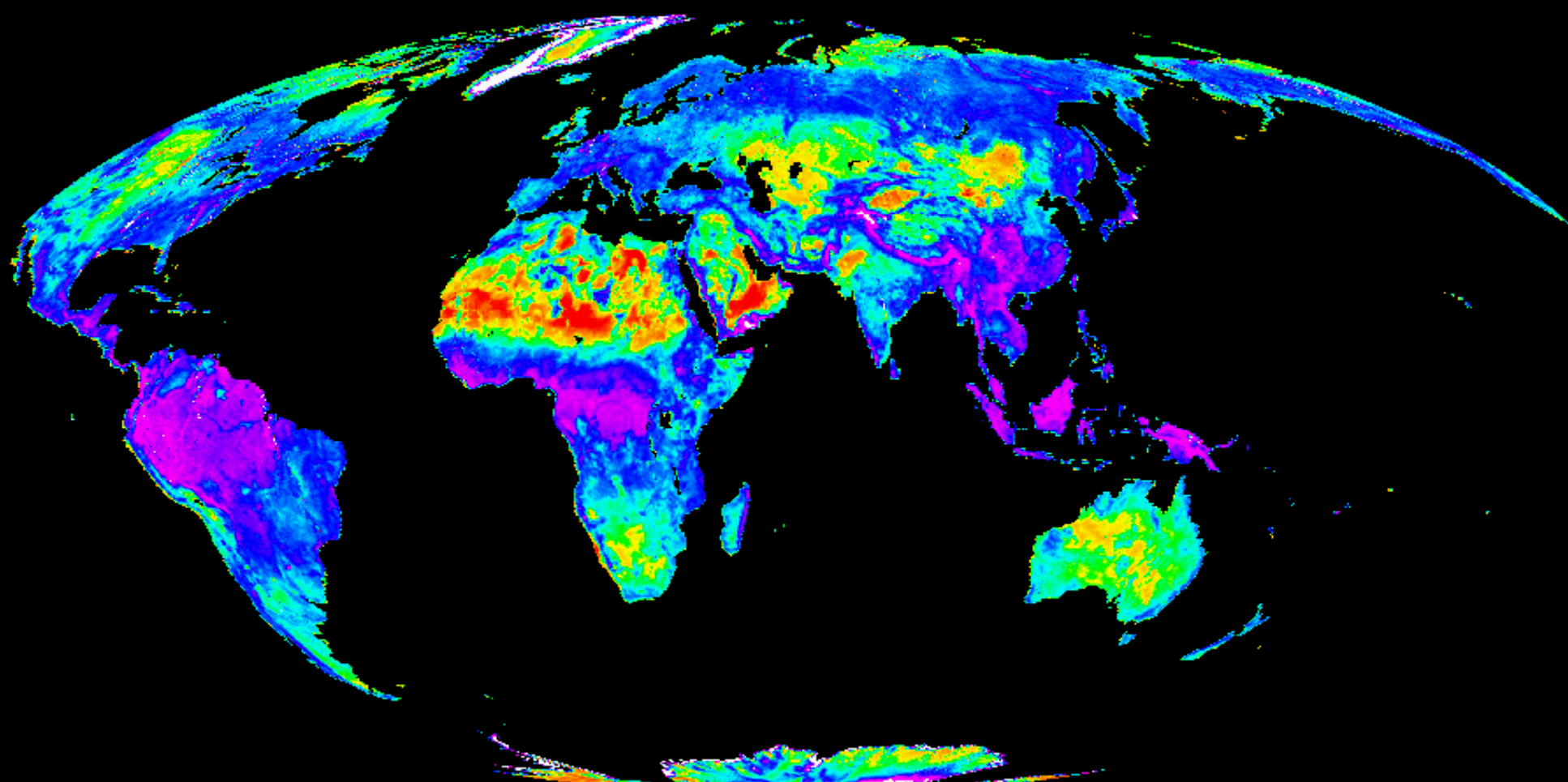


-25.5

-16.5 -15.5 -12.5 -9.5 -6.5 (dB)

May 1992

ERS Scatterometer: global image of $\sigma^0(40^\circ)$

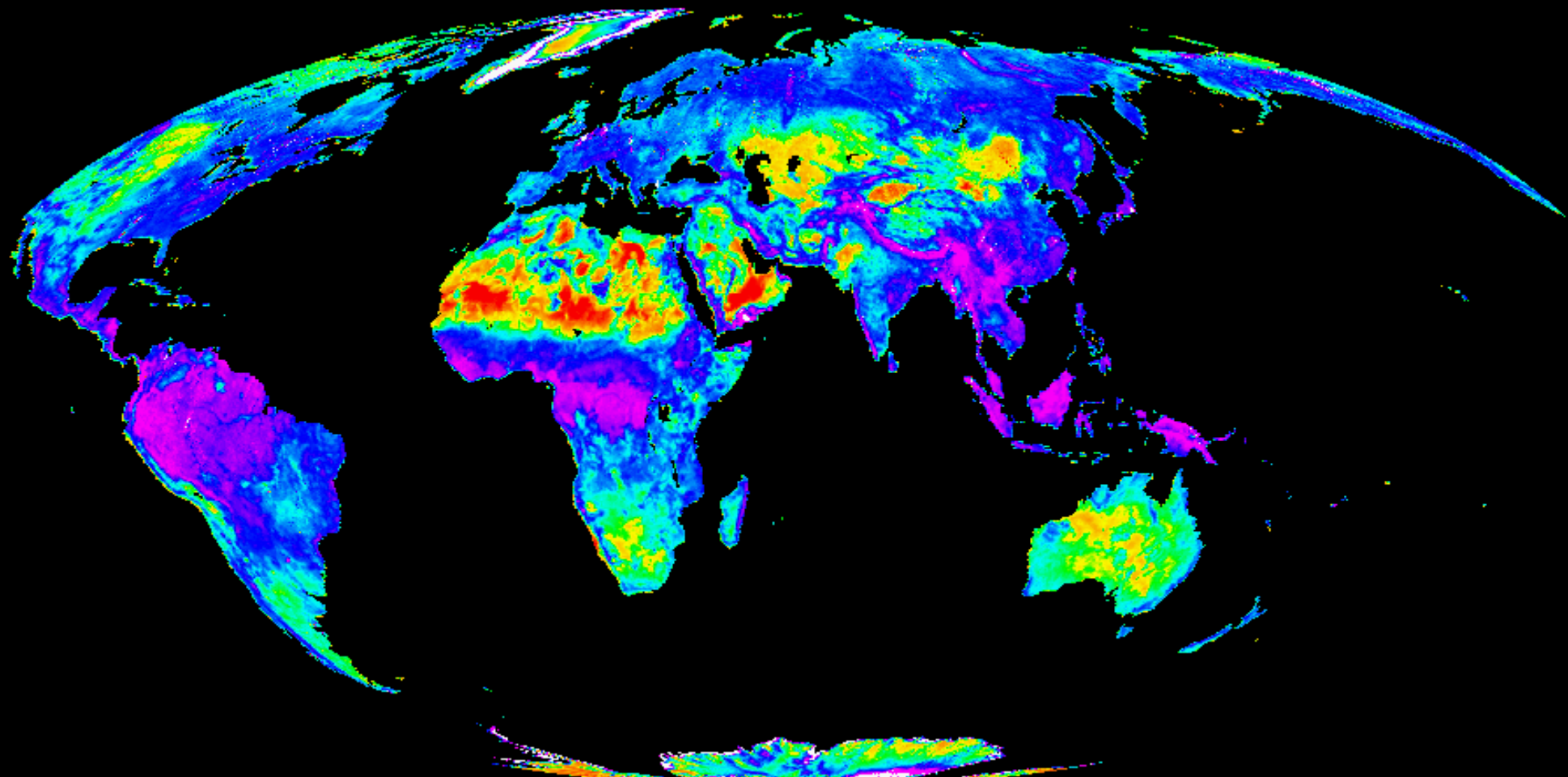


-25.5

-16.5 -15.5 -12.5 -9.5 -6.5 (dB)

June 1992

ERS Scatterometer: global image of $\sigma^0(40^\circ)$

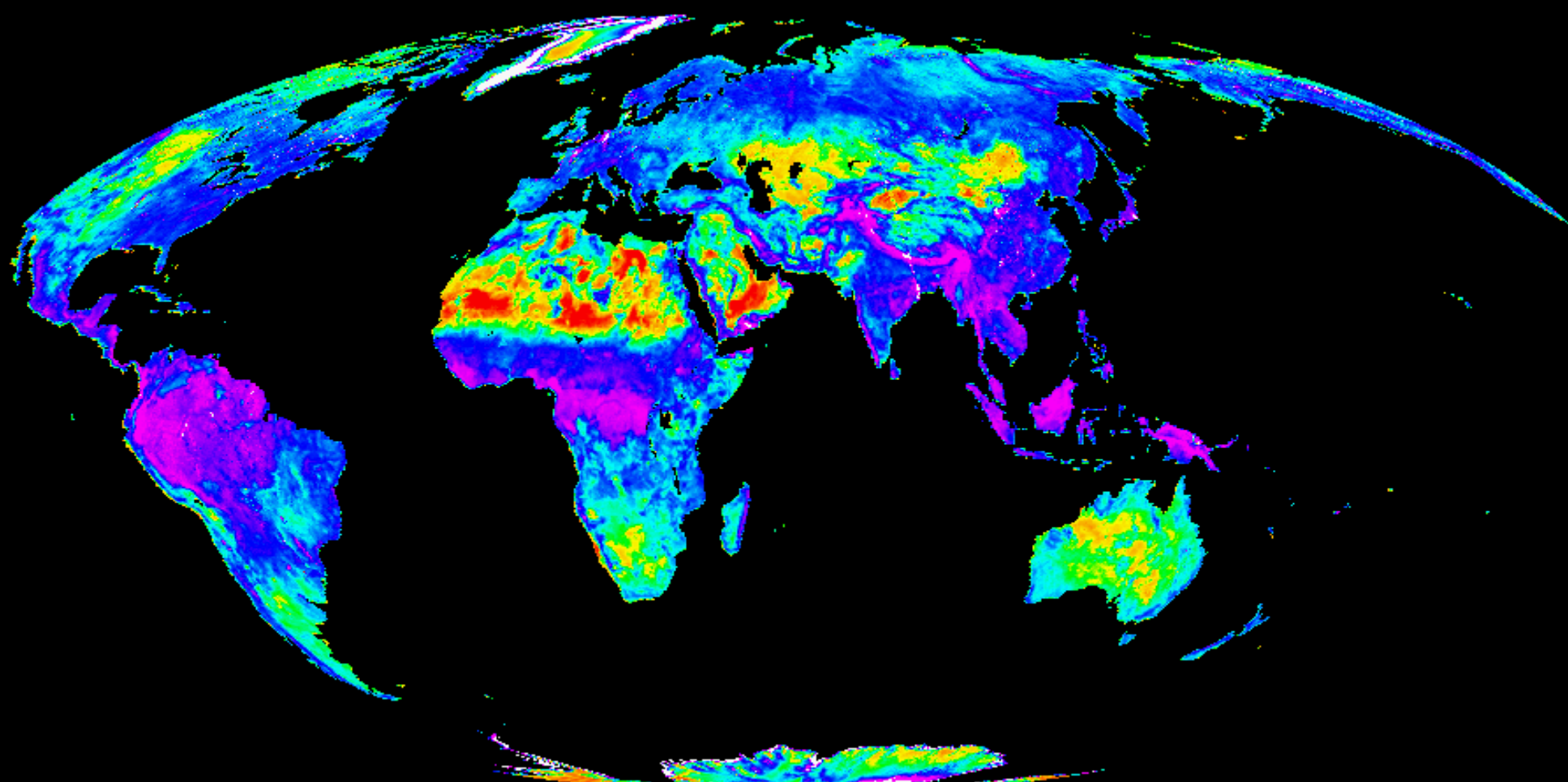


-25.5

-16.5 -15.5 -12.5 -9.5 -6.5 (dB)

July 1992

ERS Scatterometer: global image of $\sigma^0(40^\circ)$

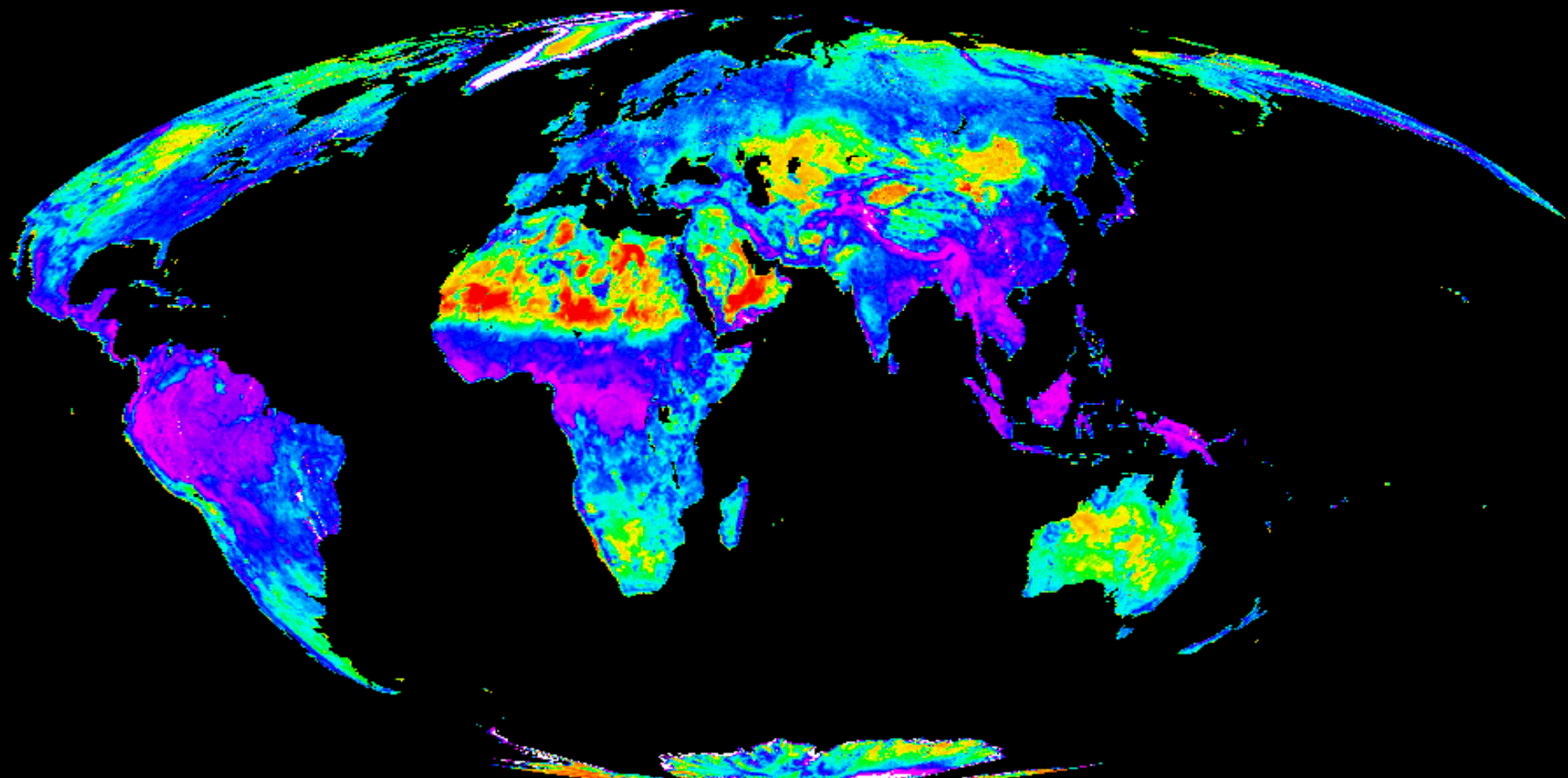


-25.5

-16.5 -15.5 -12.5 -9.5 -6.5 (dB)

August 1992

ERS Scatterometer: global image of $\sigma^0(40^\circ)$

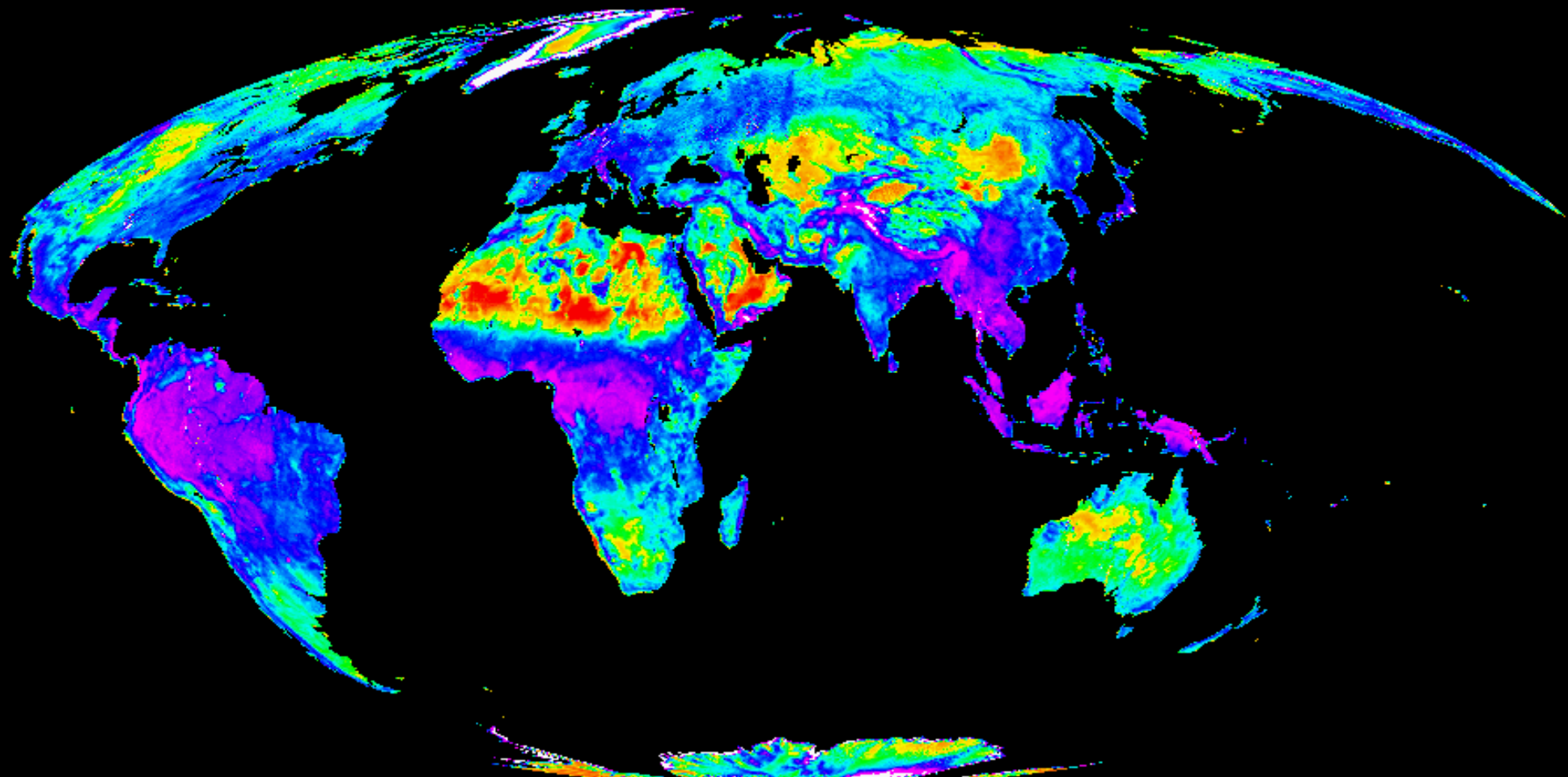


-25.5

-16.5 -15.5 -12.5 -9.5 -6.5 (dB)

Sept. 1992

ERS Scatterometer: global image of $\sigma^0(40^\circ)$

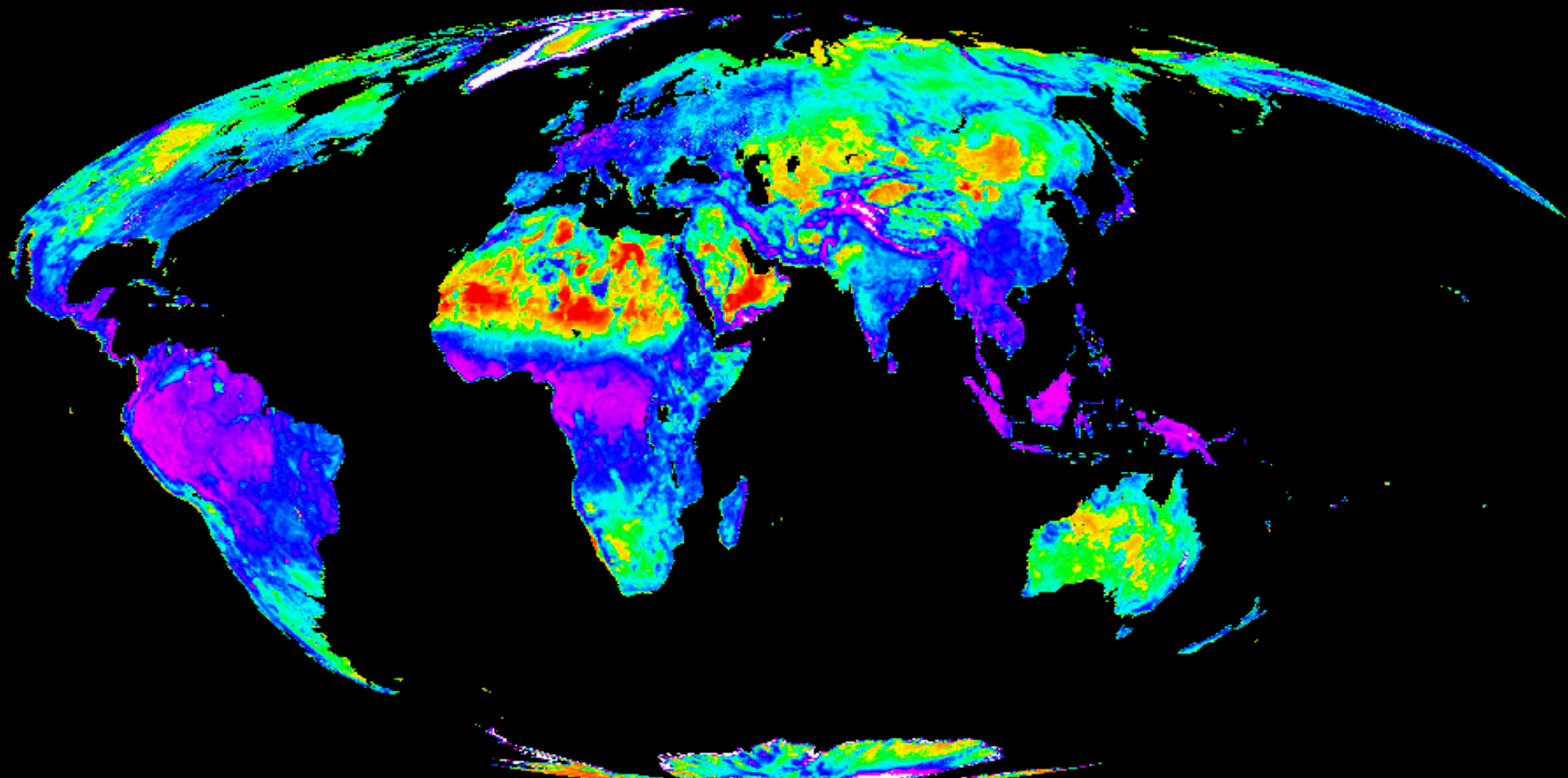


-25.5

-16.5 -15.5 -12.5 -9.5 -6.5 (dB)

October 1992

ERS Scatterometer: global image of $\sigma^0(40^\circ)$

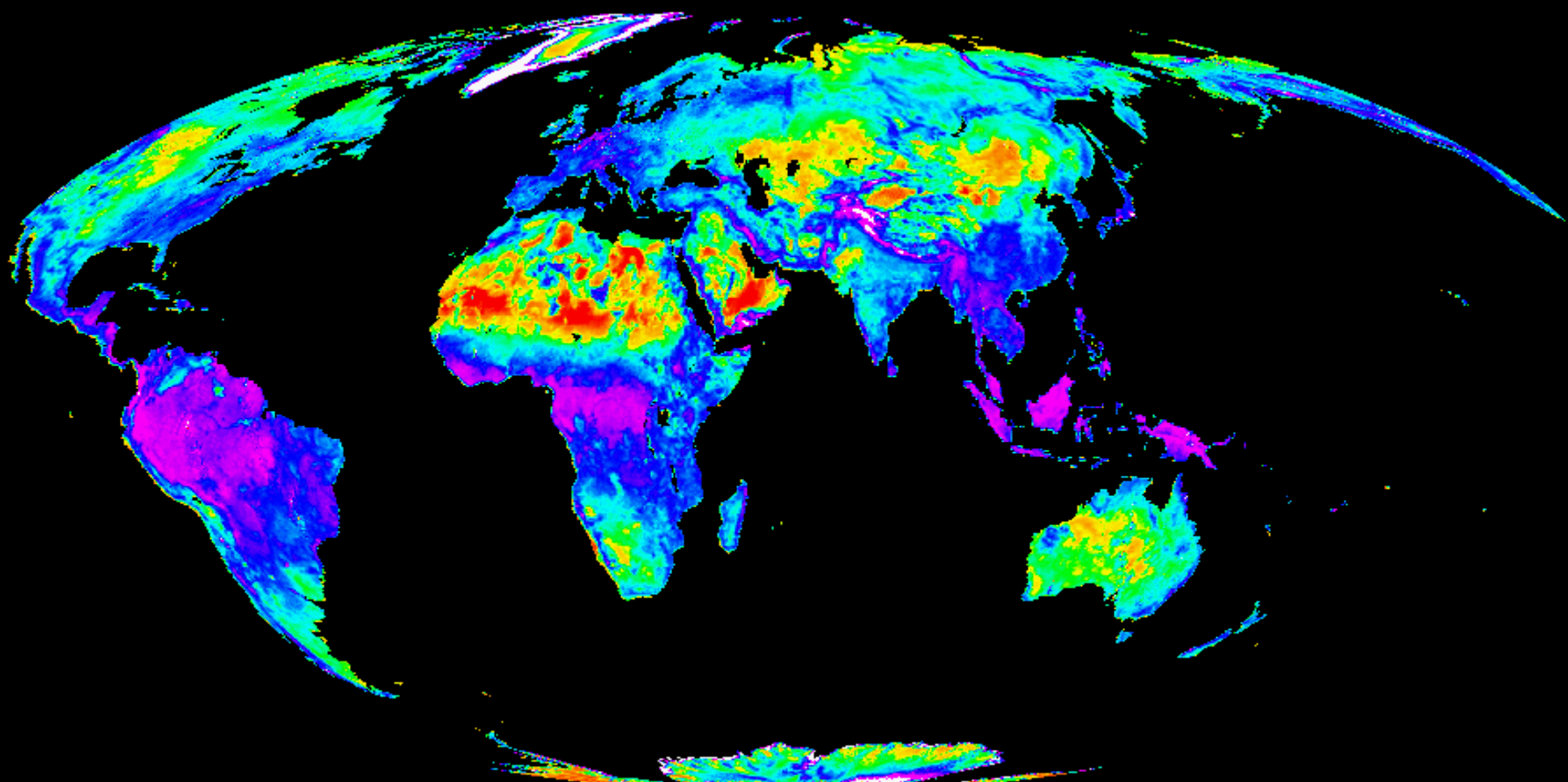


-25.5

-16.5 -15.5 -12.5 -9.5 -6.5 (dB)

Nov. 1992

ERS Scatterometer: global image of $\sigma^0(40^\circ)$

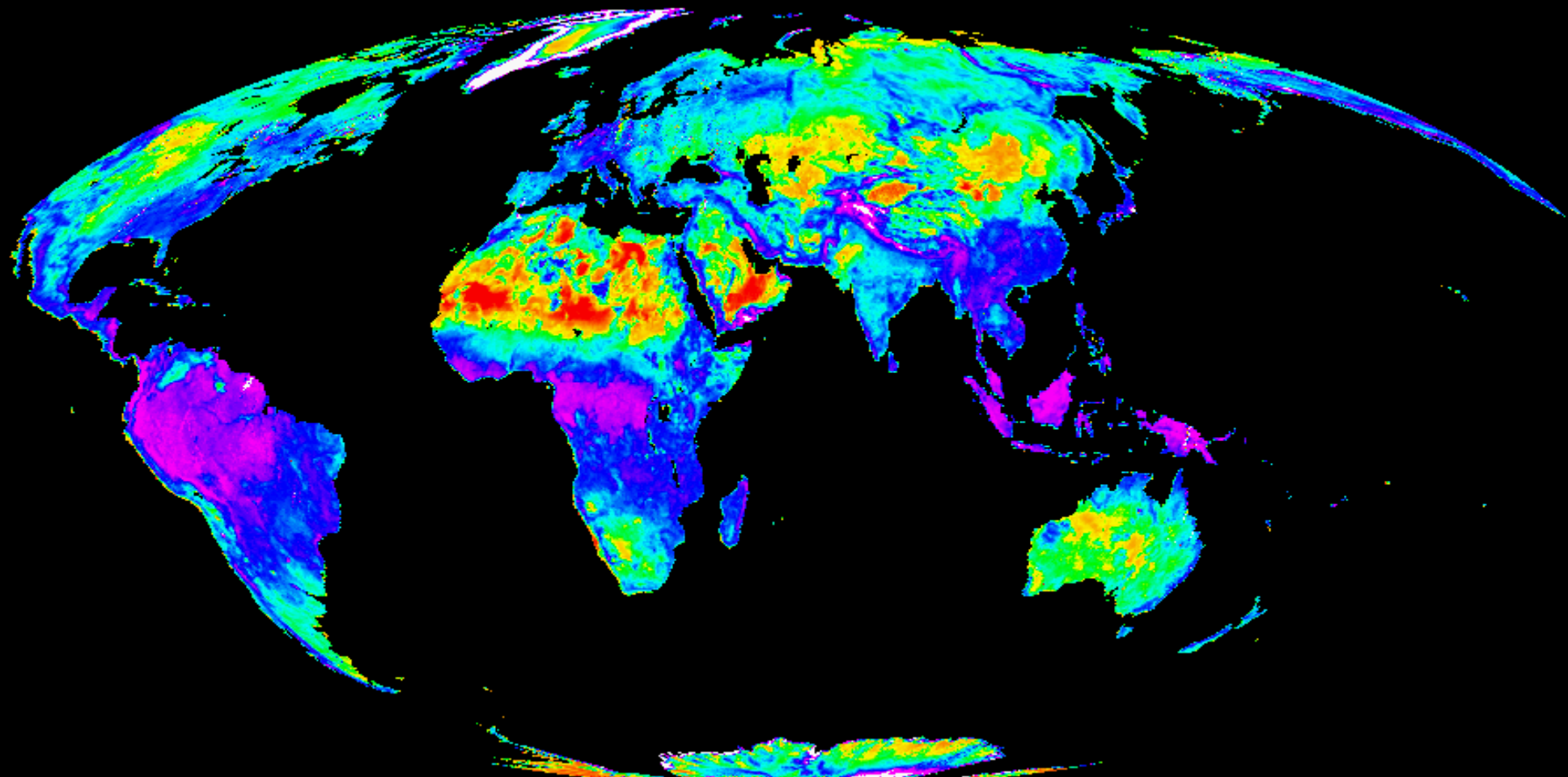


-25.5

-16.5 -15.5 -12.5 -9.5 -6.5 (dB)

Dec. 1992

ERS Scatterometer: global image of $\sigma^0(40^\circ)$



-25.5

-16.5 -15.5

-12.5

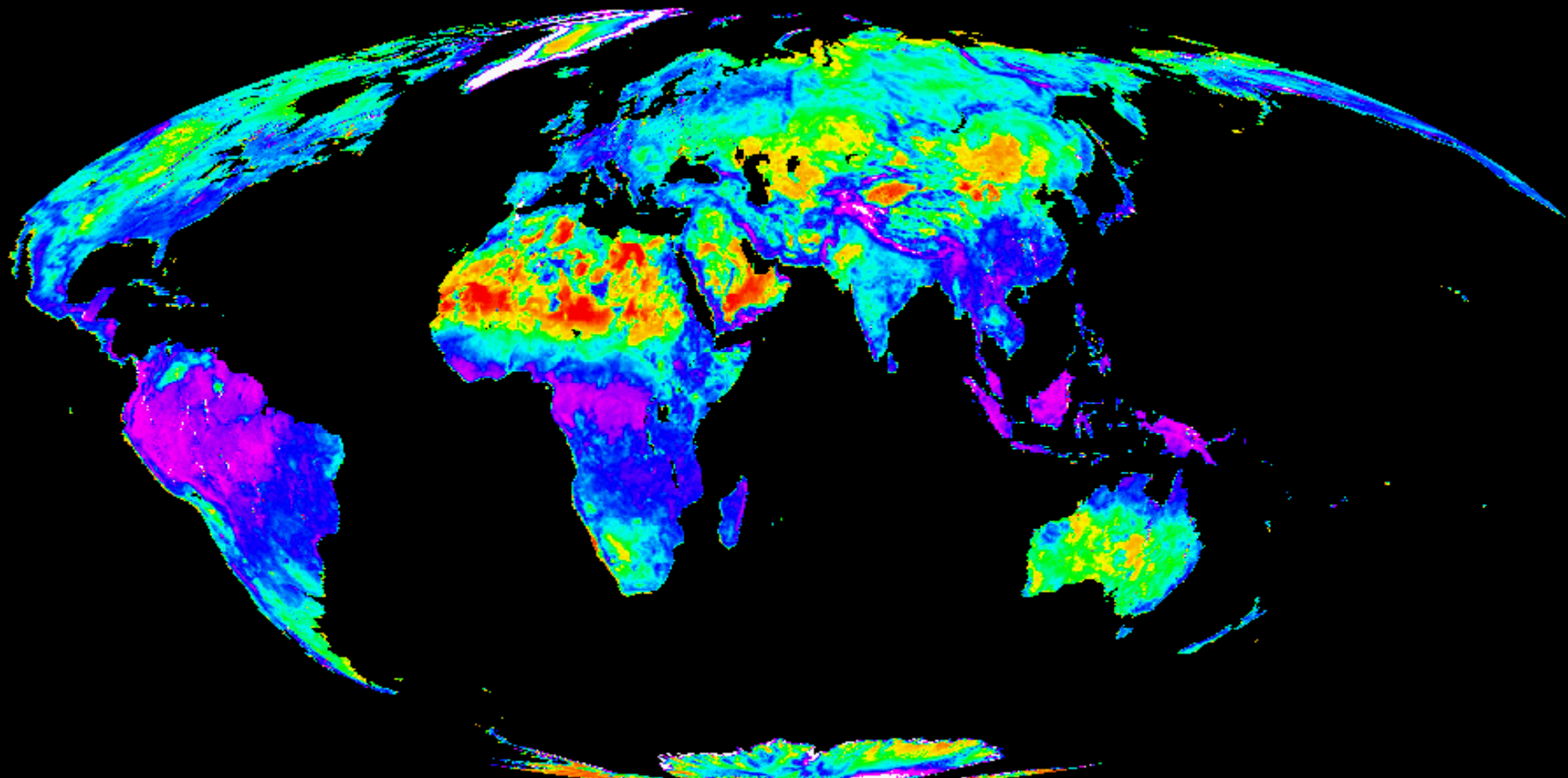
-9.5

-6.5

(dB)

January 1993

ERS Scatterometer: global image of $\sigma^0(40^\circ)$



-25.5

-16.5 -15.5

-12.5

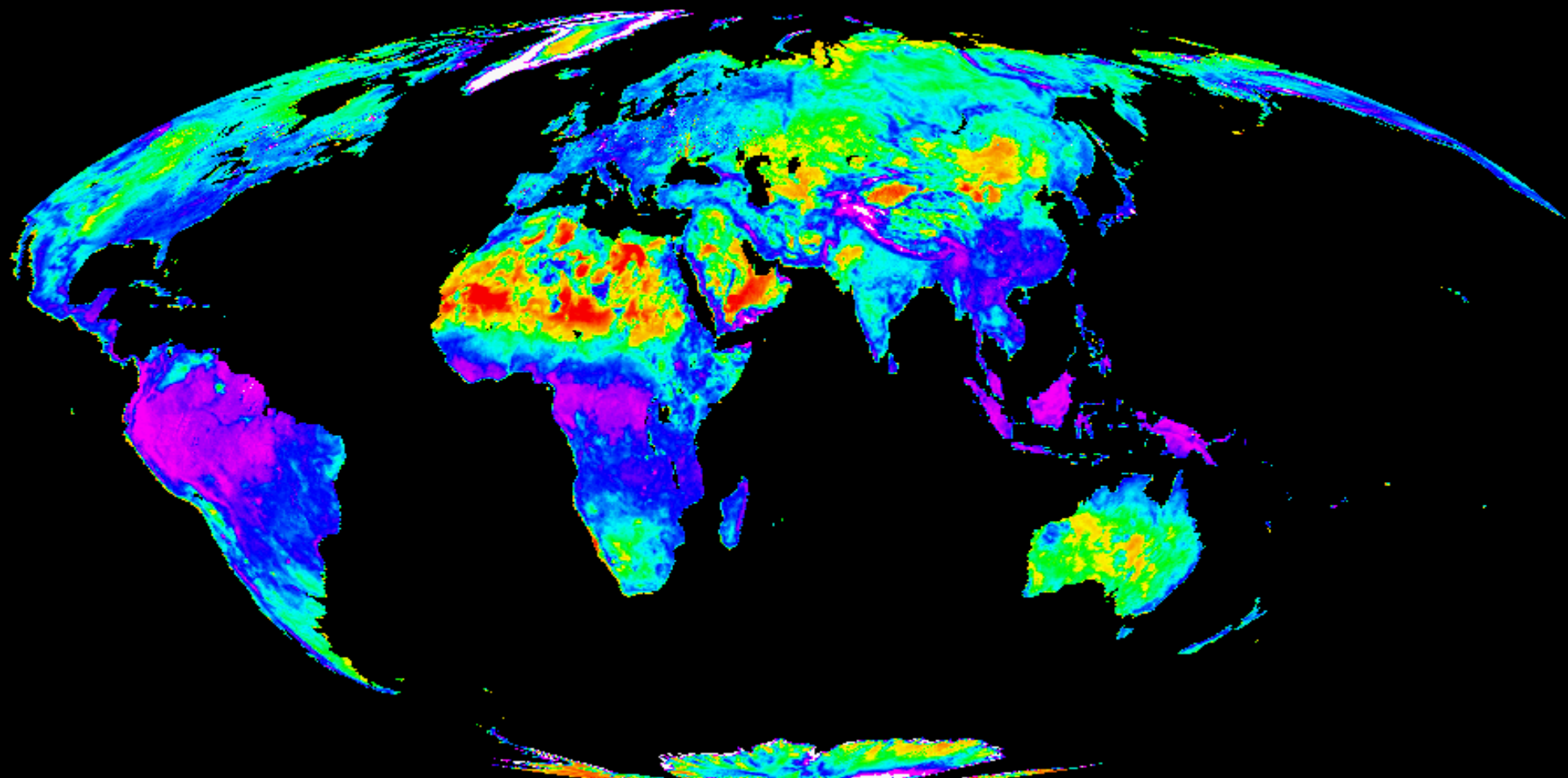
-9.5

-6.5

(dB)

February 1993

ERS Scatterometer: global image of $\sigma^0(40^\circ)$

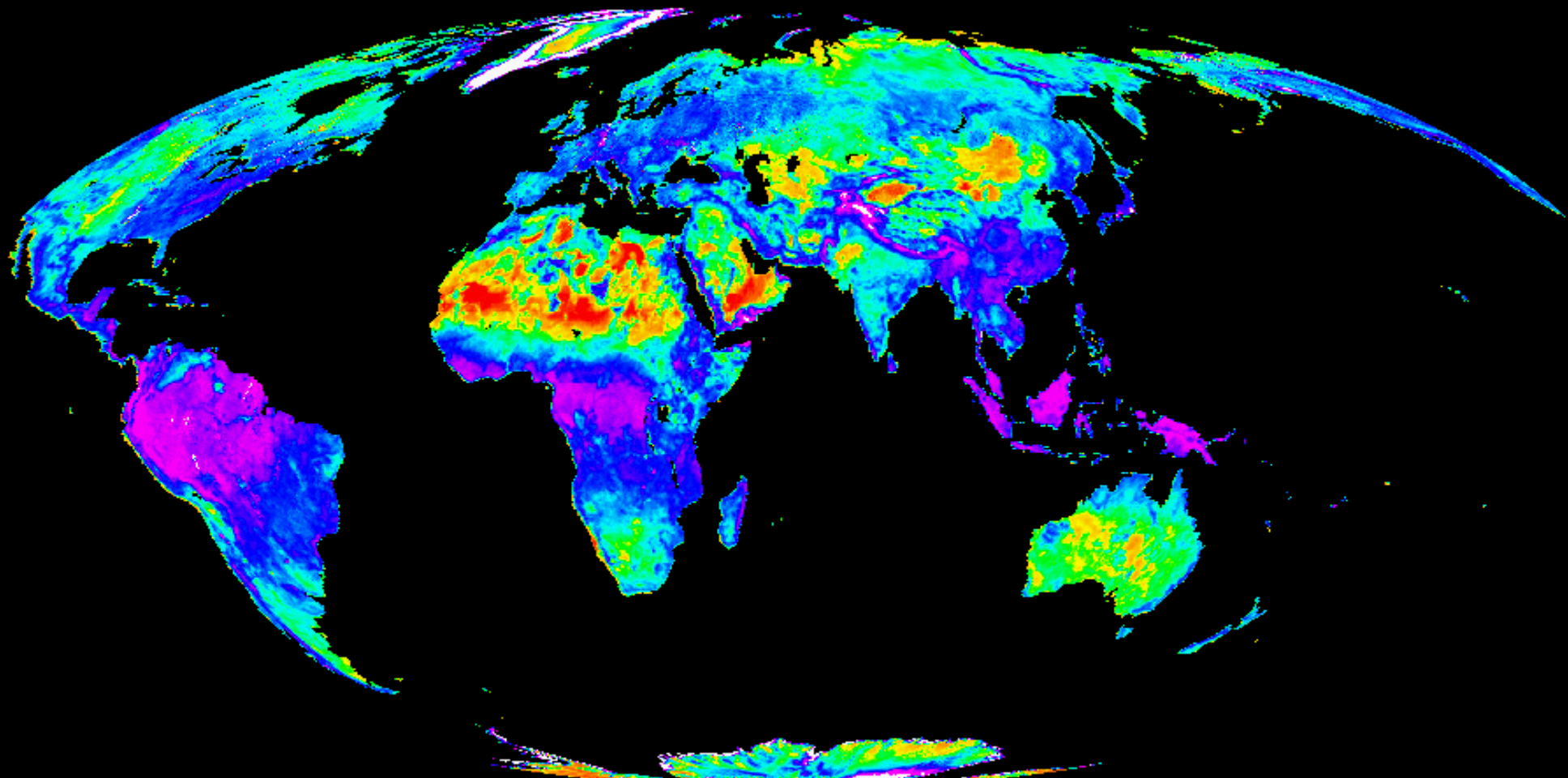


-25.5

-16.5 -15.5 -12.5 -9.5 -6.5 (dB)

March 1993

ERS Scatterometer: global image of $\sigma^0(40^\circ)$

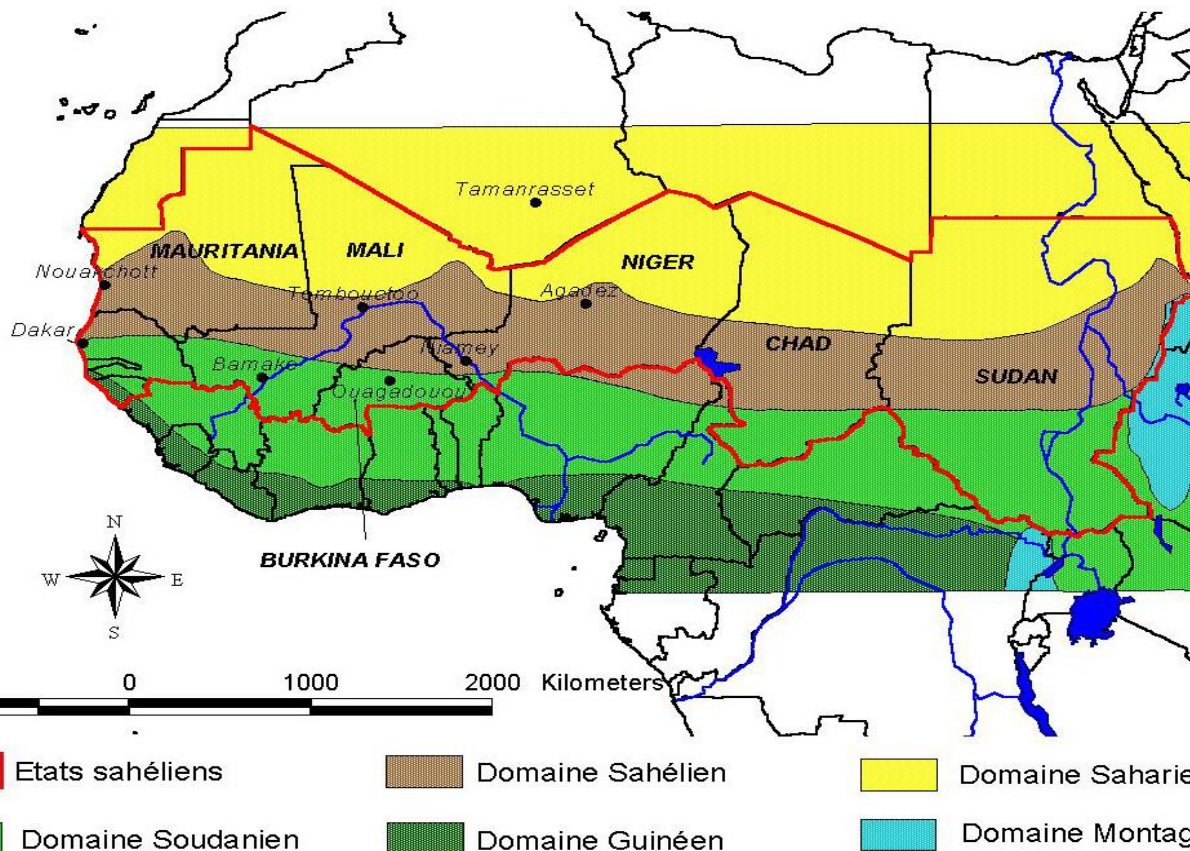


-25.5

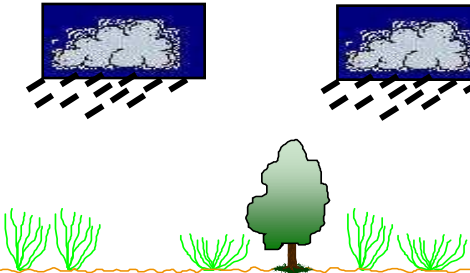
-16.5 -15.5 -12.5 -9.5 -6.5 (dB)

April 1993

The African Sahel



- A large dry season (from October to June) followed by a short rainy season (June-September)



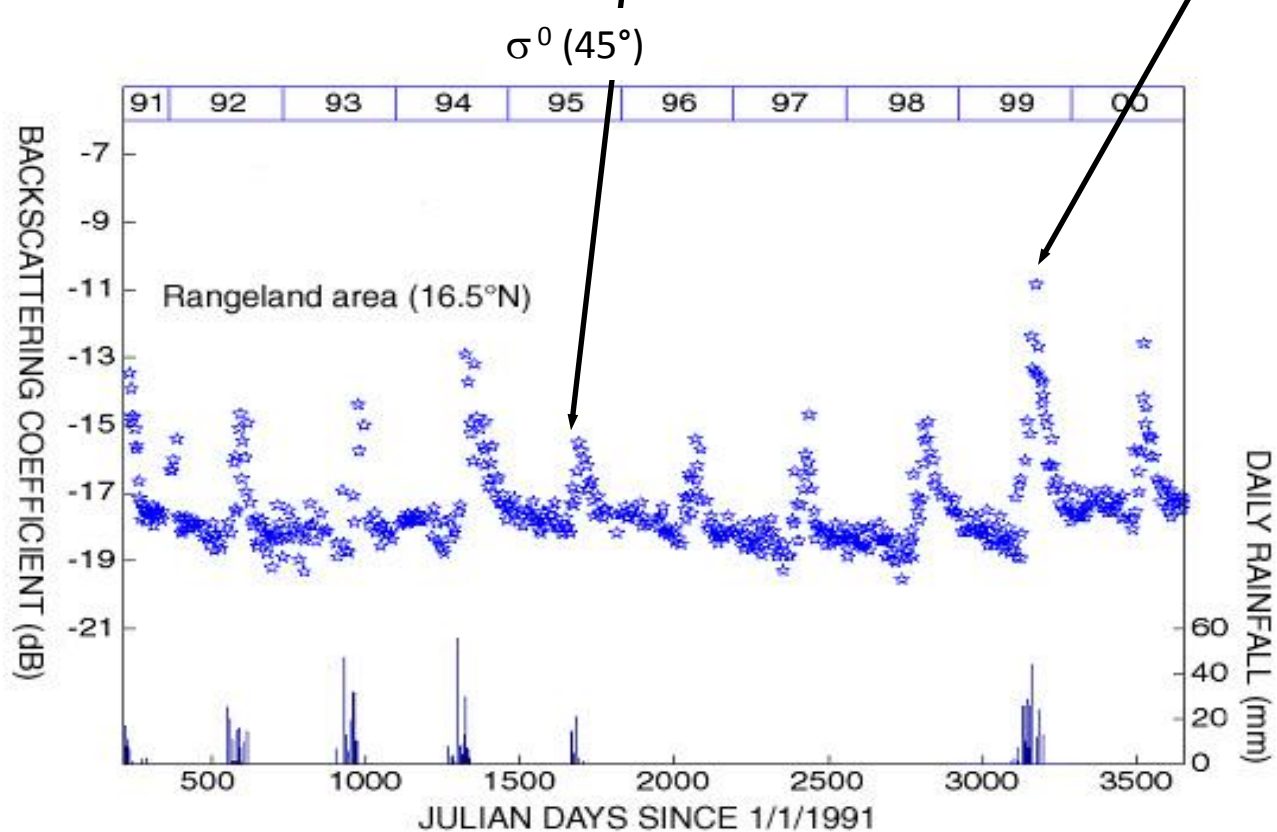
- Vegetation (natural or crops)
⇒ strongly linked to precipitation system

Temporal evolution of $\sigma^0(45^\circ)$: Rharous

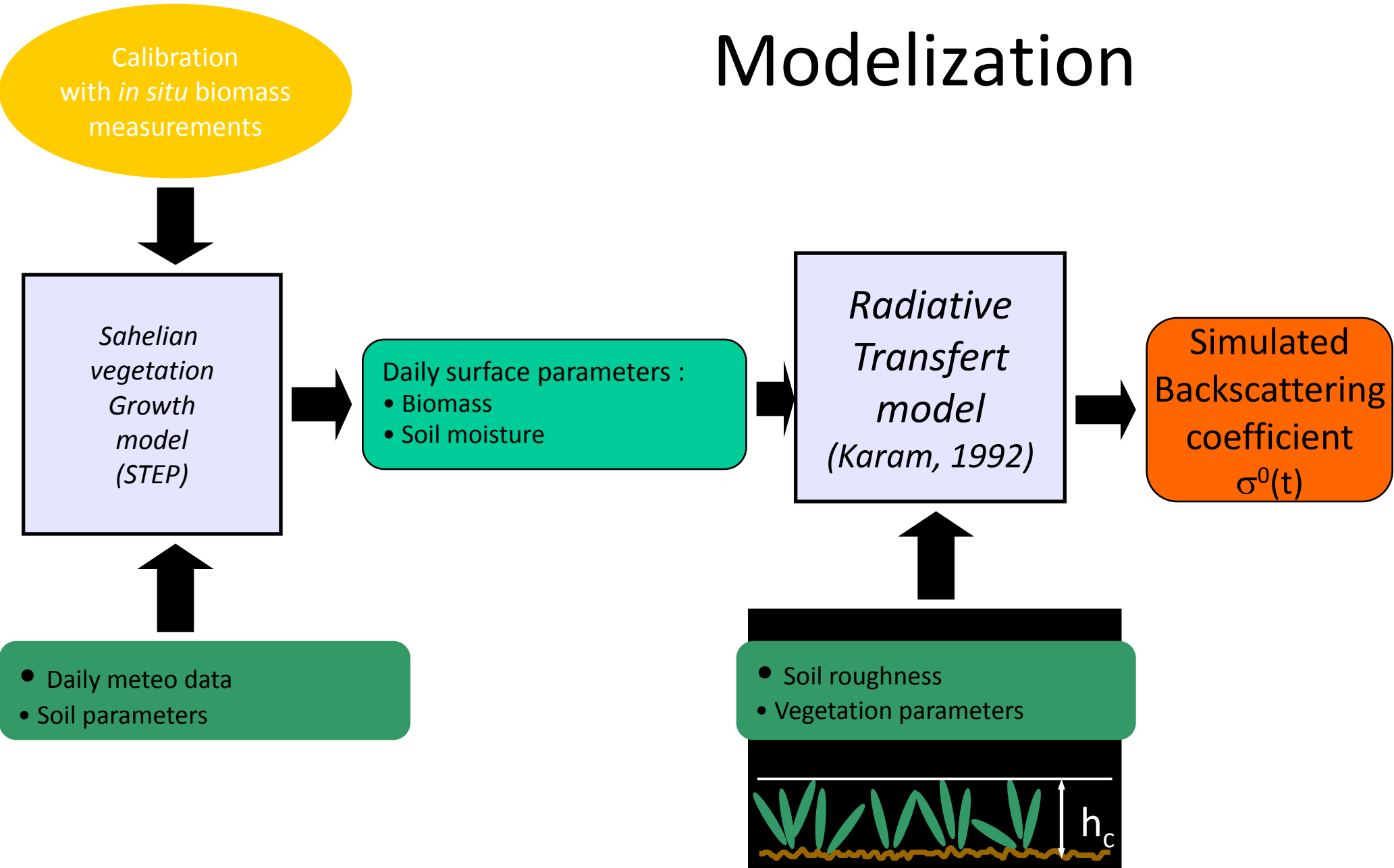
Dry year



Wet year

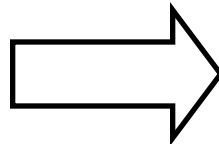
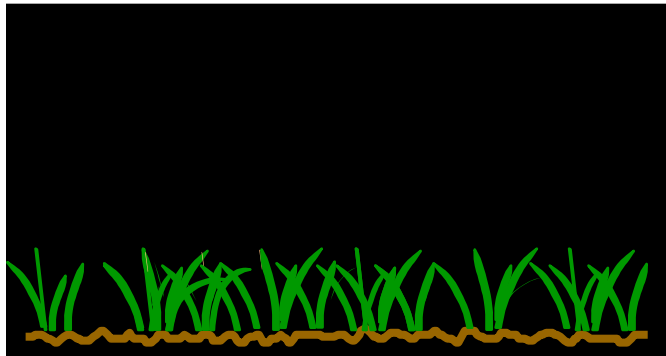


Modelization

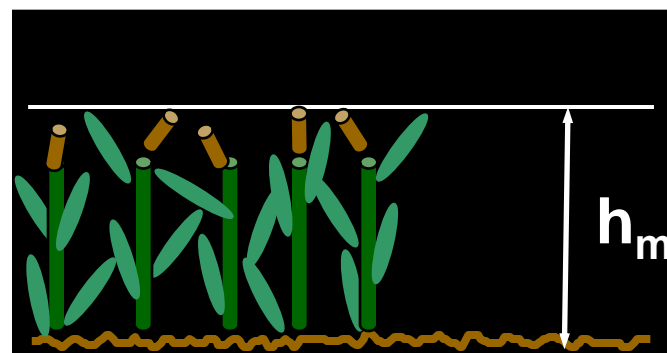
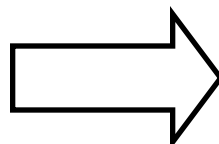
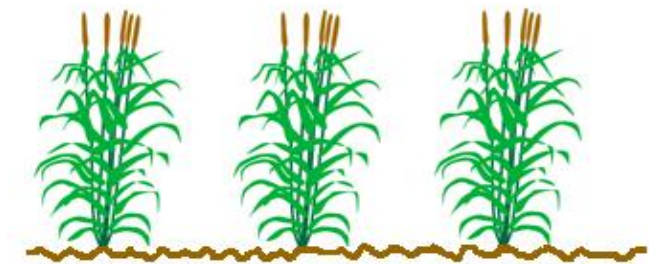
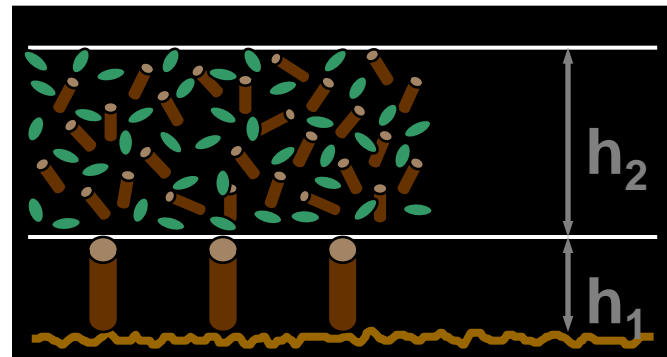
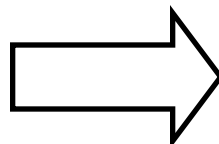
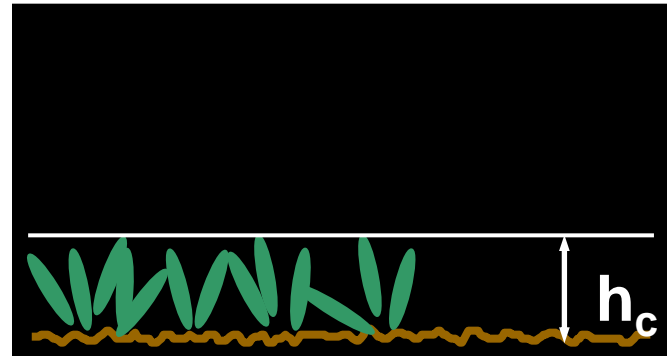


Radiative transfert model

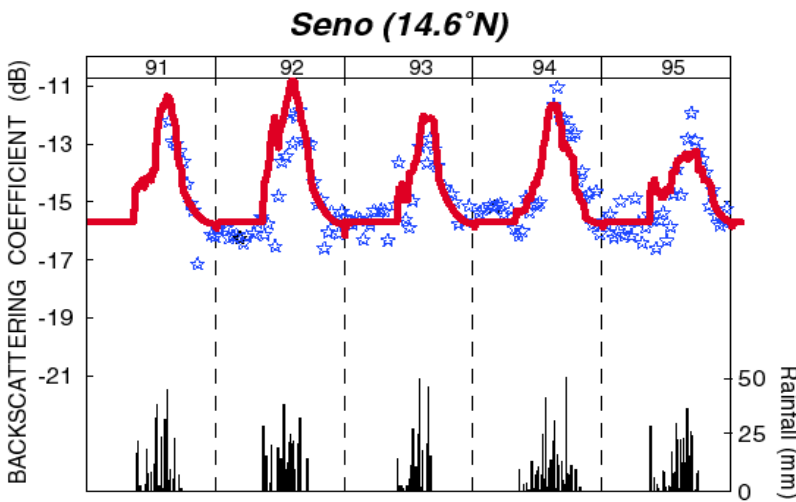
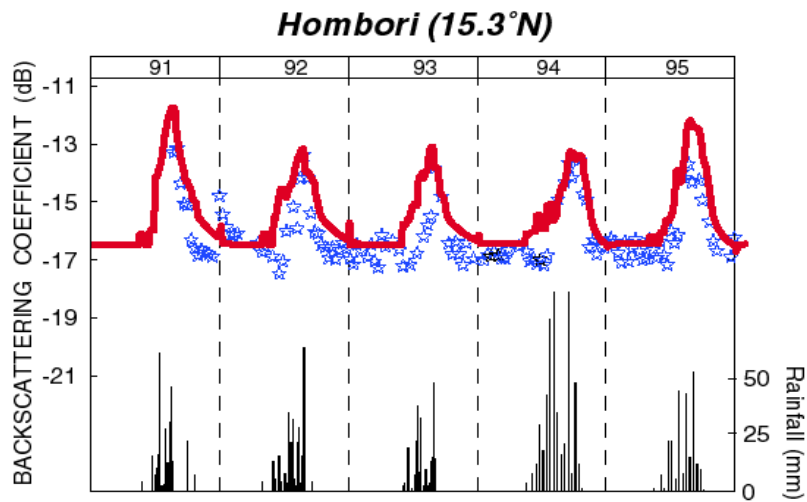
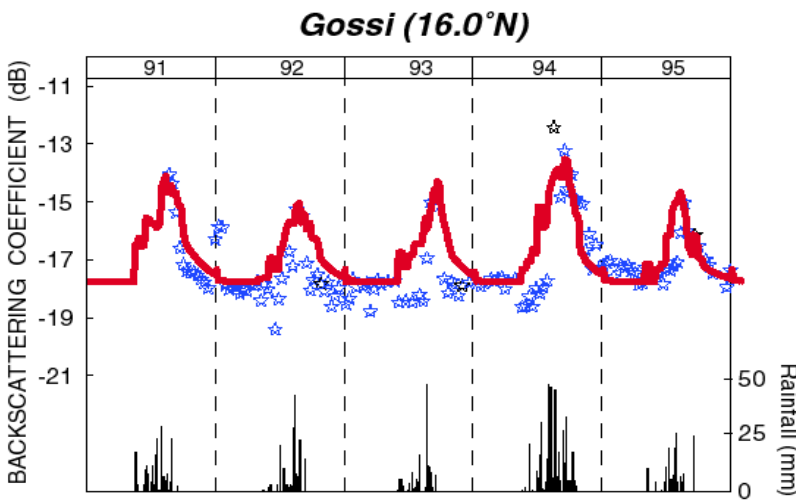
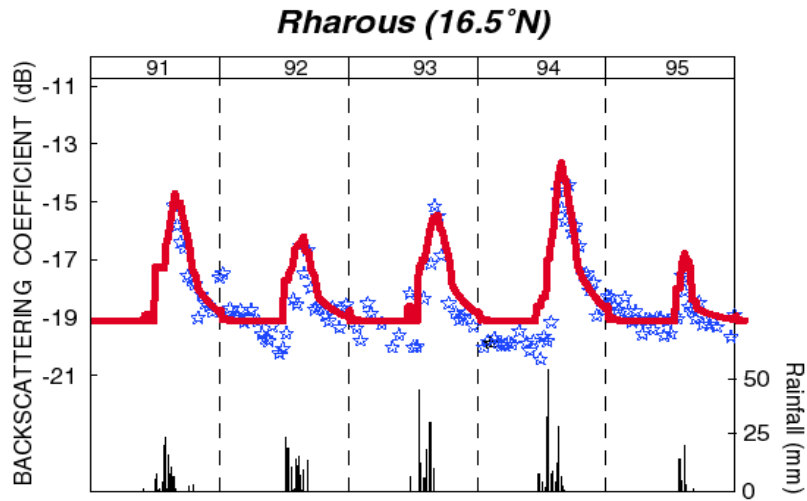
Observed scene



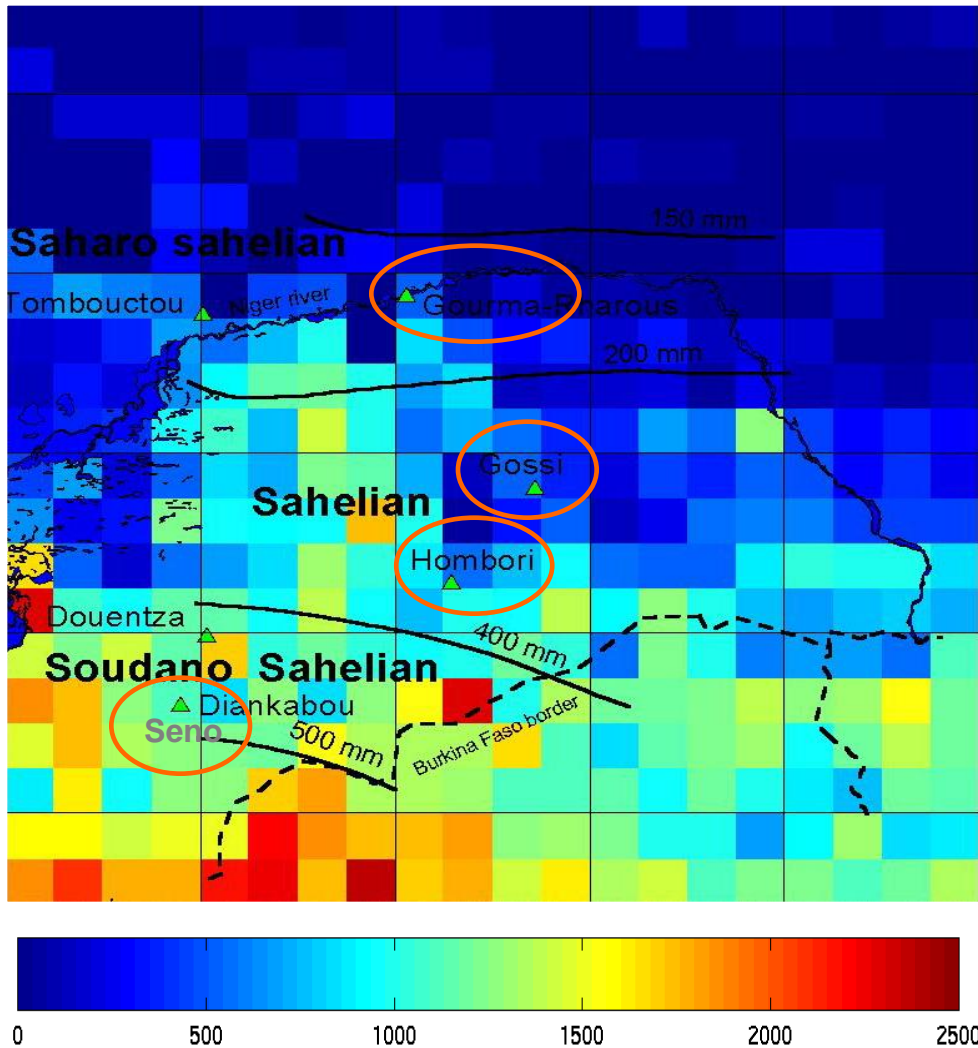
Simulated scene



Résultats de modélisation à 45°



Inversion method : *Biomass production map at a regional scale*



Biomass + soil moisture:
→ ERS WSC + METEOSAT

Validated over 4 pastoral sites
(Gourma and Seno regions)

Absolute errors:

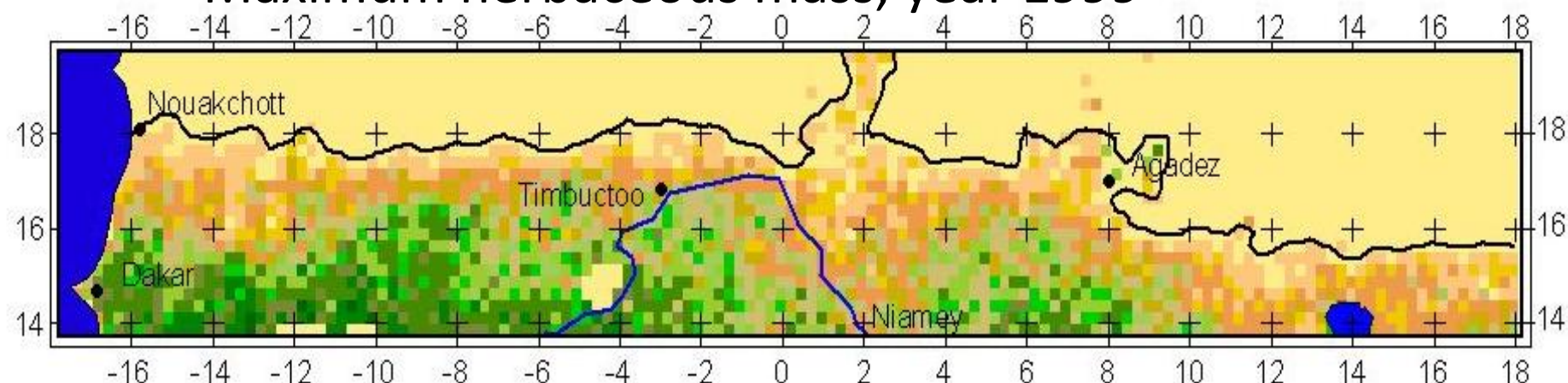
~ 200 kg DM / ha

* Relative error : 17 %

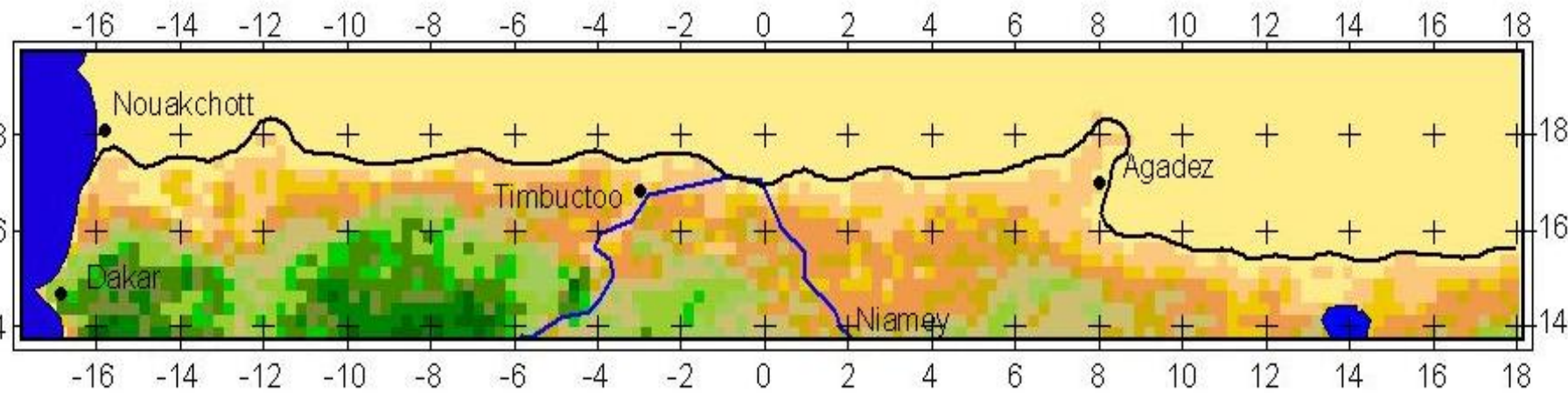
Spatialisation : Comparaison à VEGETATION/SPOT4 (2)

Maximum herbaceous mass, year 1999

ERS WSC



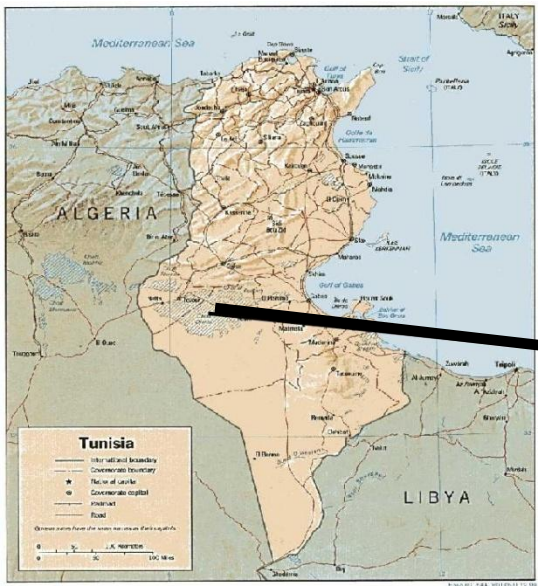
SNDVI
VEGETATION



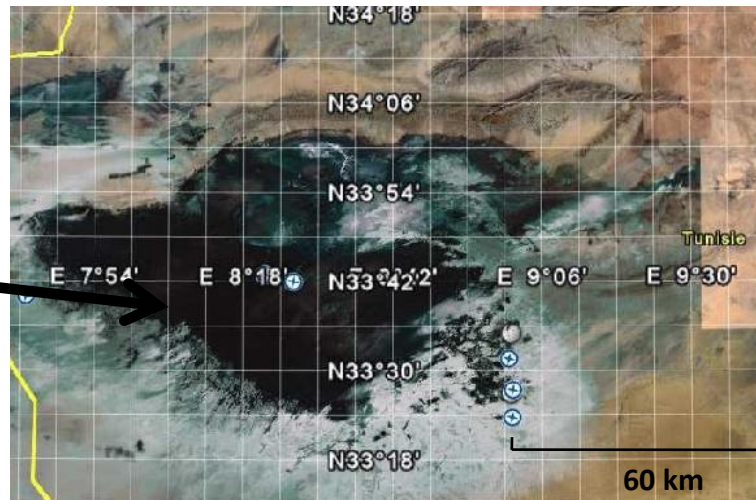
overall good agreement between both sensors

weaker values with respect to vegetation

The Chott El Jerid, Tunisia



A vast evaporitic (80 x 120 km) playas (evaporite = saline deposits)



Discharge playa from a major aquifer + occasional runoff from neighbouring playa (Fedjadj).

→ **Temporary flooding**



Flooded / dry surface

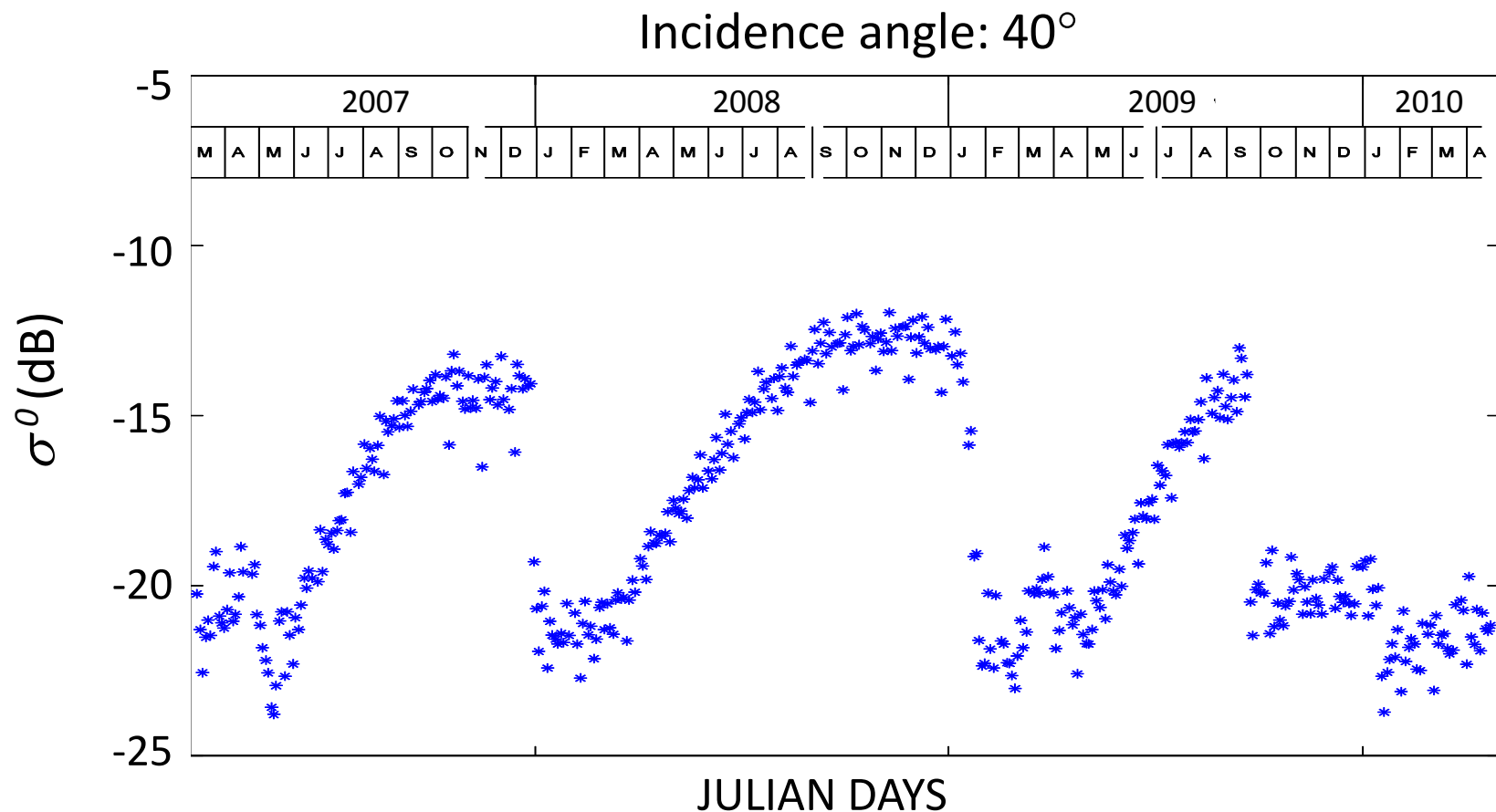
Wettest months

sudden smoothing due to dissolution of saline crust
+ dramatic change of diel. const. (saline solution)

Summer months:

evaporation → halite crystal growth → increase of roughness

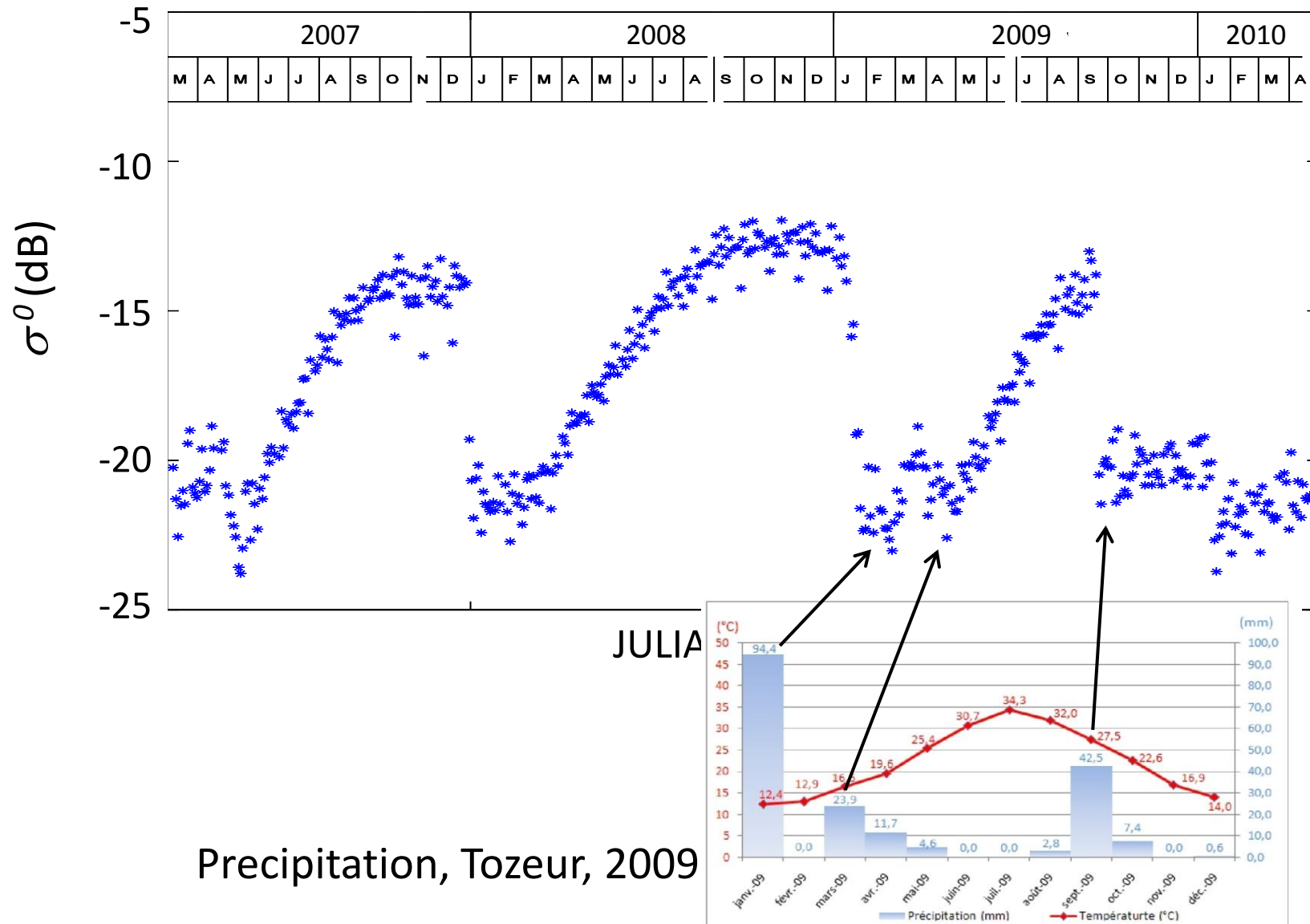
ASCAT temporal signature over the *Chott el Jerid*



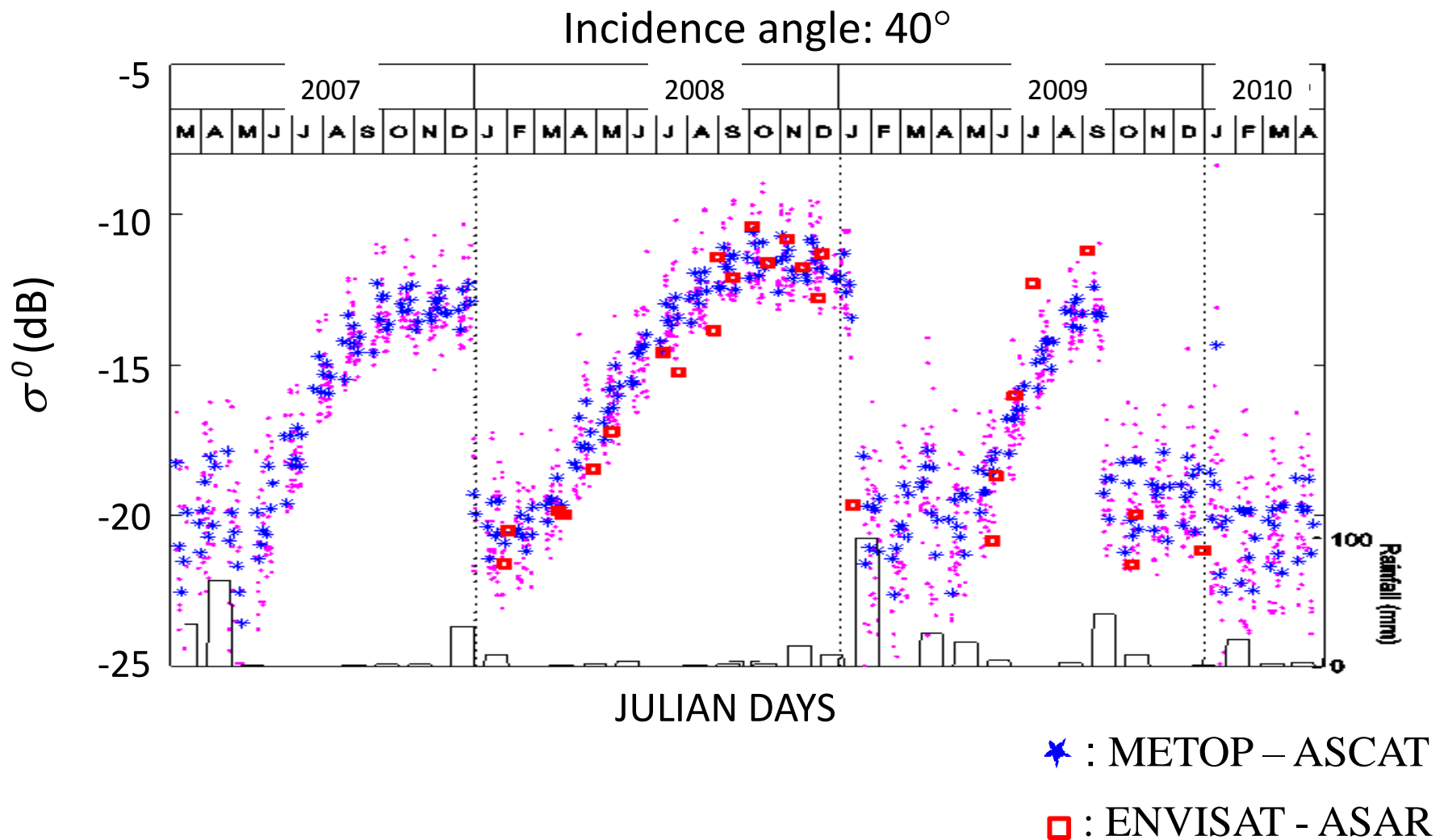
High temporal dynamic (> 10 dB)
Linked to environment seasonal variations

ASCAT temporal signature over the *Chott el Jerid*

Incidence angle: 40°

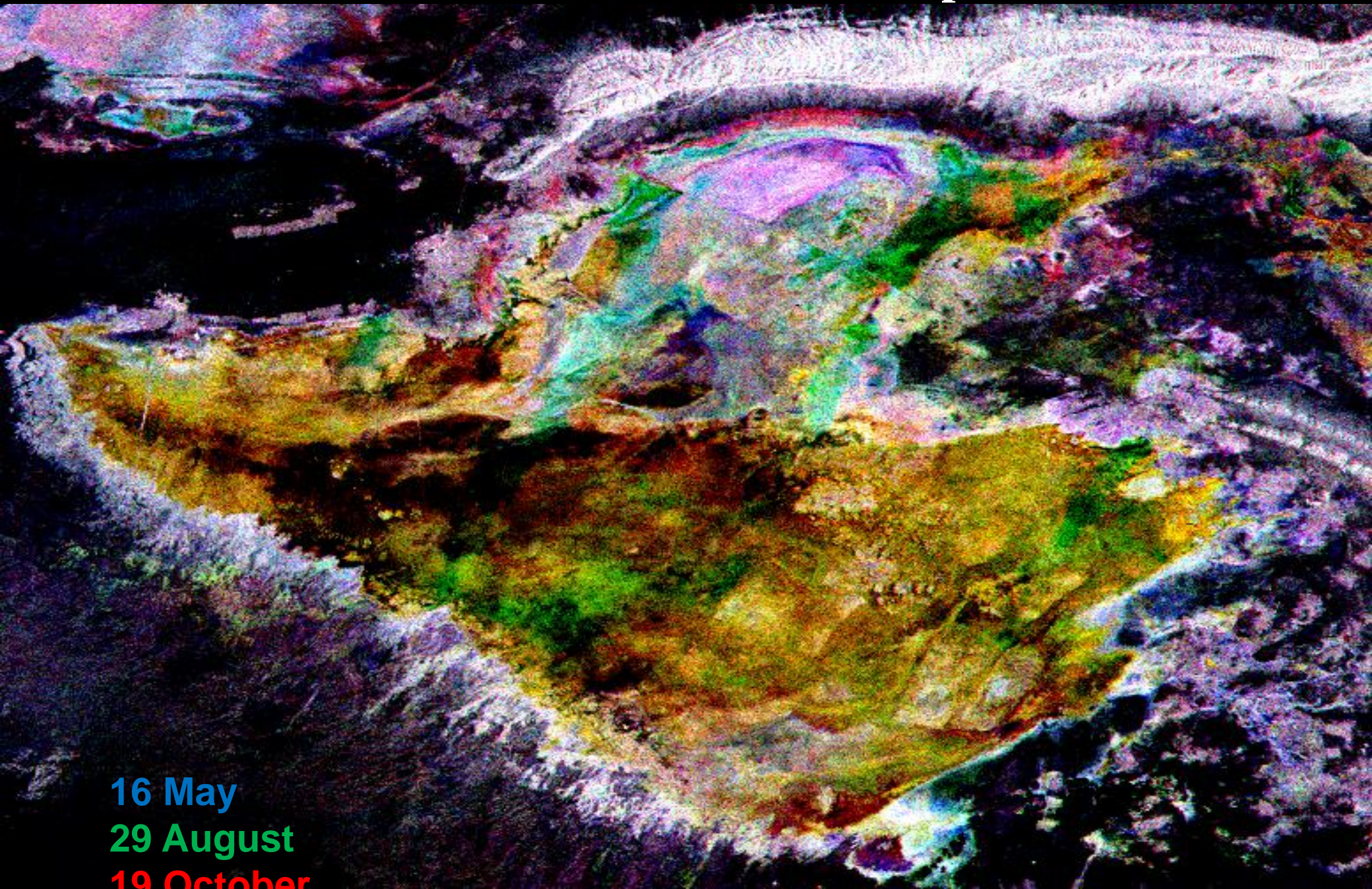


ASCAT temporal signature over the *Chott el Jerid*



Satellometer temporal frequency (< 2 days) well suited for monitoring seasonnal dynamic

ASAR – WIDE SWATH: Multidate composition (year 2009)



16 May

29 August

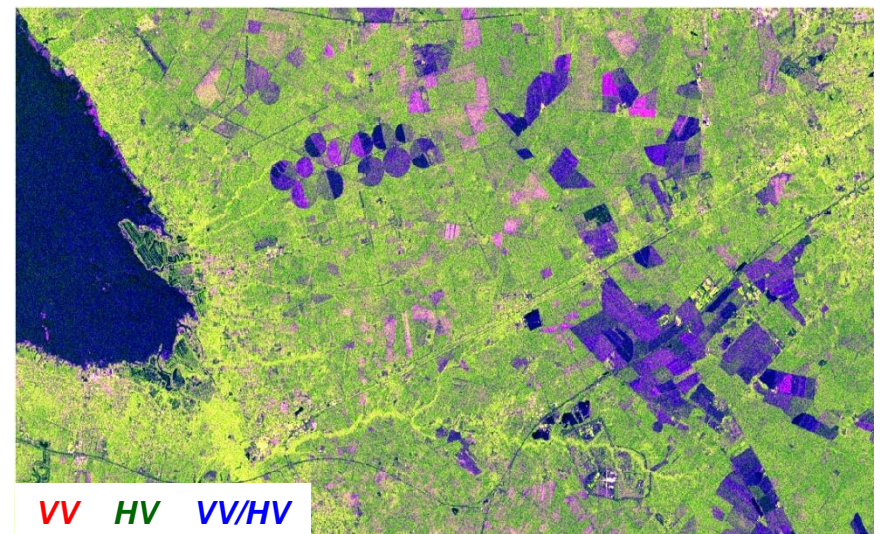
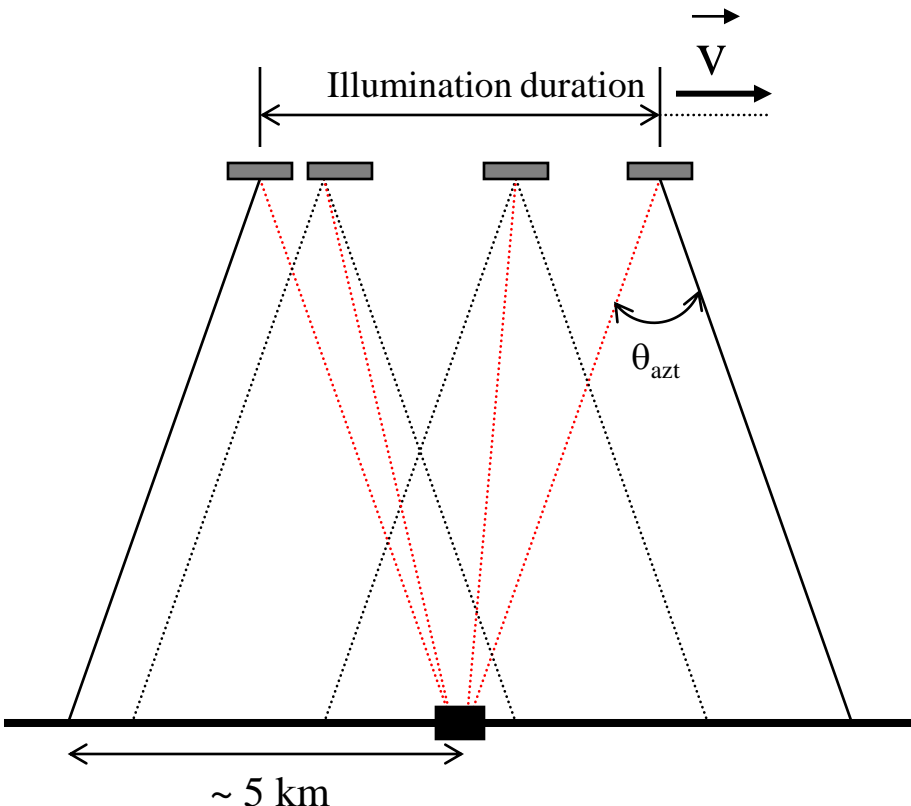
19 October

Side looking radar sensors

SAR:

☞ *surface imaging*

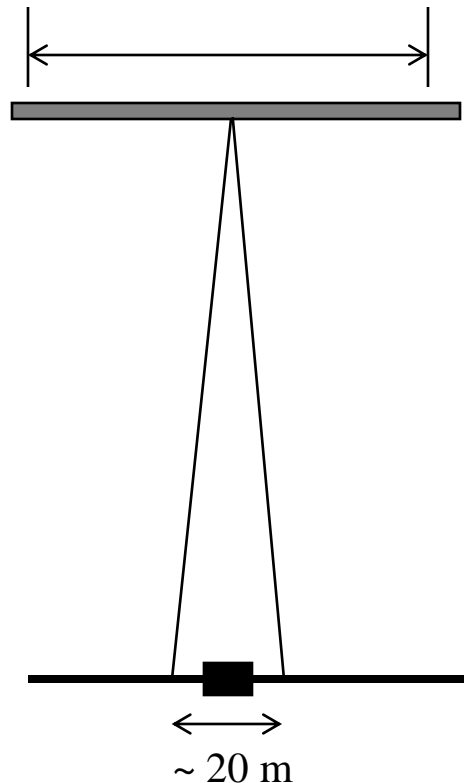
- **high spatial resolution:** $\sim 10 \text{ m}$
- **low frequency of acquisition ($\sim \text{month}$)**



Sentinel-1
Les Landes – March 2015

Side looking radar sensors

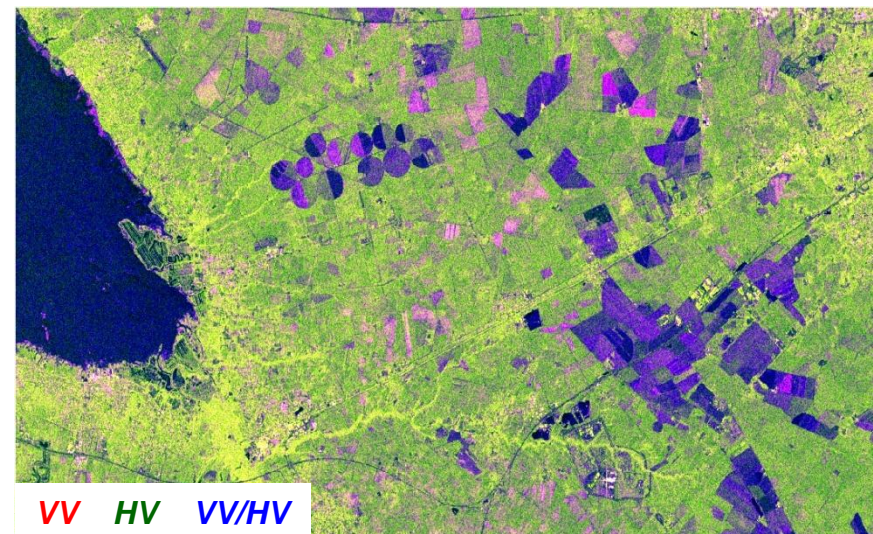
Large unique synthetic antenna



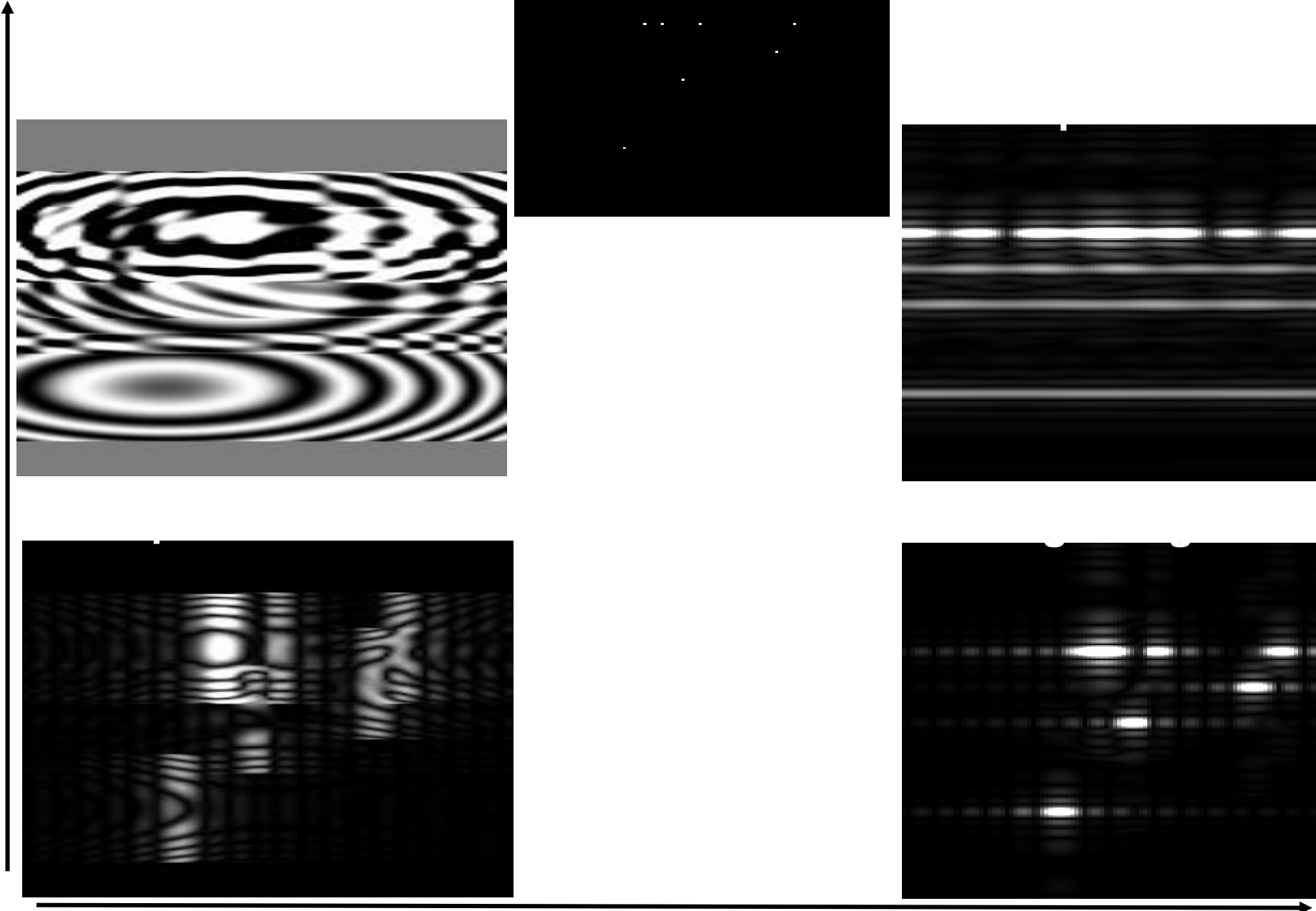
SAR:

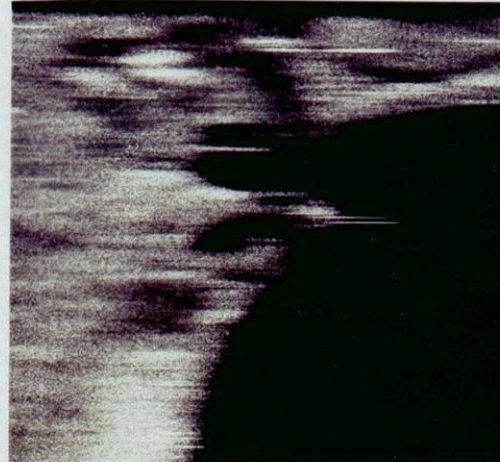
☞ *surface imaging*

- **high spatial resolution:** ~ 10 m
- **low frequency of acquisition (~ month)**



Sentinel-1
Les Landes – March 2015

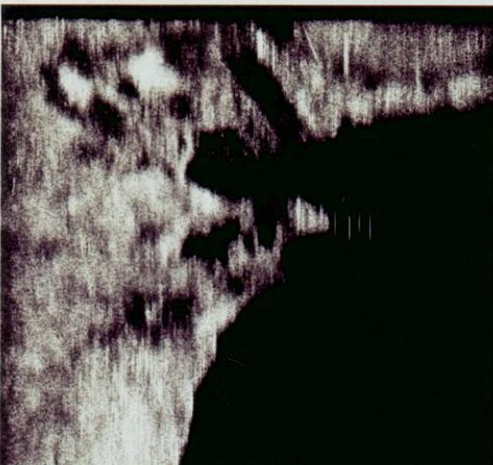




NON COMPRIME DISTANCE
NON COMPRIME AZIMUT

NON COMPRIME DISTANCE
COMPRIME AZIMUT

Document CNES



COMPRIME DISTANCE
NON COMPRIME AZIMUT

COMPRIME DISTANCE
COMPRIME AZIMUT

Frequency - wavelength

Radar band frequencies / wavelengths

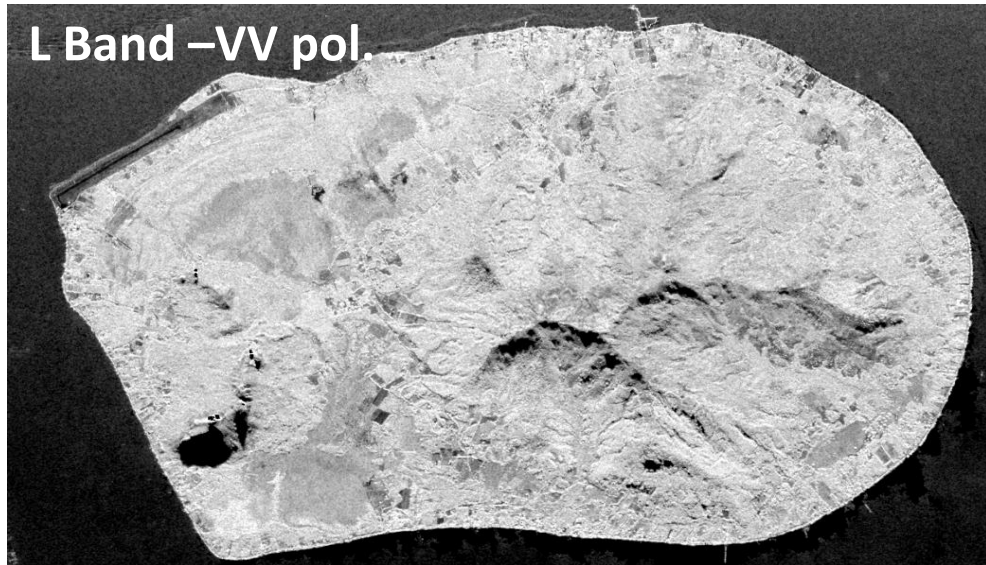
$$\lambda = c T = \frac{c}{f_0}$$

Band X	$\lambda \sim 3 \text{ cm}$	F ~10 GHz
Band C	$\lambda \sim 6 \text{ cm}$	F~5 GHz
Band L	$\lambda \sim 25 \text{ cm}$	F~1,2 GHz
Band P	$\lambda \sim 60 \text{ cm}$	F~500 MHz

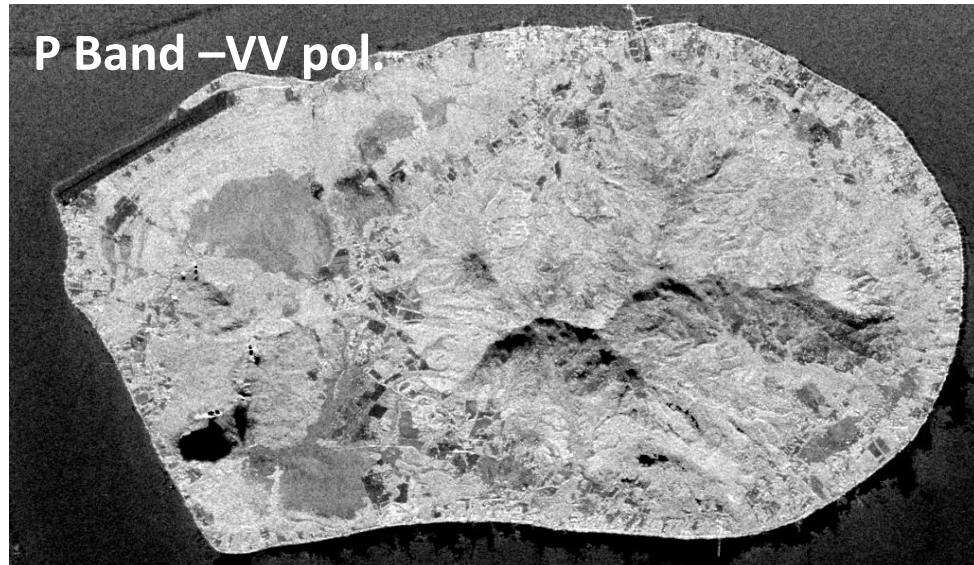
Frequency - wavelength

Tubuai Island, Vegetation discrimination

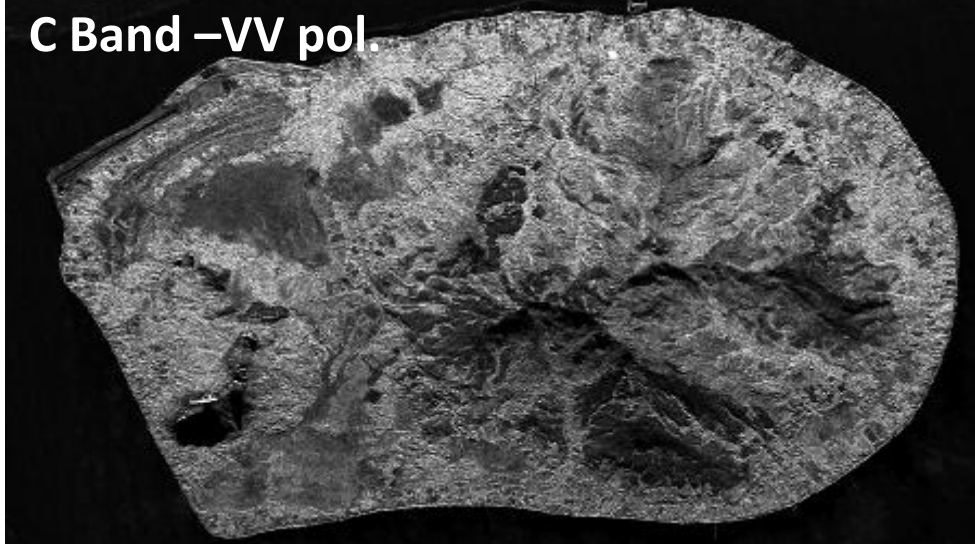
L Band –VV pol.



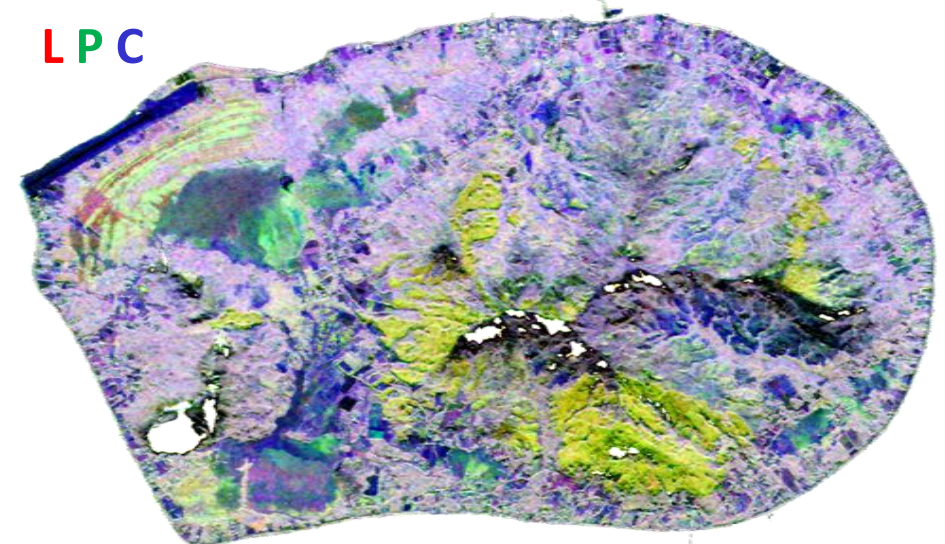
P Band –VV pol.



C Band –VV pol.



L P C



Comparison between C and L band

ASAR ($\lambda = 6 \text{ cm}$)

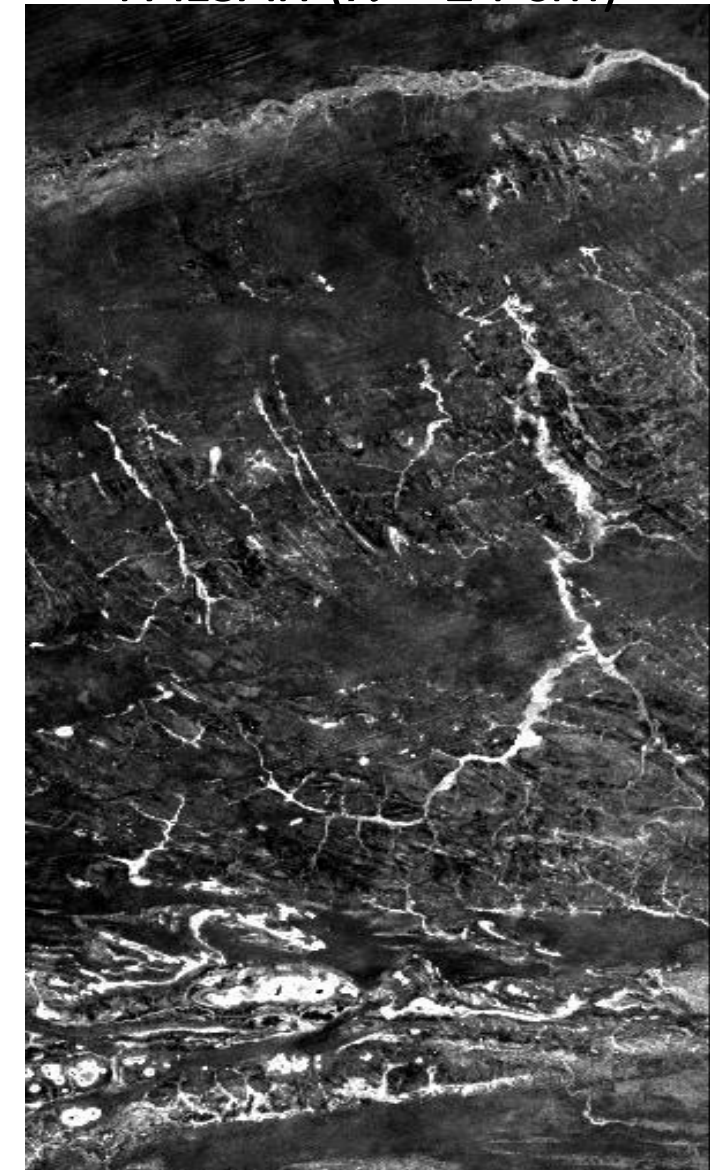


*C Band (ASAR):
Sensitive to sandy soils*

*L Band (PALSAR):
Better discrimination of
buried geological features*

Remnant of alluvial systems

PALSAR ($\lambda = 24 \text{ cm}$)

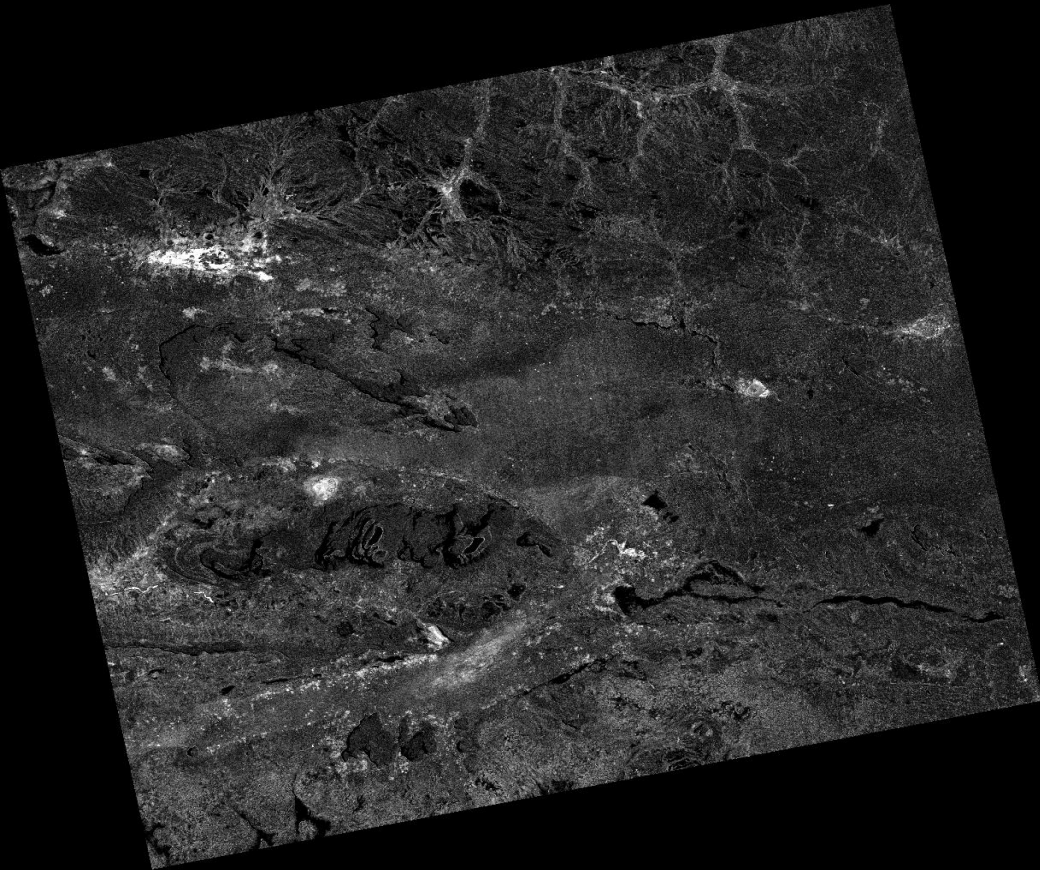


Higher penetration of L band over sandy soils

Comparison C band / L band for change detection

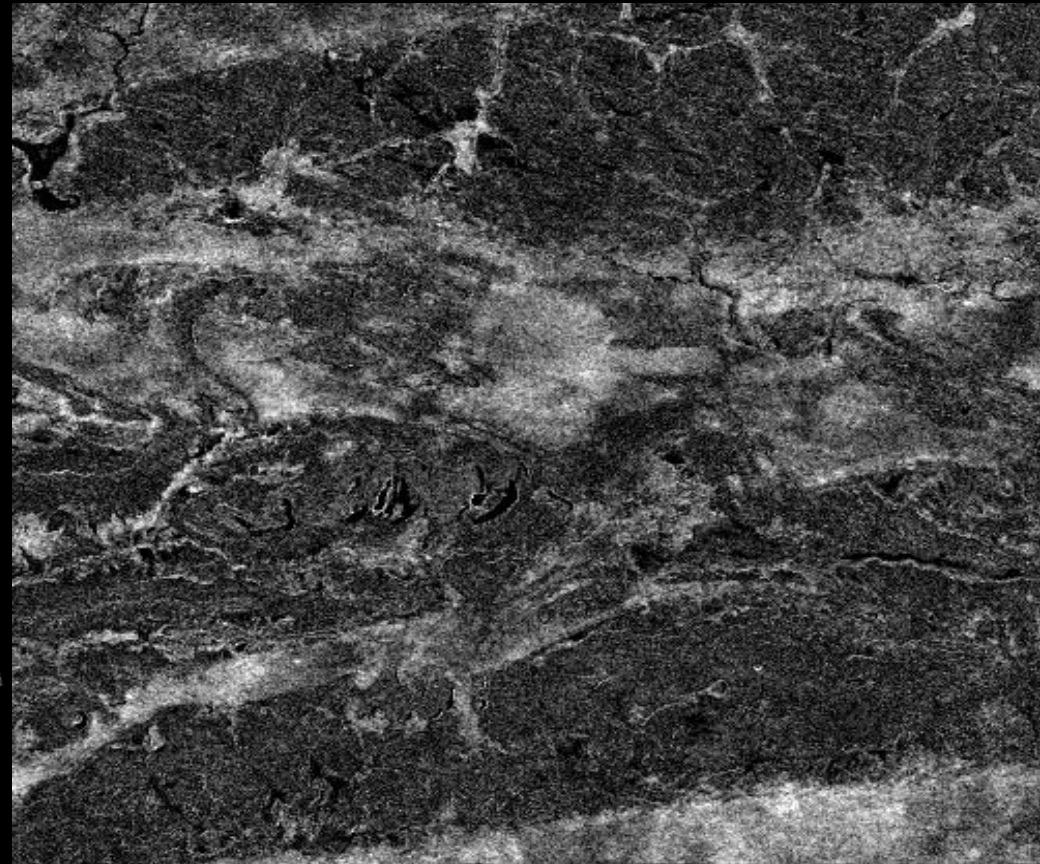
PALSAR ($\lambda = 24$ cm)

12 images: Jan. 2007 – avr. 2009



ASAR ($\lambda = 6$ cm)

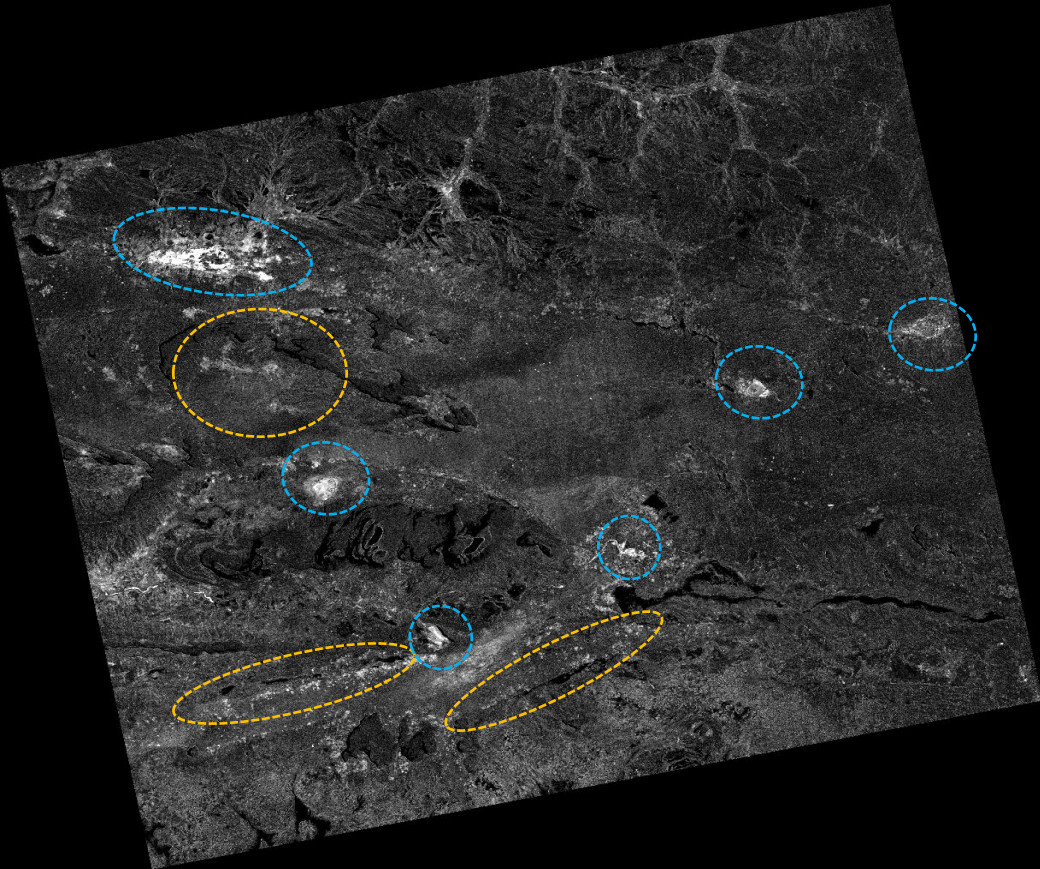
5 images: Jul. 2005 – Dec. 2005



Comparison C band / L band for change detection

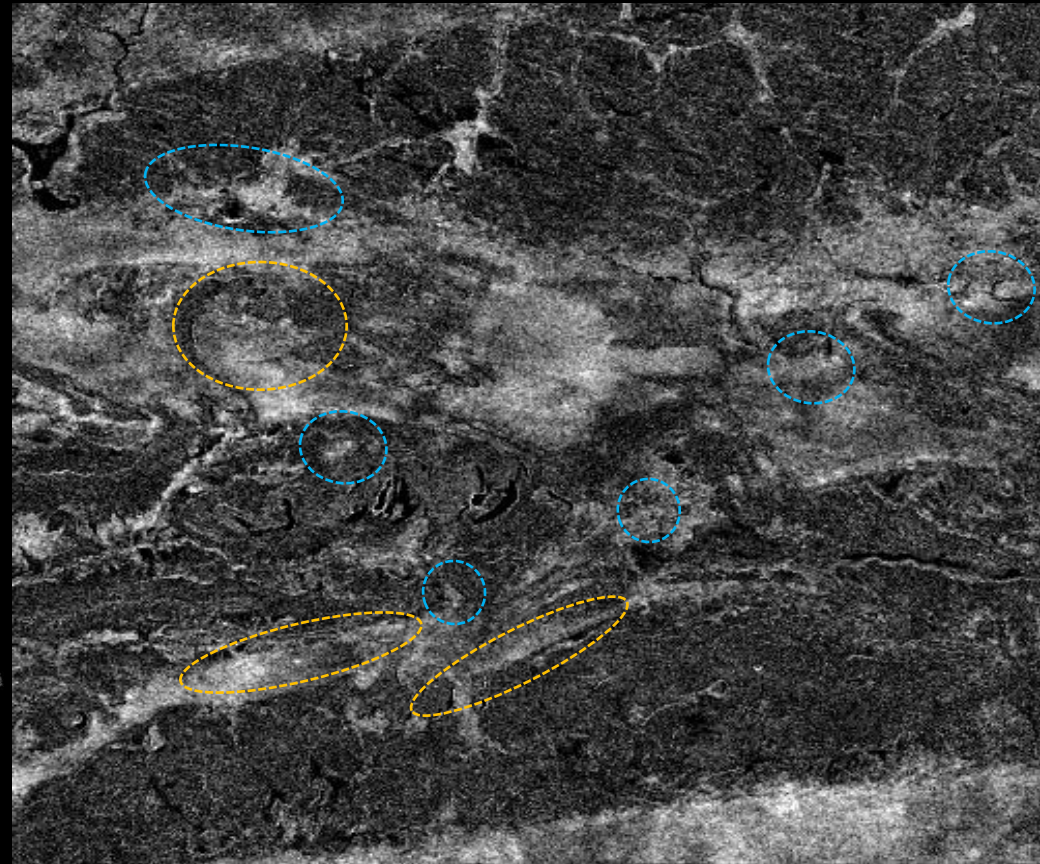
PALSAR ($\lambda = 24$ cm)

12 images: Jan. 2007 – avr. 2009



ASAR ($\lambda = 6$ cm)

5 images: Jul. 2005 – Dec. 2005



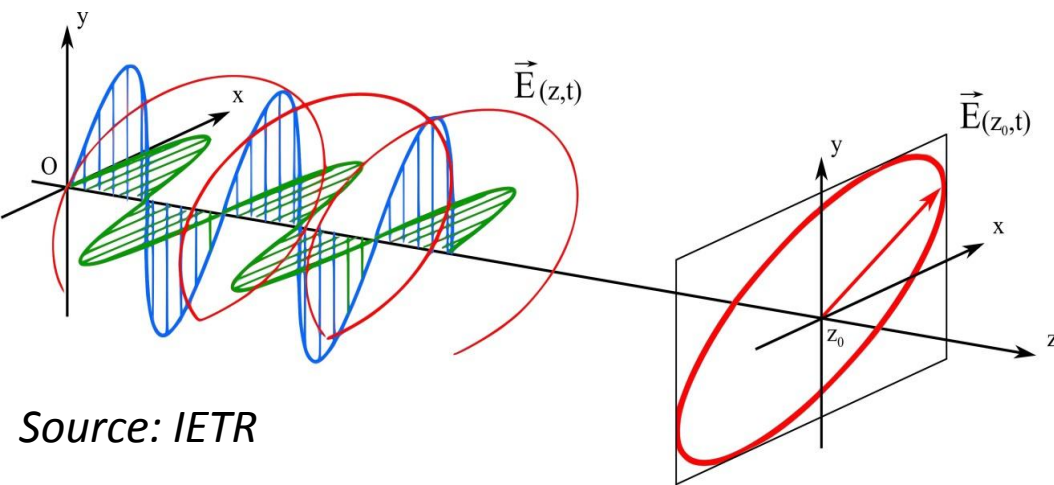
High penetration over sandy soils
changes over **water ponds**
+ **millet fields**

Low penetration over sandy soils
changes due to surface states variations
+ **water ponds**

Polarization

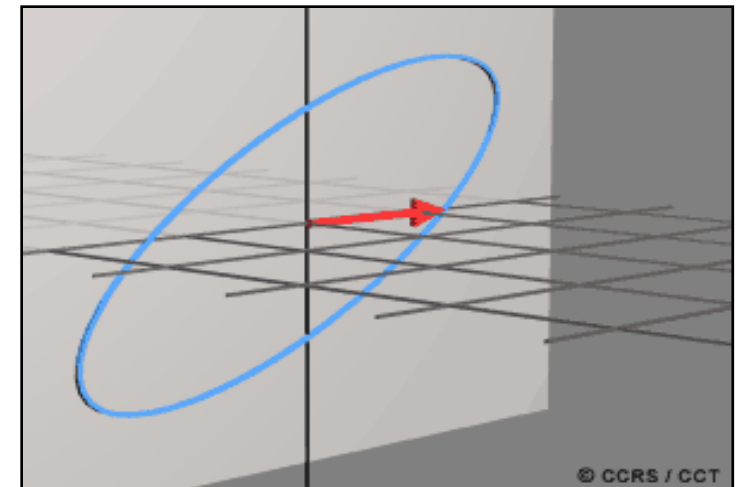
Important characteristics of coherent EMW:

Electromagnetic field evolution is predictable



Source: IETR

Most general: *Elliptical polarization*



© CCRS / CCT

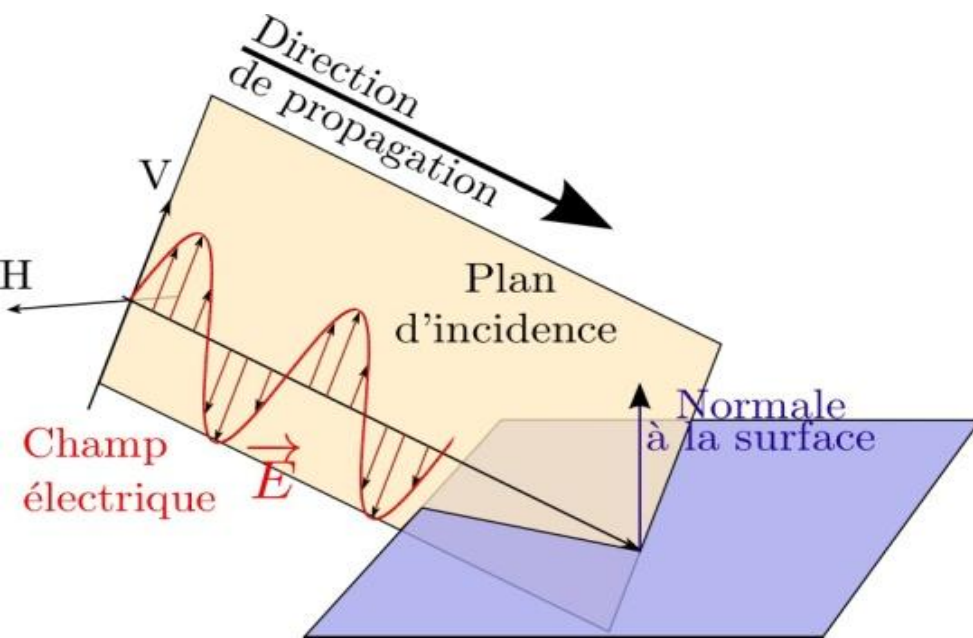
Polarization

Radar :

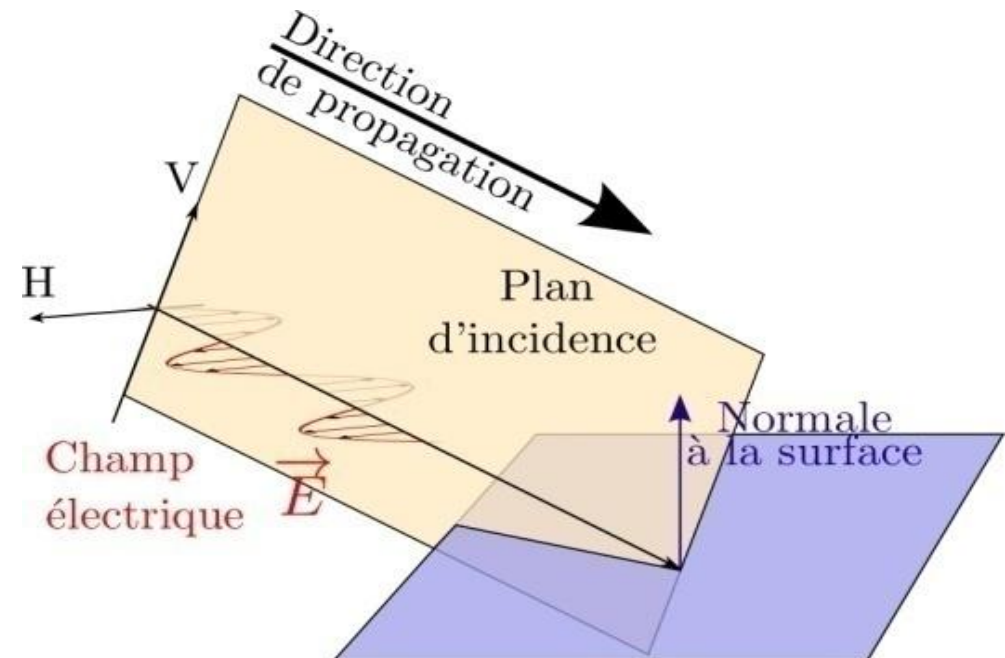
transmits a EMW in a given polarization

measures the backscattered wave contribution in a given polarization

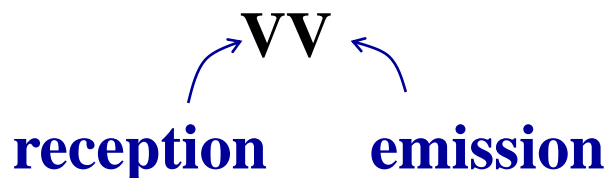
Vertical polarization



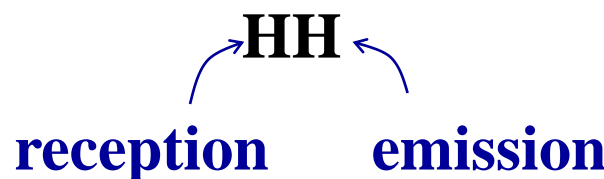
horizontal polarization



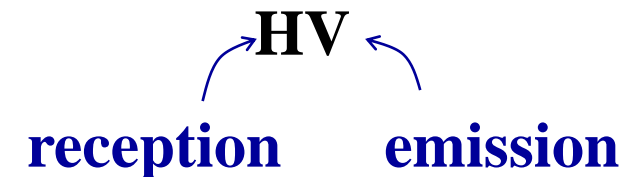
Polarization characterisation of a radar acquisition:



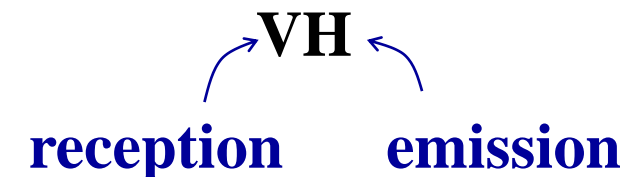
ERS, ASAR



JERS, RADARSAT, PALSAR

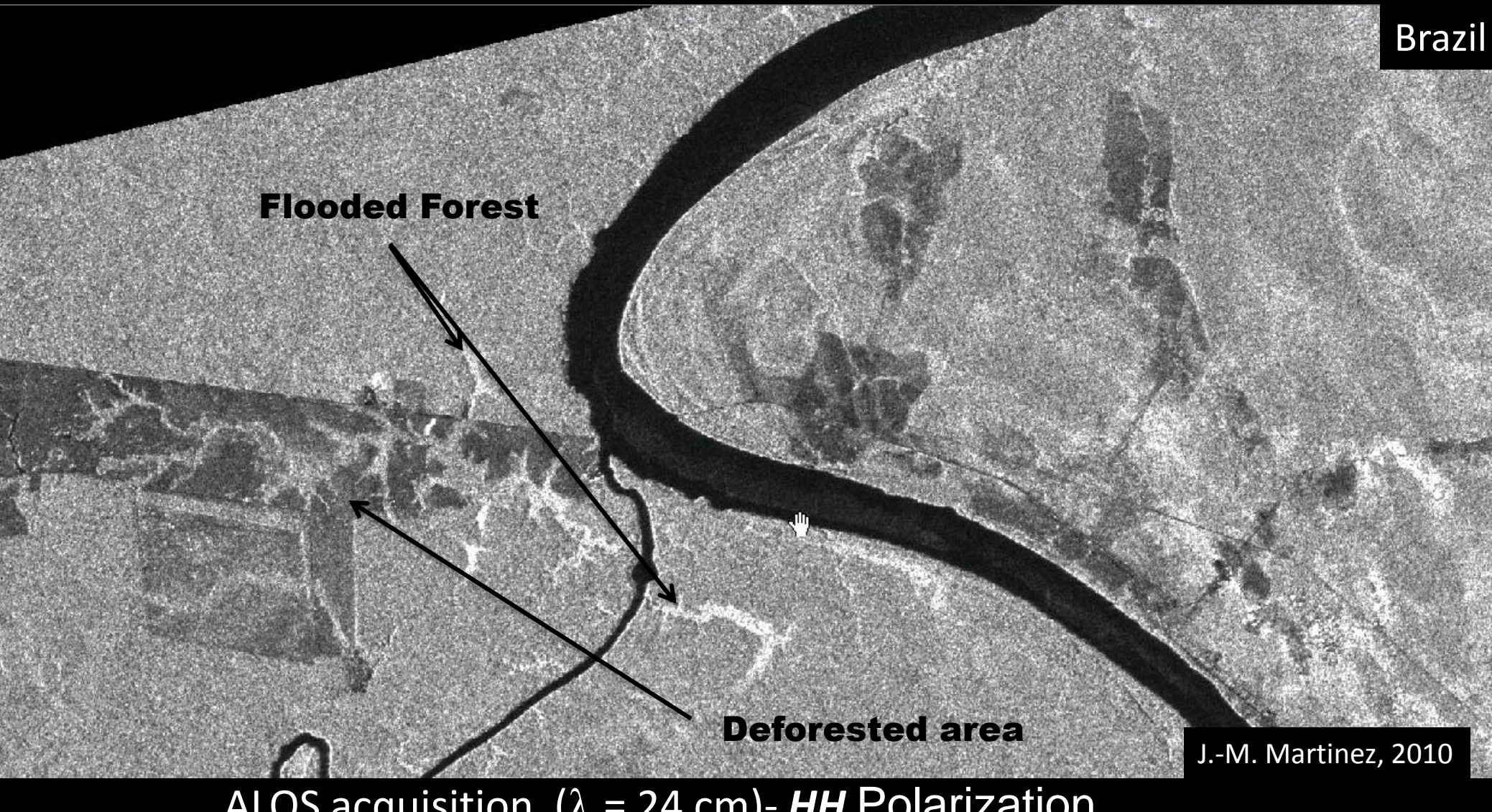


ASAR, PALSAR



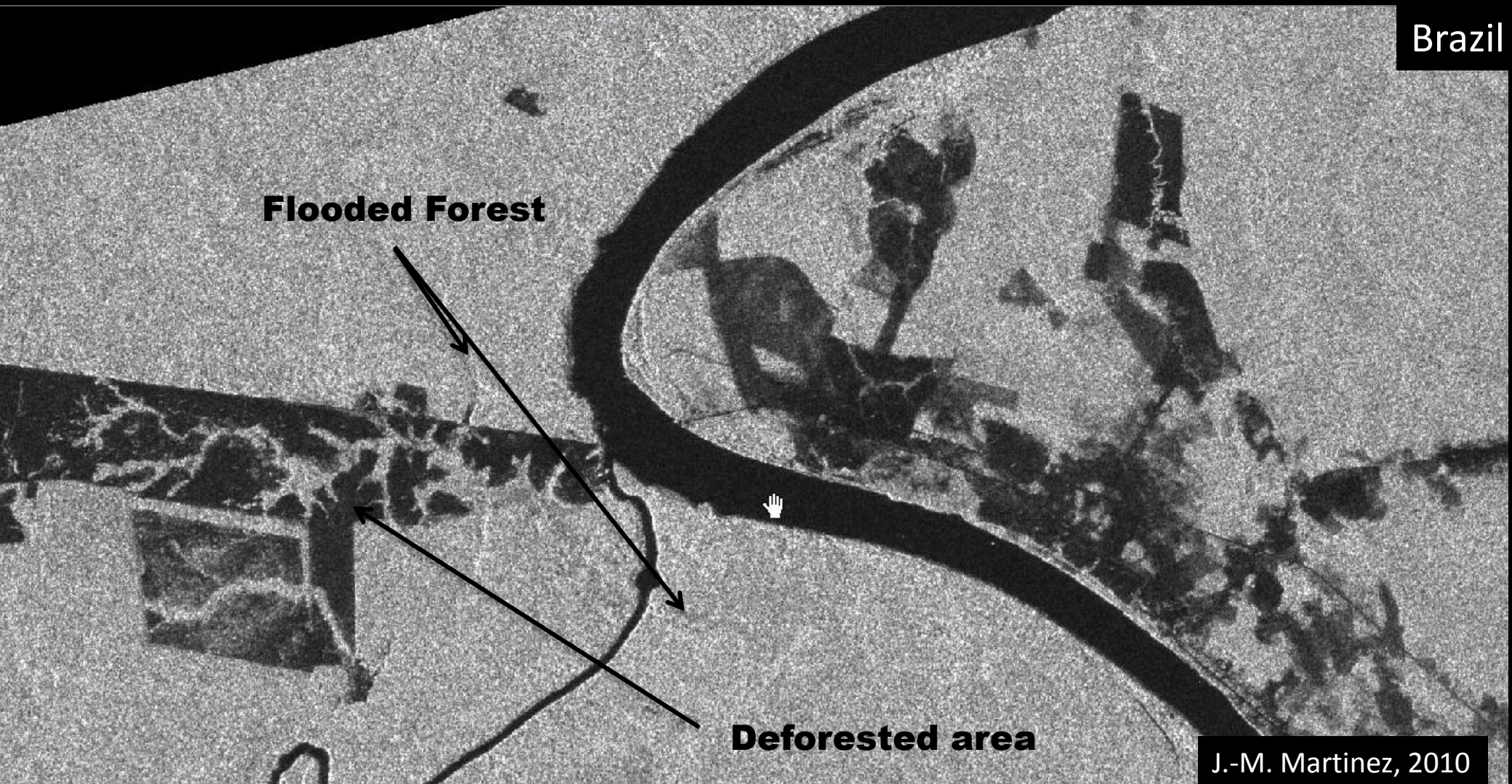
ASAR, PALSAR

Polarization



J.-M. Martinez, 2010

Polarization



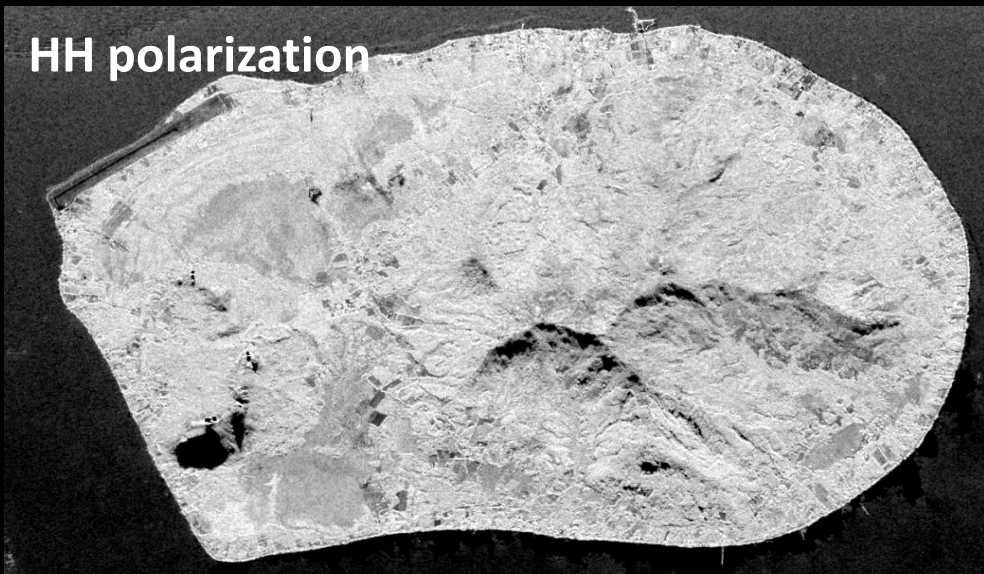
ALOS acquisition ($\lambda = 24 \text{ cm}$)- **HV** Polarization

J.-M. Martinez, 2010

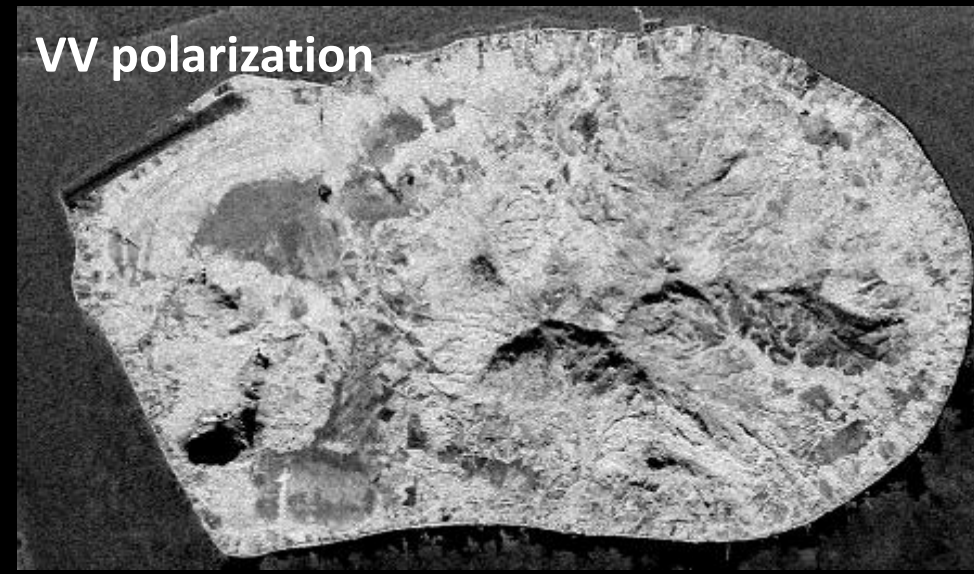
Polarization

Tubuai Island, vegetation discrimination, L Band

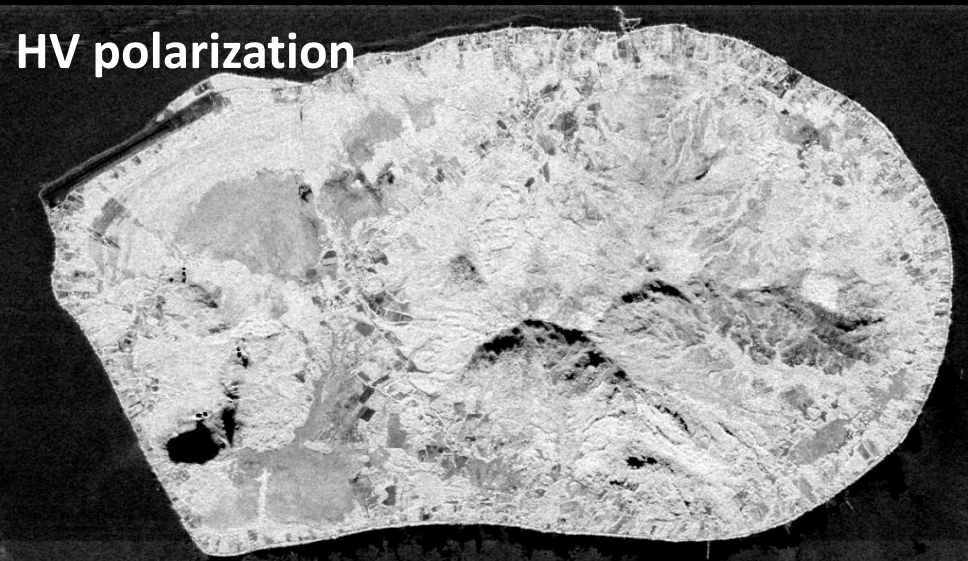
HH polarization



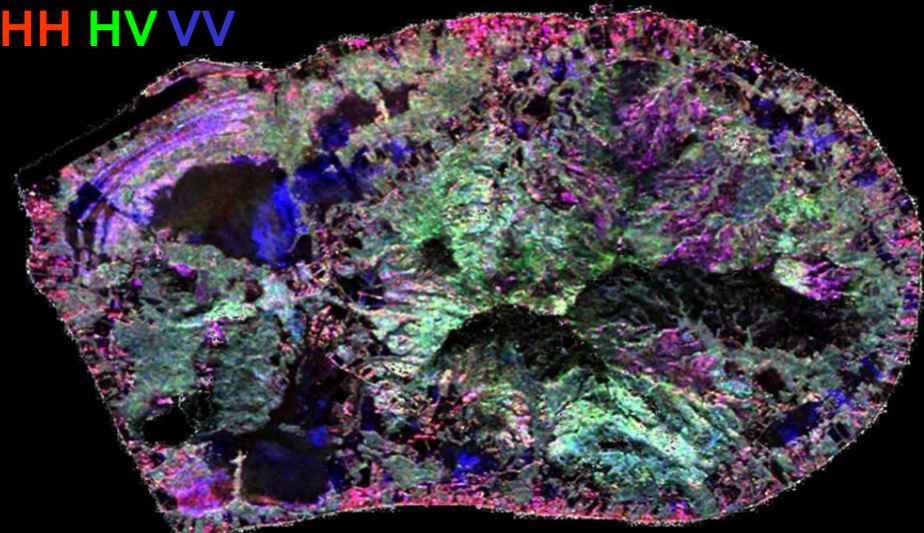
VV polarization



HV polarization



HH HV VV

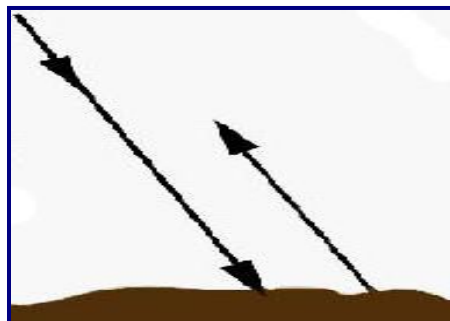


SAR polarimetry for vegetation cartography

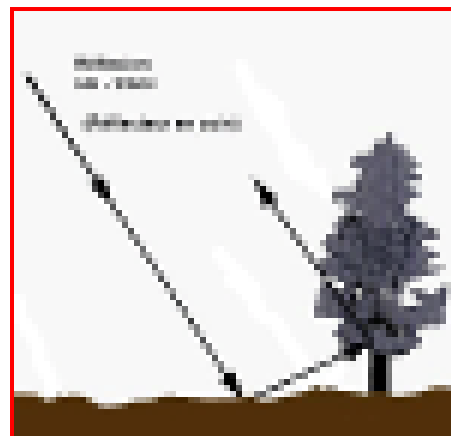
Radar polarimetry:

sensitive to ***scattering mechanisms*** within a resolution cell

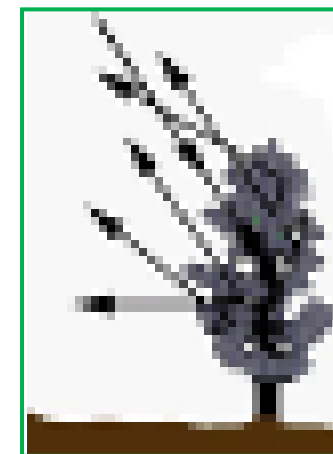
=> Sensitive to ***vegetation geometrical structure***



Surface scattering (bare soil)



Double bounds (flooded vegetation or urban areas)



Volume scattering (dense vegetation)

SAR polarimetry for vegetation cartography

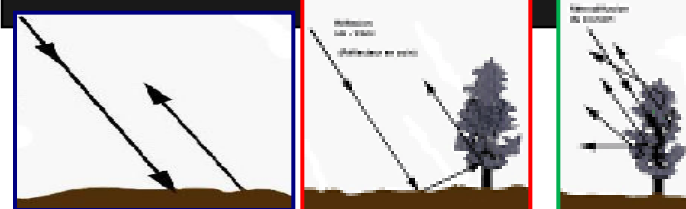
Île de Tubuai, Polynésie française



Quickbird



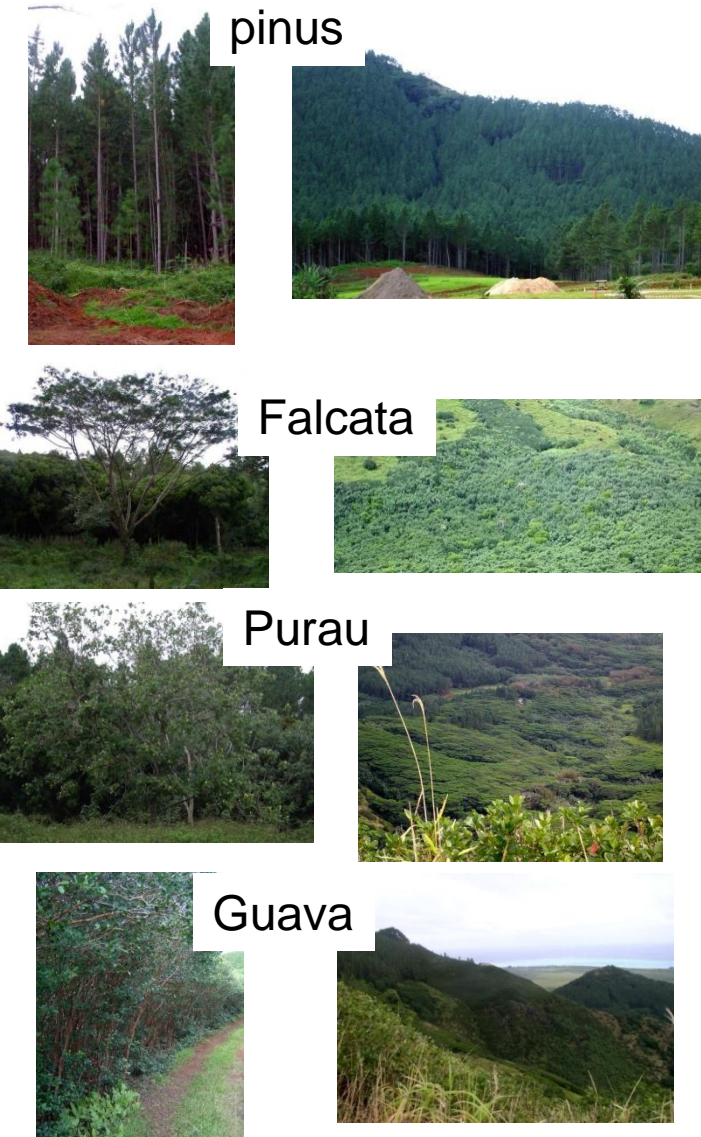
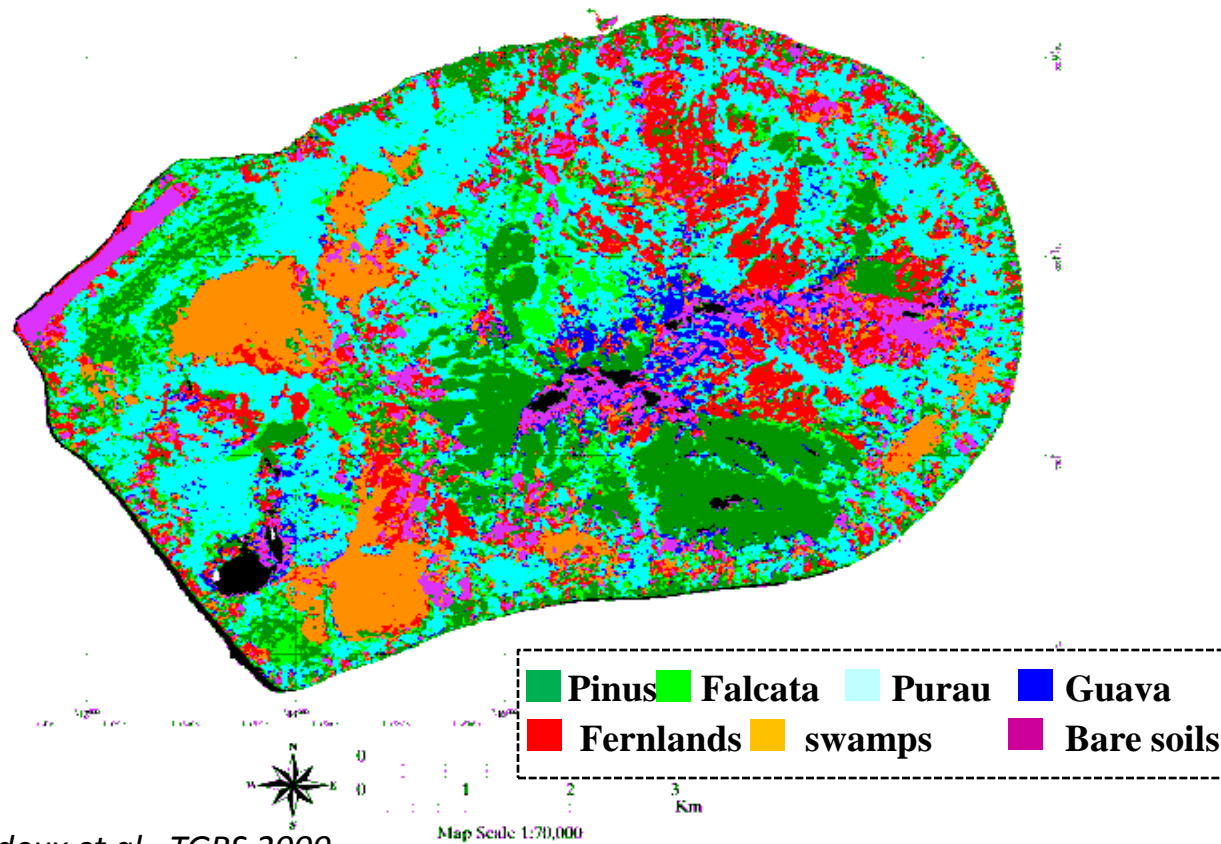
AIRSAR, bande L
Août 2004



SAR polarimetry for vegetation cartography

Classification polarimetric data

Tubuai Island - AIRSAR data



☞ REDD+ ==> collaborations ONF -International

The Sentinel-1 missions

Sentinel-1A: launched the 3rd April 2014

==> SAR data from March 2015

Revisit time: 12 days

Sentinel-1B: launched the 22th April 2016

==> SAR data from September 2016

Revisit time: 12 days

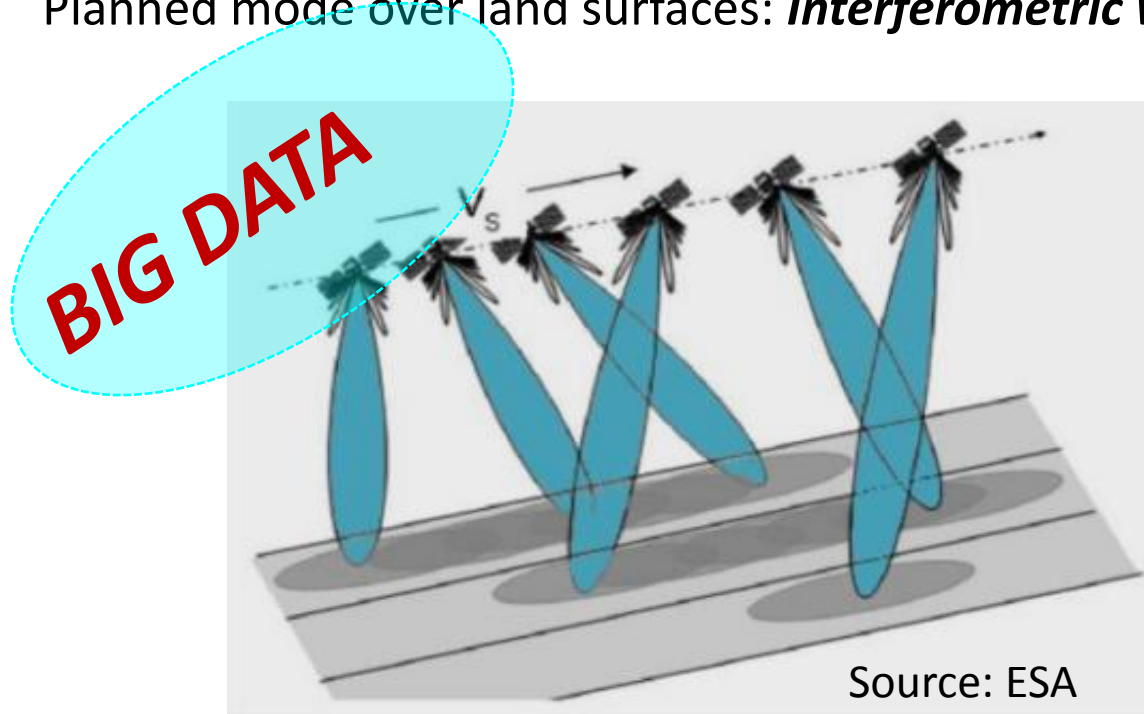
- C band
- Spatial resolution: 20 m
- Swath width: 250 km
- Two polarizations over land surfaces: VV and VH

6 days!!

SAR ← → SENTINEL-1 ← → Scatterometers

Acquisitions period: **12 days** (S1-A) – **6 days** (S1- A+B)

Planned mode over land surfaces: ***Interferometric Wide (IW)***



2 Polarisations: **$VV - VH$**

Swath: 250 km (3 sub-swaths)

GRD Products :

Spatial resolution: **20 m**

Pixel: 10 m

SLC Products

Spatial resolution: 3 x 20 m;

Pixel: 2 x 14 m (rge x az.)

Temporal monitoring of seasonal variations of land surfaces

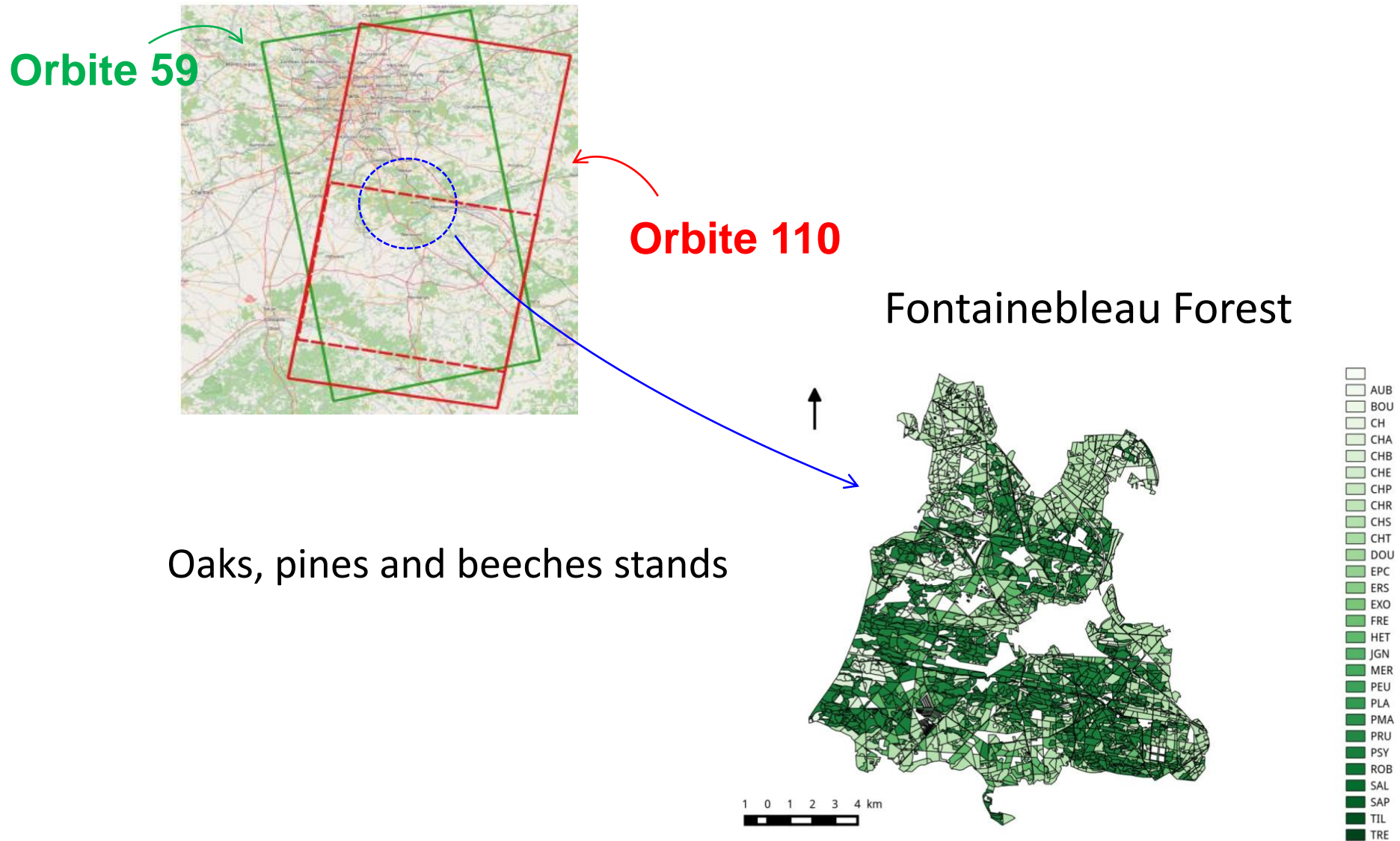
Radar Backscattering Coefficient

$$\sigma^0$$

Interferometric Coherence

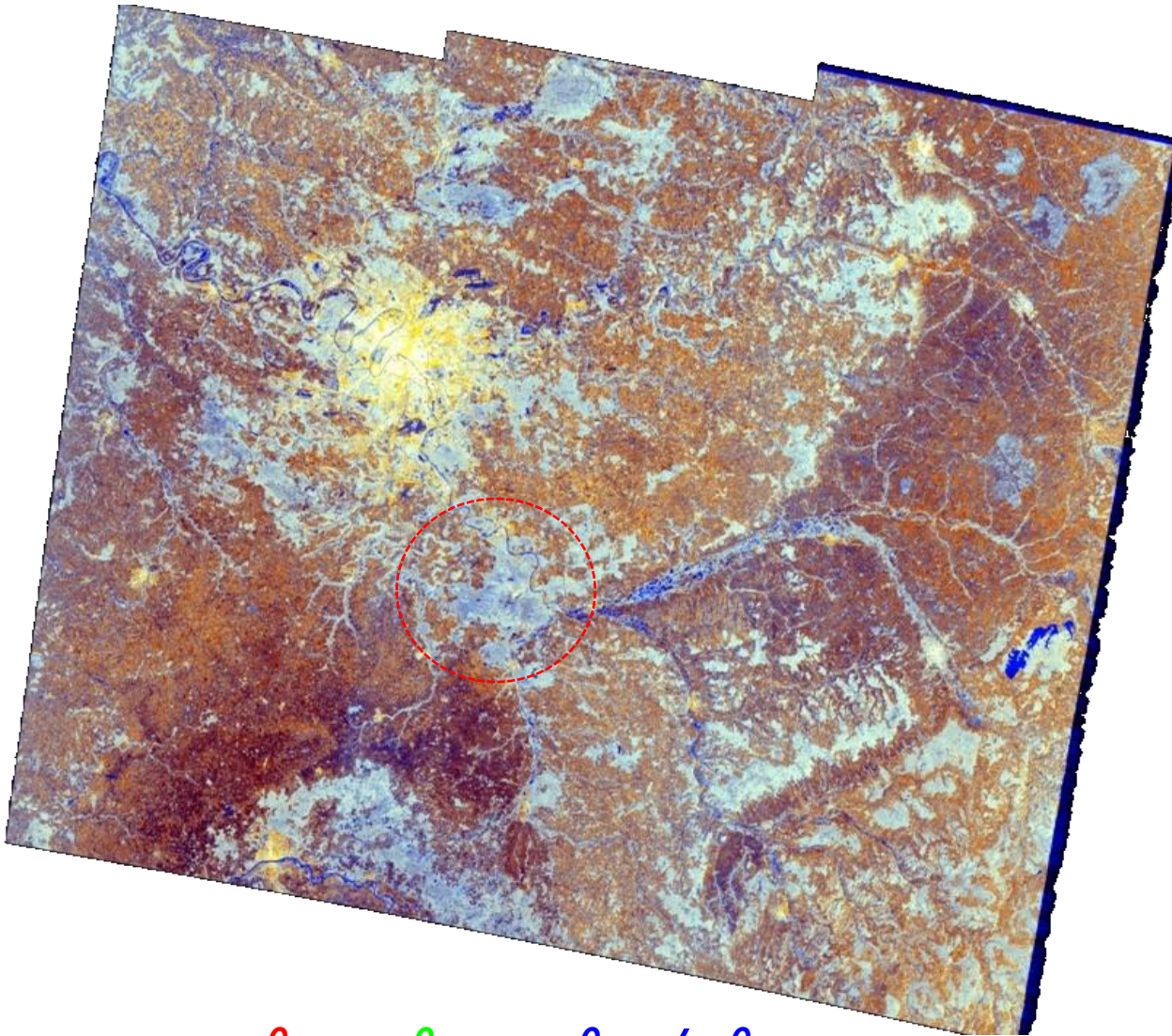
$$|\rho|$$

Acquisitions over the Paris region



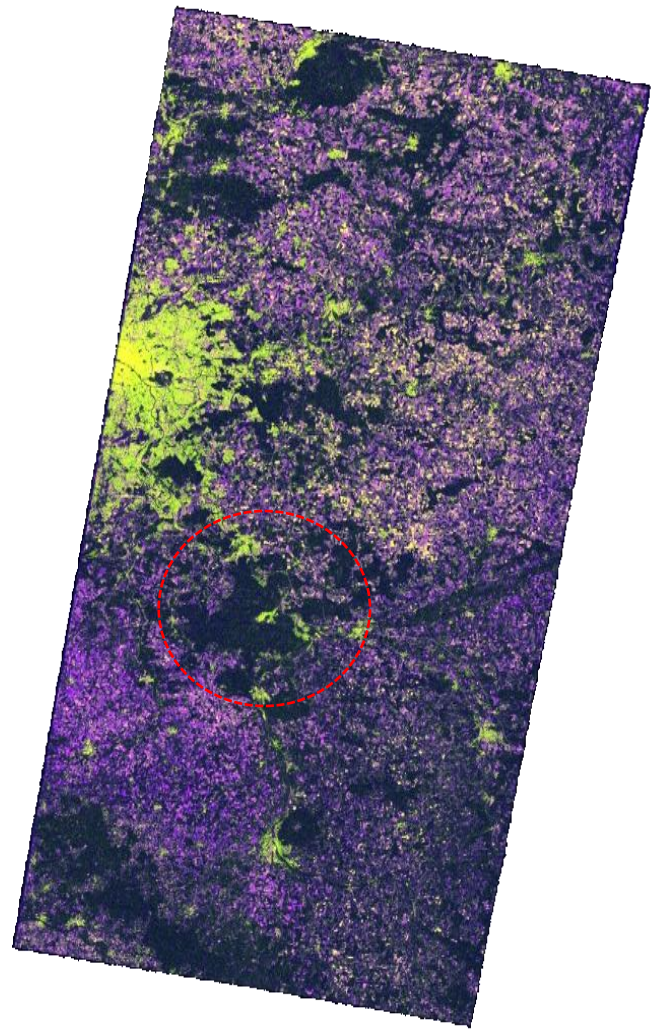
18th March 2015 IW Acquisition

Radar reflectivity (σ^0) image



σ^0_{VV} σ^0_{VH} $\sigma^0_{VH} / \sigma^0_{VV}$

18 – 30 March coherence image

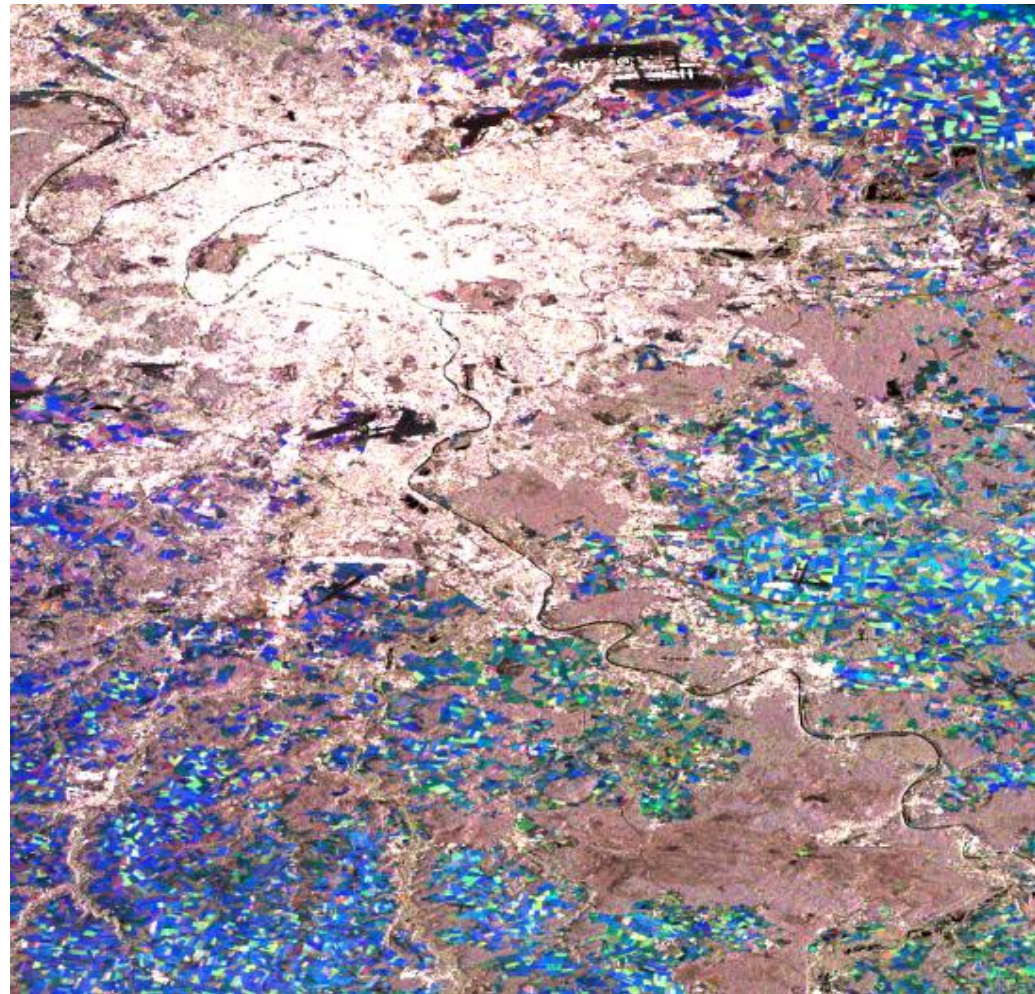


$|\rho_{VV}|$ $|\rho_{VH}|$ $\rho_{VV} / |\rho_{VH}|$

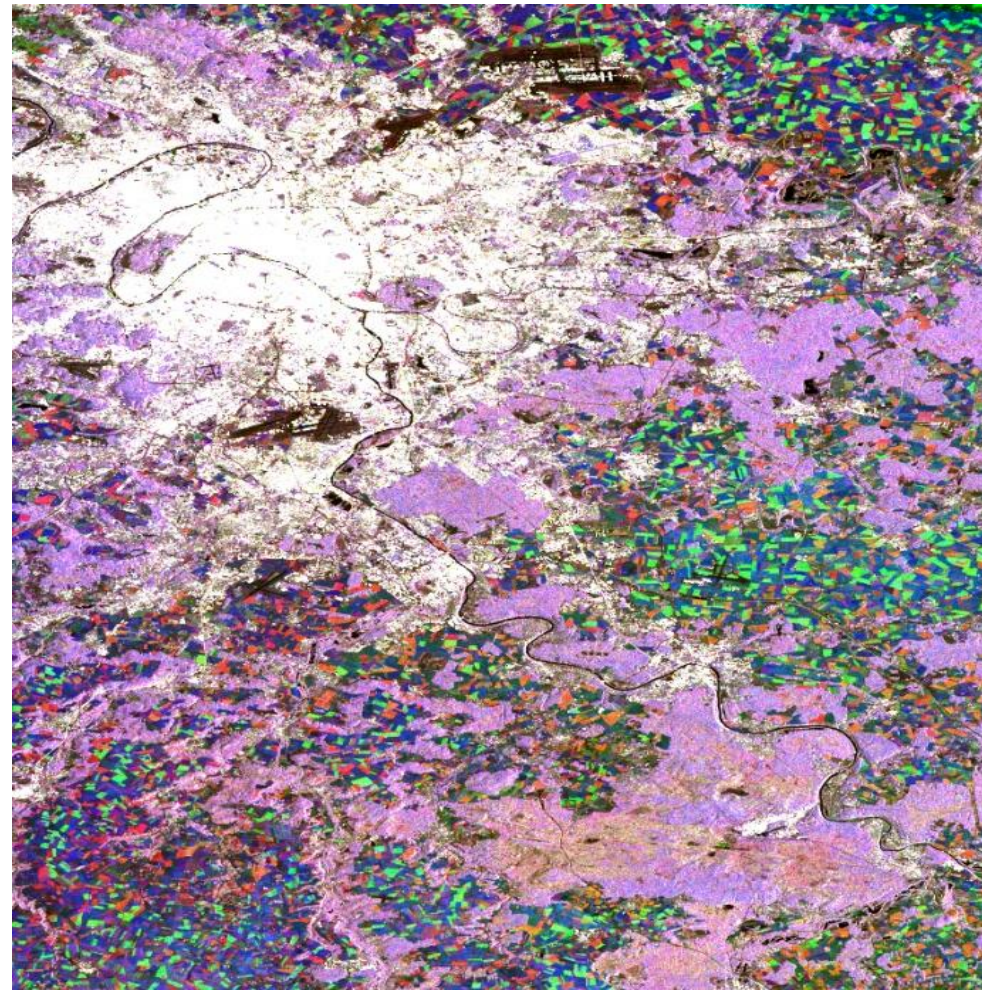
σ^0 Color composite image

5 May - 2 Sept. - 19 Dec. 2015

Polarisation VV



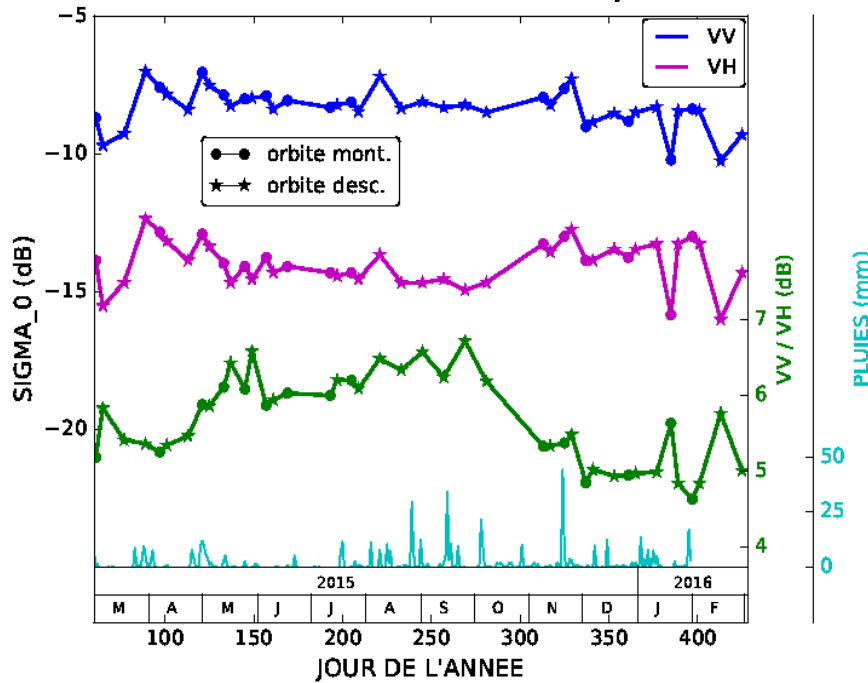
Polarisation VH



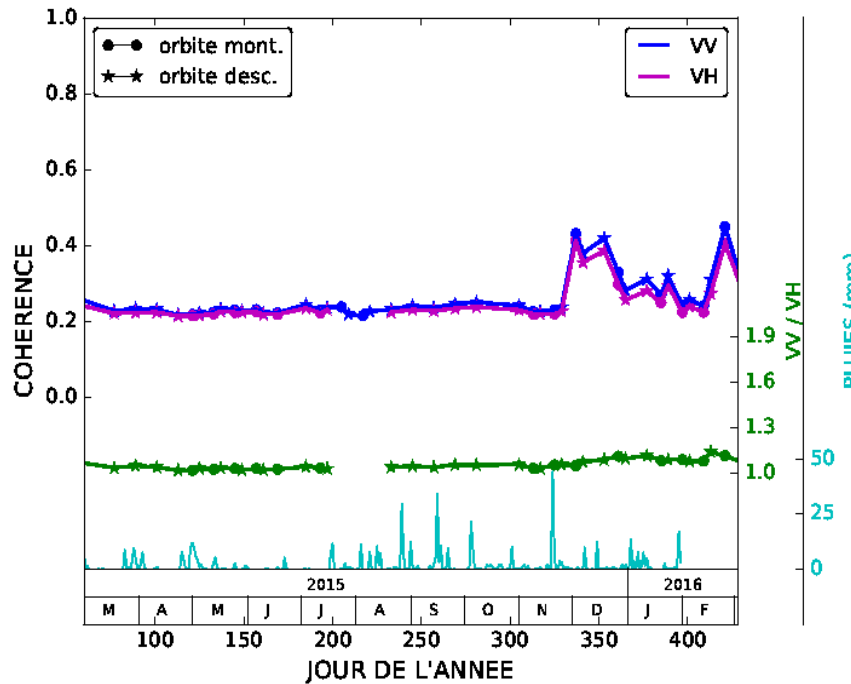
⌚ High spatio-temporal variability over crop fields

Fontainebleau Forest

Radar reflectivity



coherence



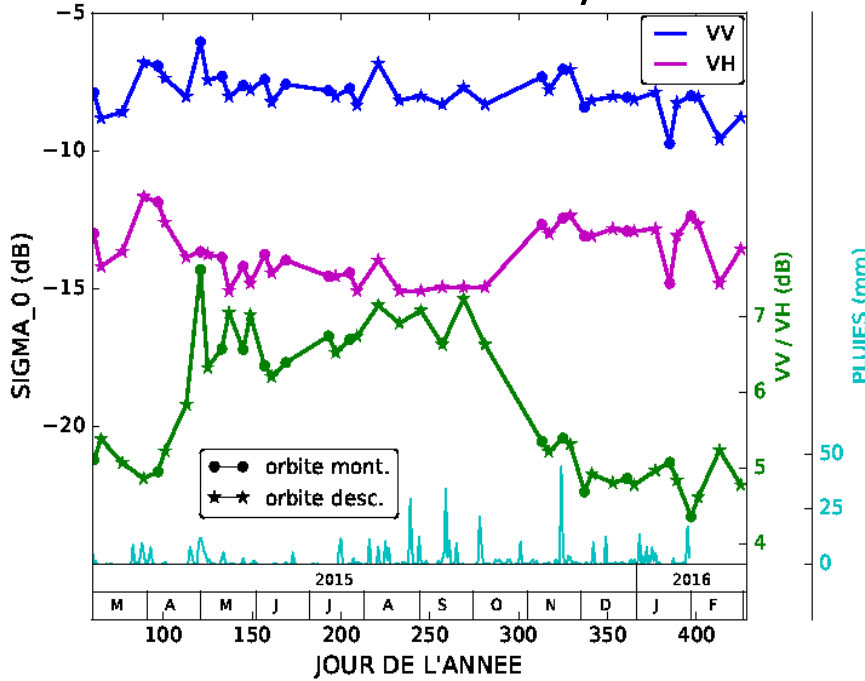
- No seasonal cycle σ^0_{VV}
- seasonal cycle $\sigma^0_{VH} \Rightarrow \sigma^0_{VV} / \sigma^0_{VH}$

- signal low and constant (Mars-Nov.)
- $|\rho_{VV}|$ et $|\rho_{VH}|$ identical

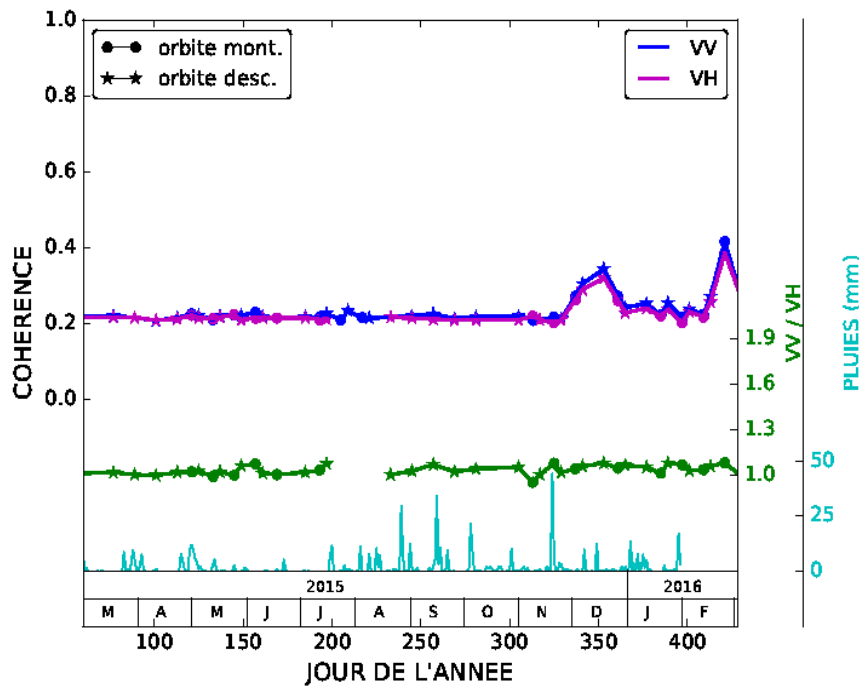
Low correlation with precipitations

Oaks stand

Radar reflectivity



coherence



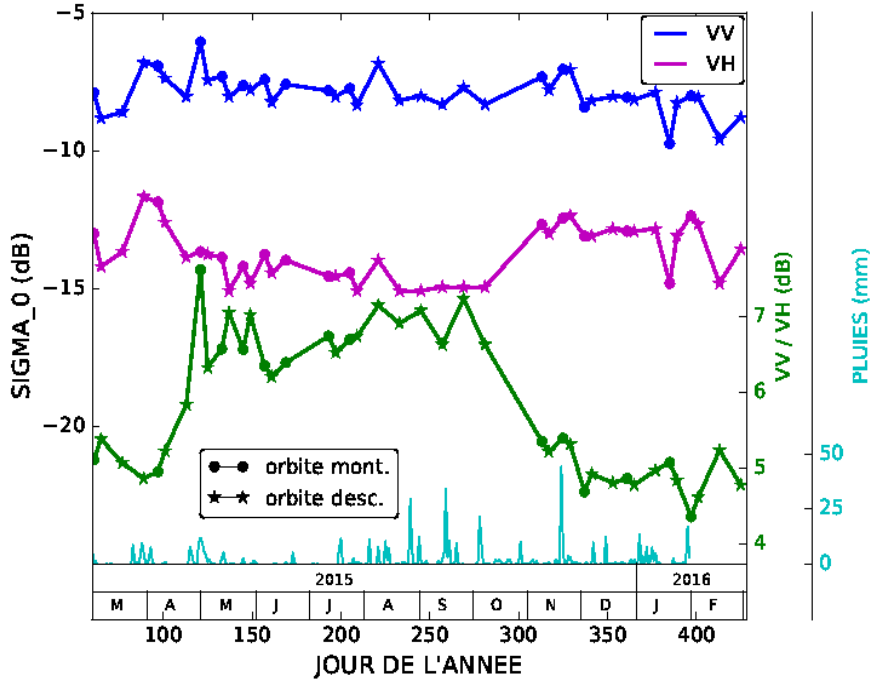
- No seasonal cycle σ^0_{VV}
- seasonal cycle $\sigma^0_{VH} \Rightarrow \sigma^0_{VV} / \sigma^0_{VH}$

- signal low and constant (Mars-Nov.)
- $|\rho_{VV}|$ et $|\rho_{VH}|$ identical

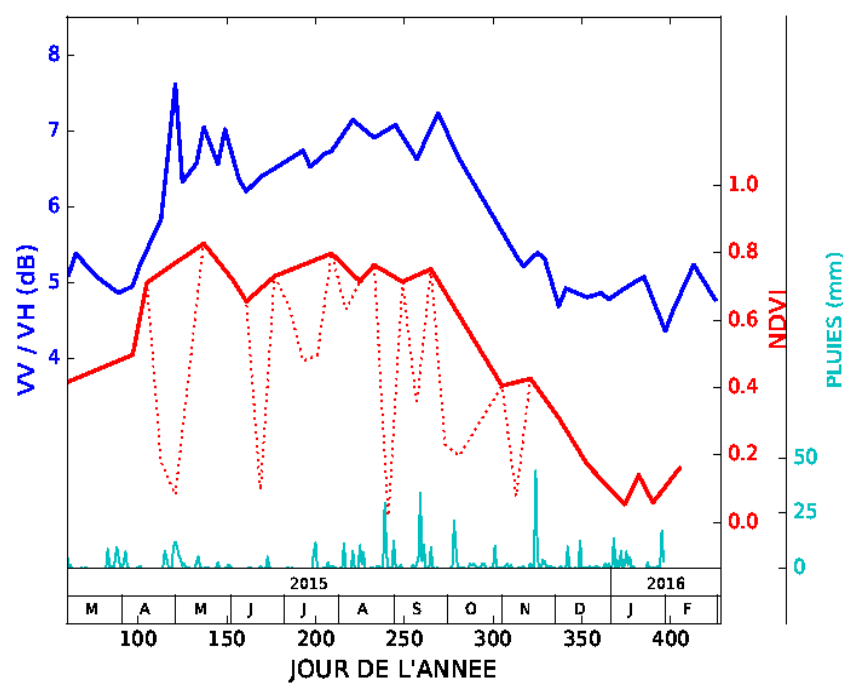
Low correlation with precipitations

Oaks stand

Radar reflectivity



$\sigma^0_{VV} / \sigma^0_{VH}$

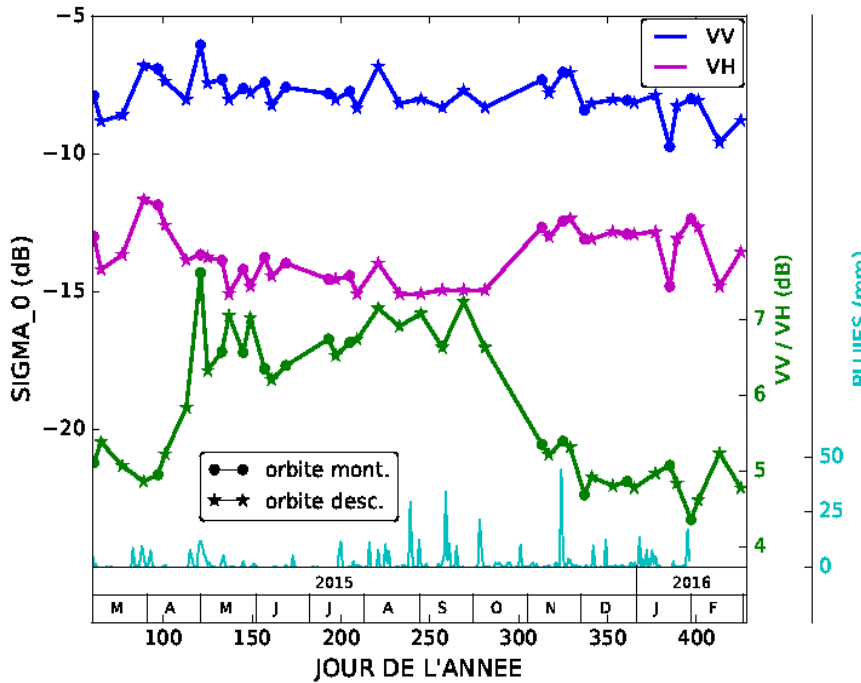


- No seasonal cycle σ^0_{VV}
- seasonal cycle $\sigma^0_{VH} ==> \sigma^0_{VV} / \sigma^0_{VH}$

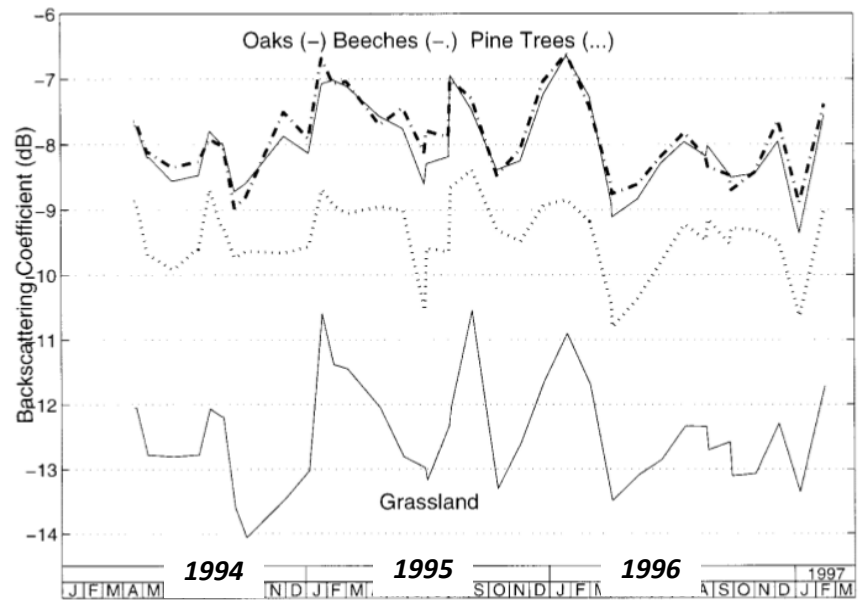
$\sigma^0_{VV} / \sigma^0_{VH}$ and NDVI in phase
==> Sensitivity of C Band to foliar activity

Oaks stand

Sentinel-1



ERS (VV pol.)



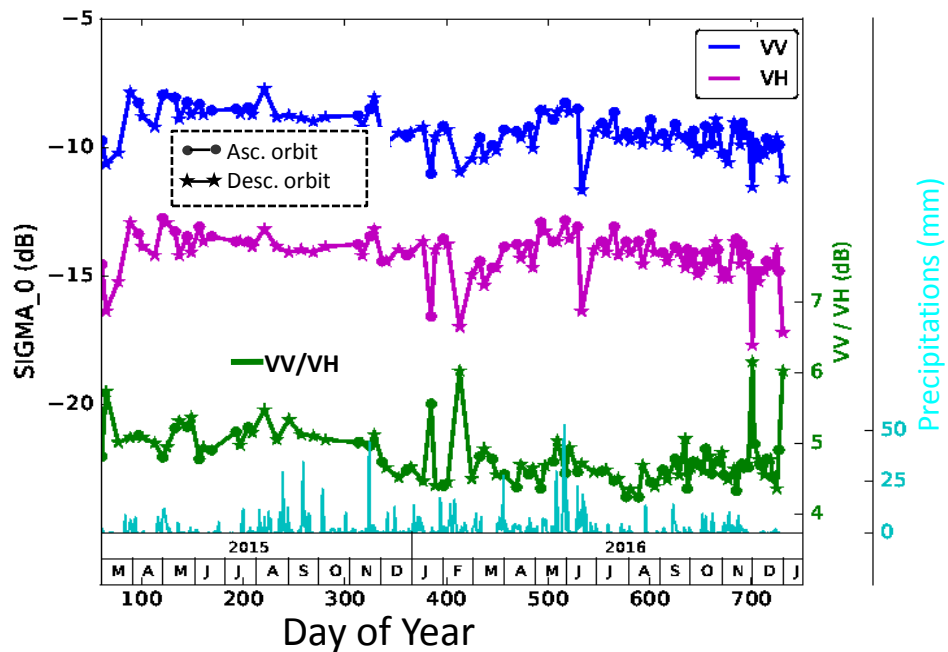
Proisy et al., 1999

- No seasonal cycle σ_{VV}^0
- seasonal cycle $\sigma_{VH}^0 \implies \sigma_{VV}^0 / \sigma_{VH}^0$

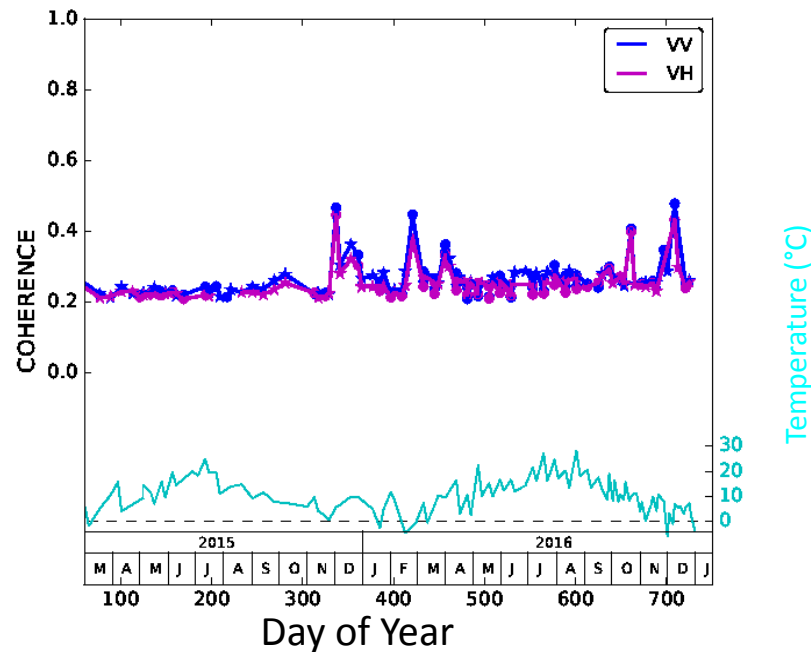
No conclusion was possible with ERS data (35 days)

Pine trees

Radar reflectivity

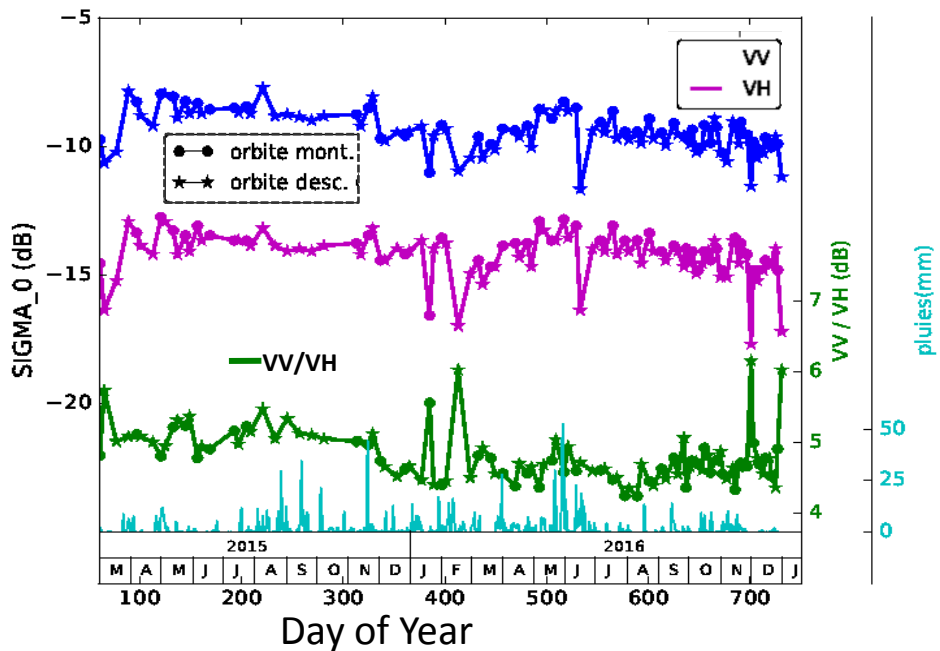


coherence

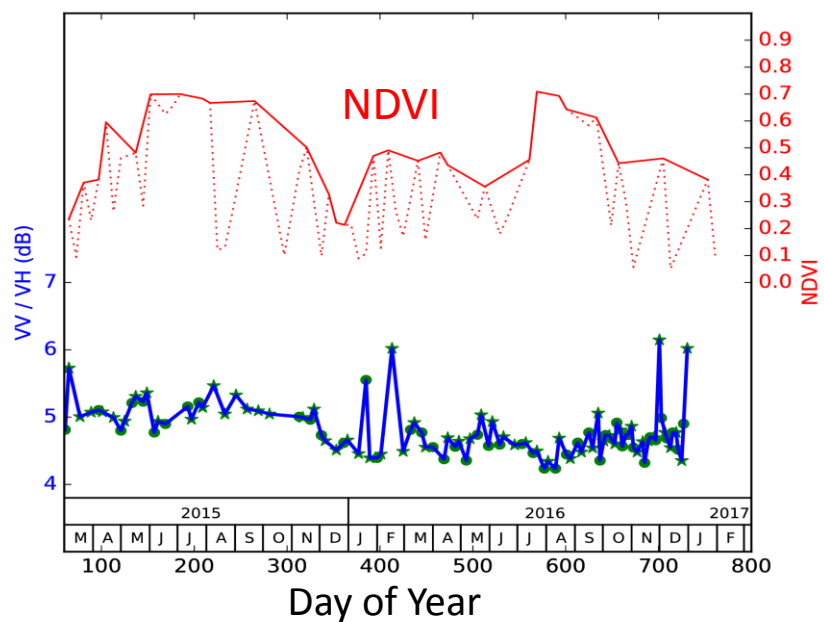


Pine trees

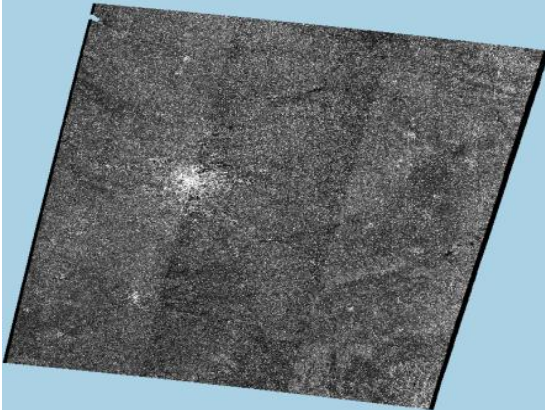
Radar reflectivity



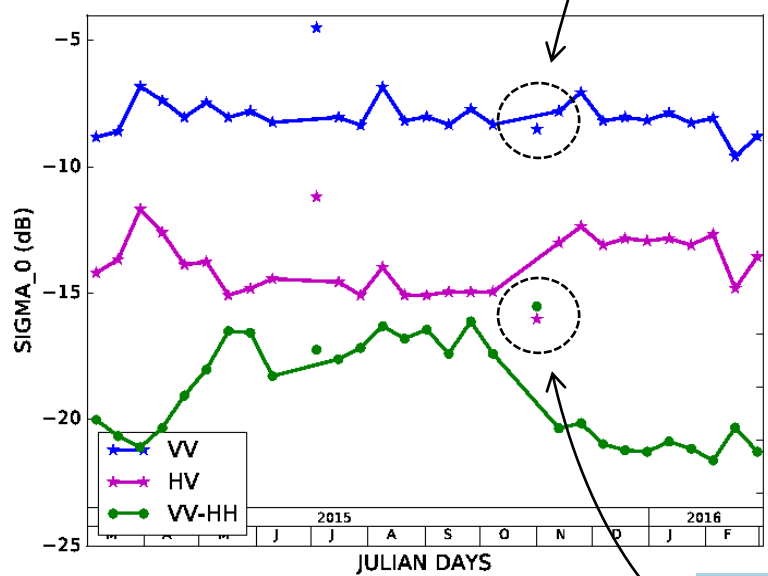
$$\sigma^0_{VV} / \sigma^0_{VH}$$



High temporal frequency



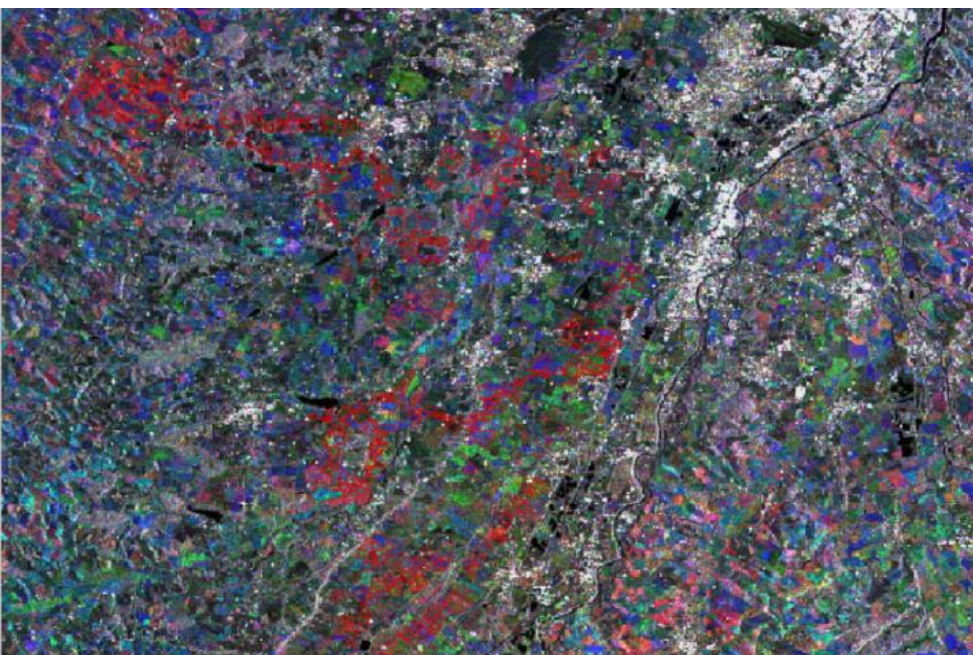
.... to detect erroneous data!



Agricultural area (Lamasquère region)

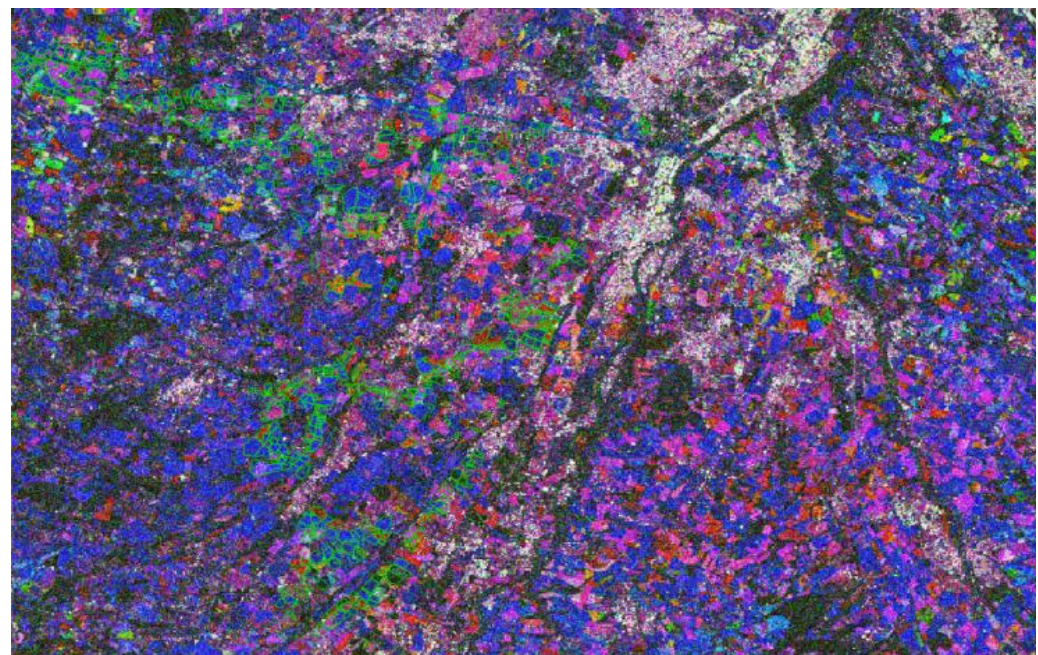
Multi-temporal color-composite images

Coeff. radar



10 June 14 Sept. 7 Dec.

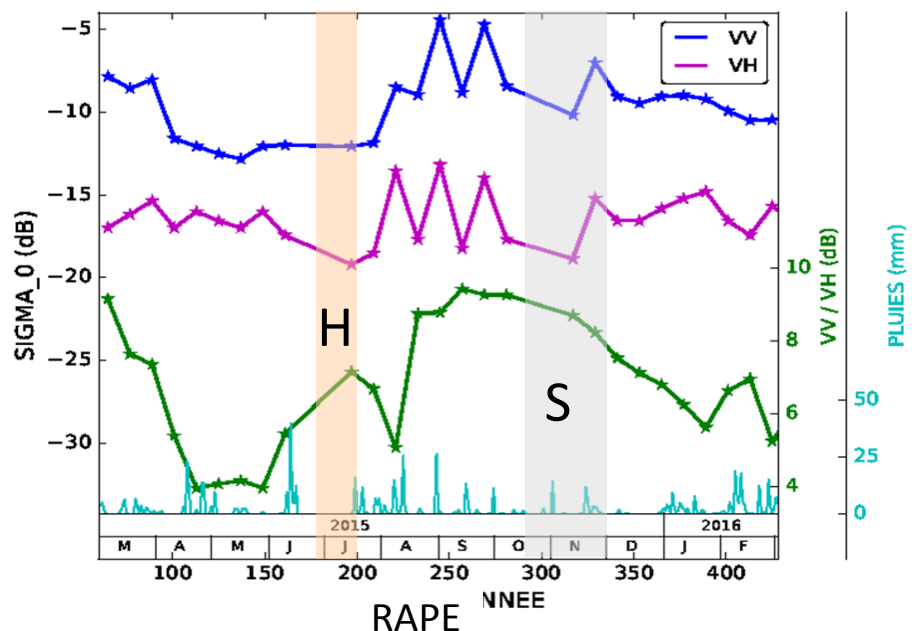
Cohérence



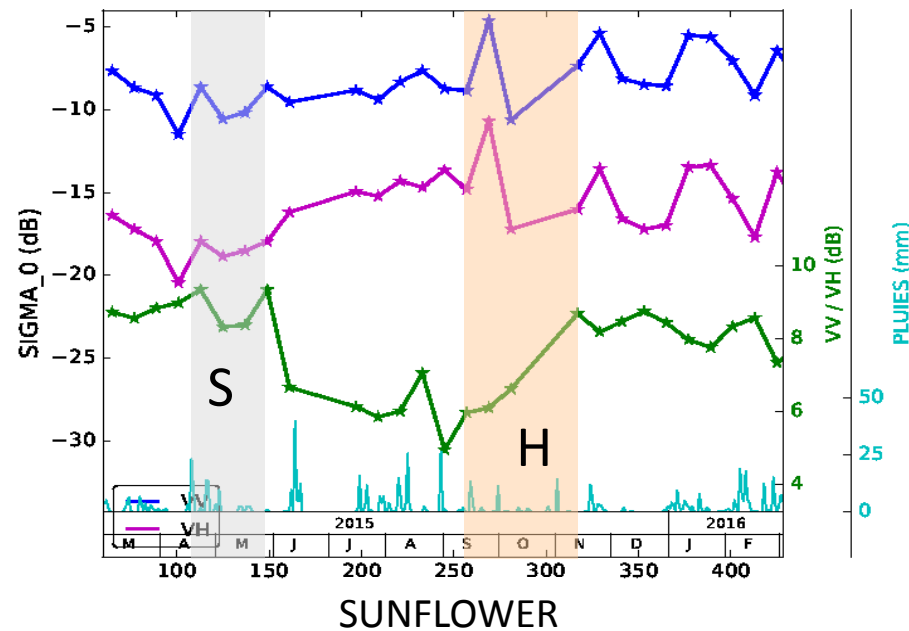
4-16 Jul. 9-16 Aug. 7-19 Dec.

CROP FIELDS: Temporal profile σ^0

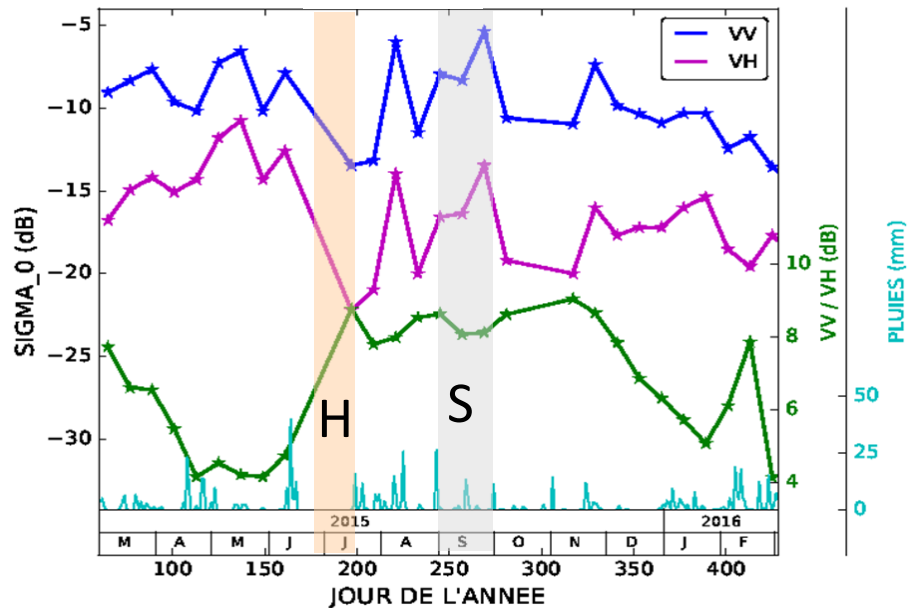
WHEAT



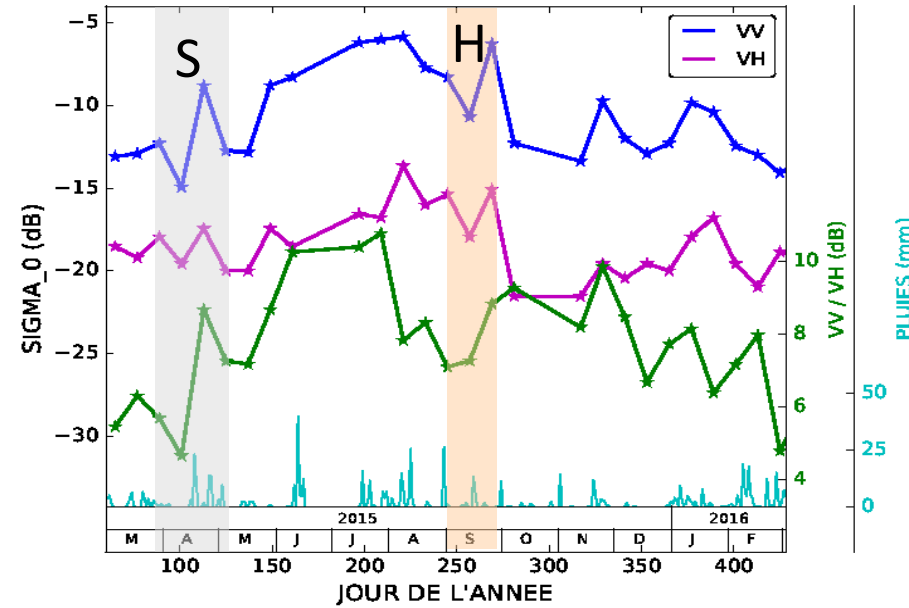
CORN – SOYA – SORGHUM



RAPE

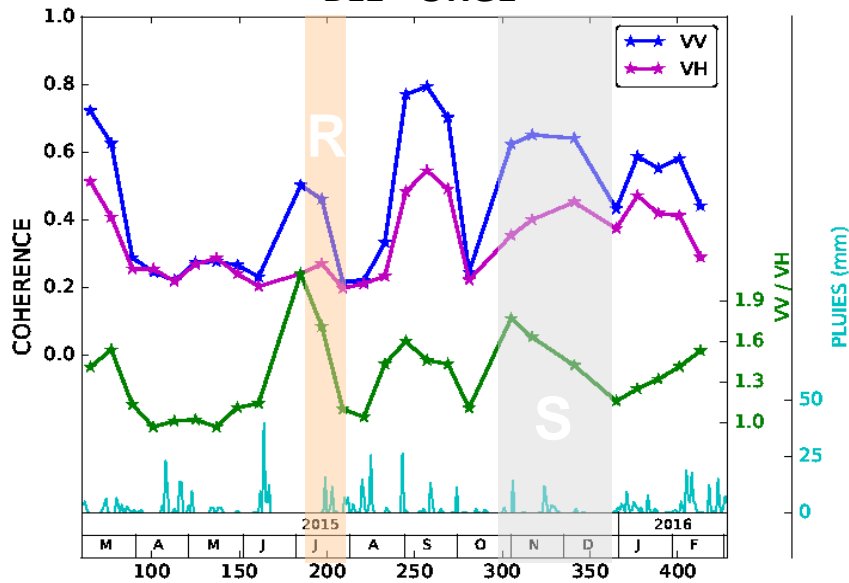


SUNFLOWER

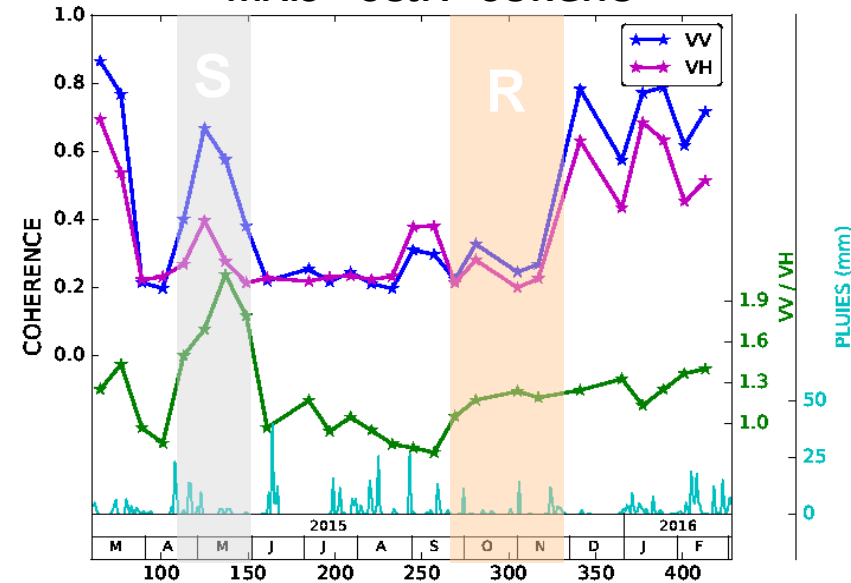


CROP FIELDS: Temporal profiles coherence

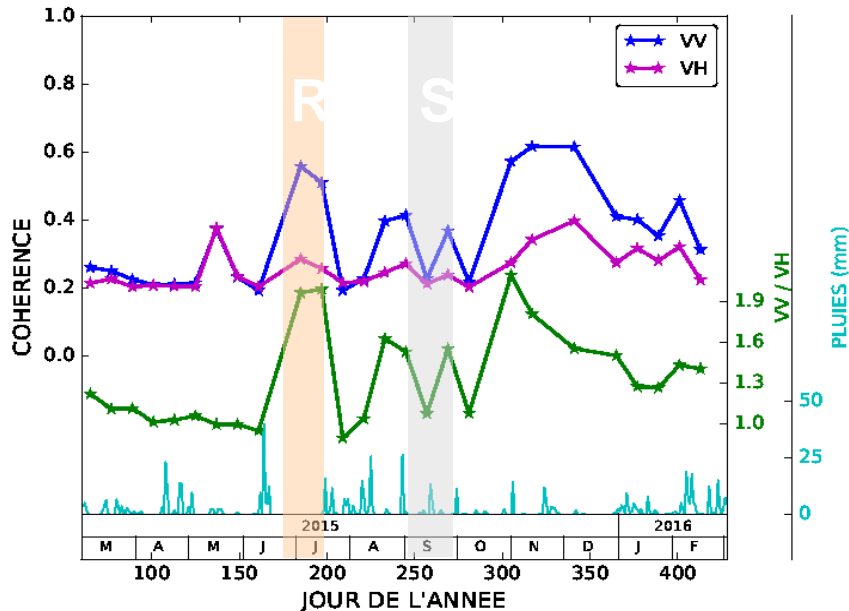
BLE - ORGE



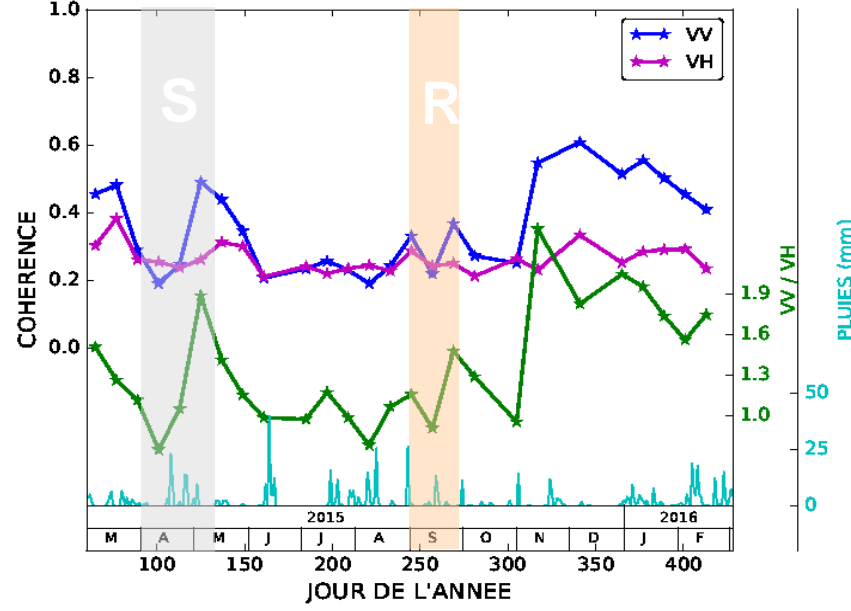
MAIS – SOJA – SORGO



COLZA



TOURNESOL



CONCLUSION

Radar brings complementary information to optical
(diversity wavelengths, polarization)

Seasonal variation of land surfaces:

☞ ***High temporal frequency*** of acquisition is necessary

Possible in the old time with ***scatterometer*** at ***regional*** scales

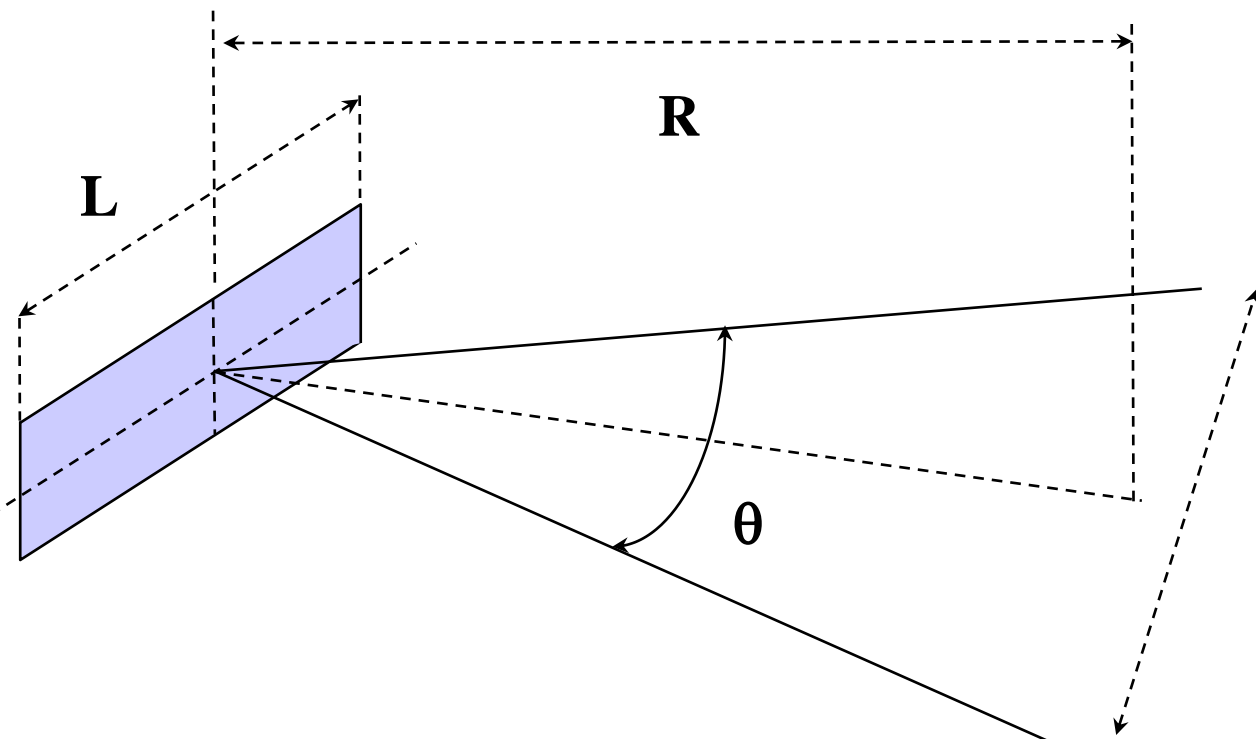
Accessible now with ***Sentinel-1*** data at ***local*** scales

Potential for ***forest*** and ***crop monitoring***

(cf. CESBIO, Th. Le Toan & Hoa Thi Phan for rice monitoring!)

Side Looking Airborne Radar (SLAR)

Rayonnement d'une antenne



$$\theta = \frac{\lambda}{L}$$

Résolution: $\delta r = \theta \cdot R$

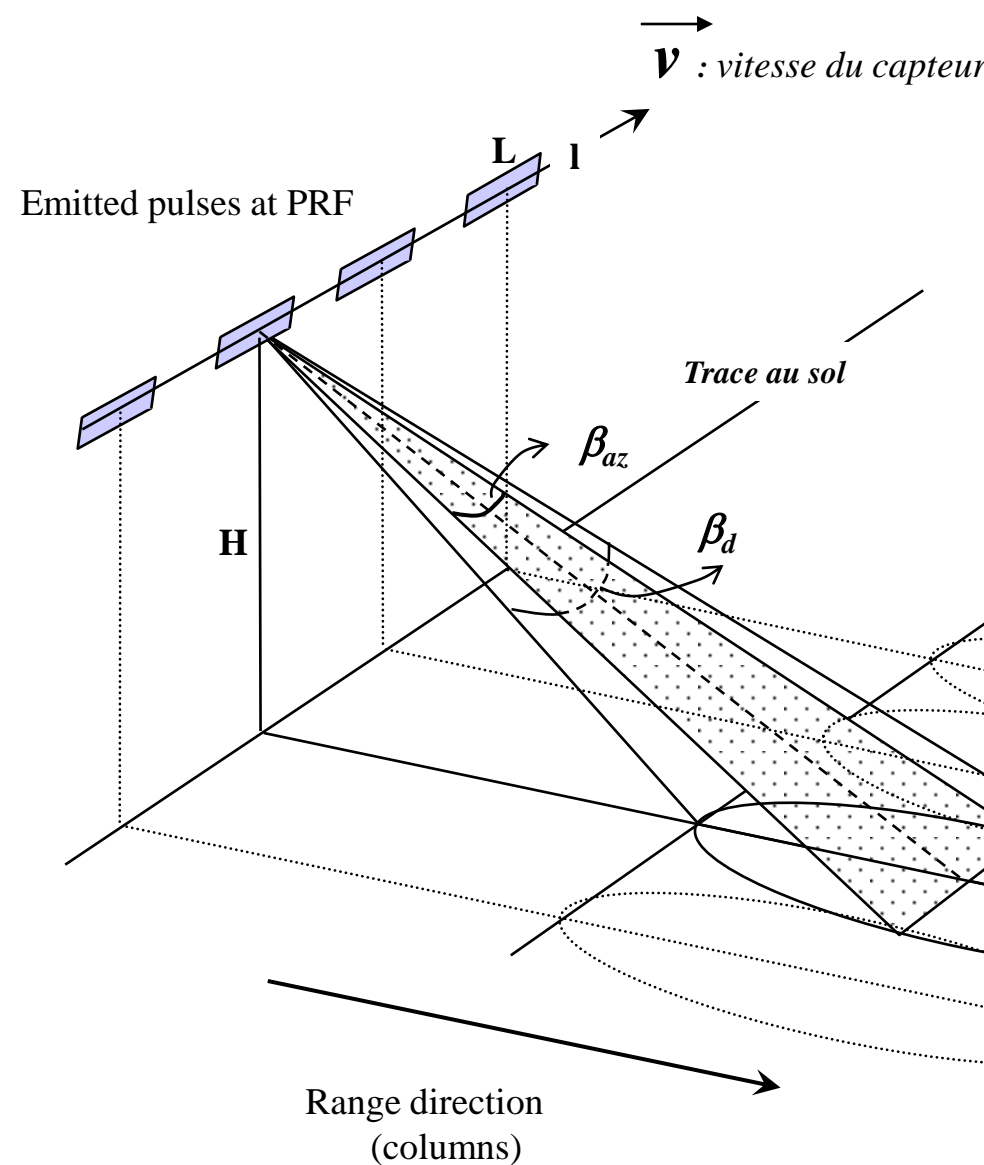
A.N.: $L = 4 \text{ m}$, $R = 4 \text{ km}$ (aéroporté), $\lambda = 3 \text{ cm}$ (bande X)

$\delta r = 30 \text{ m}$

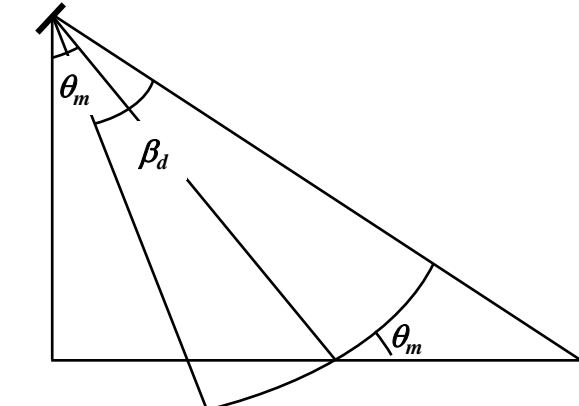
$L = 10 \text{ m}$, $R = 800 \text{ km}$ (spatial), $\lambda = 6 \text{ cm}$ (bande C)

$\delta r = 4,5 \text{ km}$

Swath width



Direction de vol



$$S \approx \frac{\lambda}{l} \frac{H}{\cos^2 \theta} \quad (\text{Flat Earth})$$

Swath S

Azimuthal direction
(lines)

A.N: $l = 1m$, $\lambda = 5.6 \text{ cm}$, $H = 700 \text{ km}$, $\theta = 23^\circ$
 $S \approx 50 \text{ km}$

Radar Imaging – spatial resolution

Range resolution

$$X_r = \frac{c \tau_p}{2} = \frac{c}{2B}$$

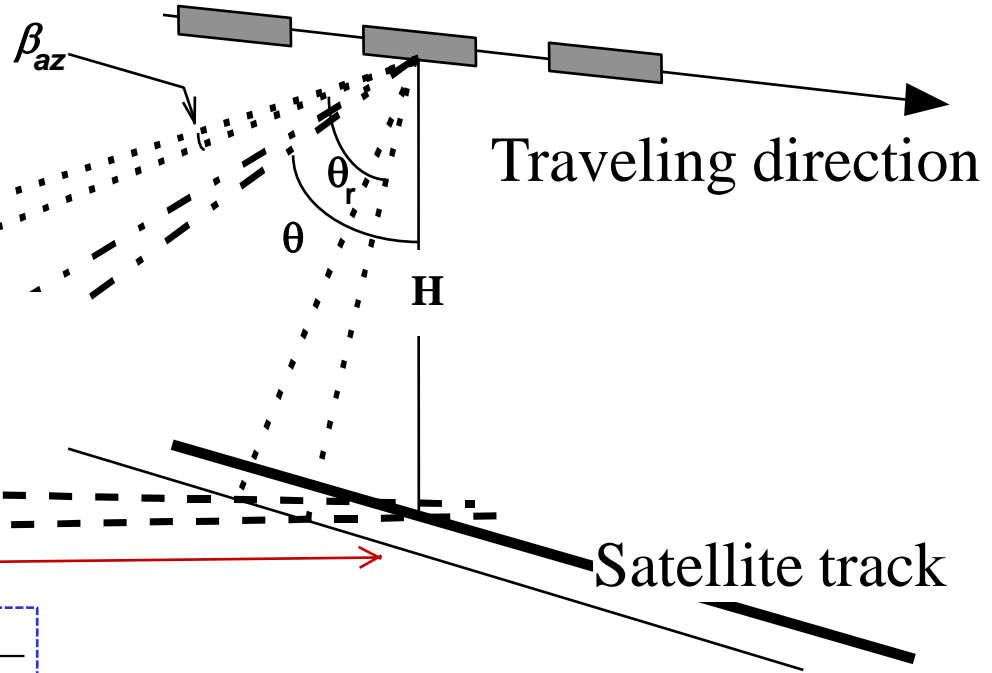
← Swath

Ground range resolution

$$X_{r_so} = \frac{c}{2B \sin \theta}$$

Azimuthal resolution

$$X_{az} = \frac{\lambda}{L} R$$



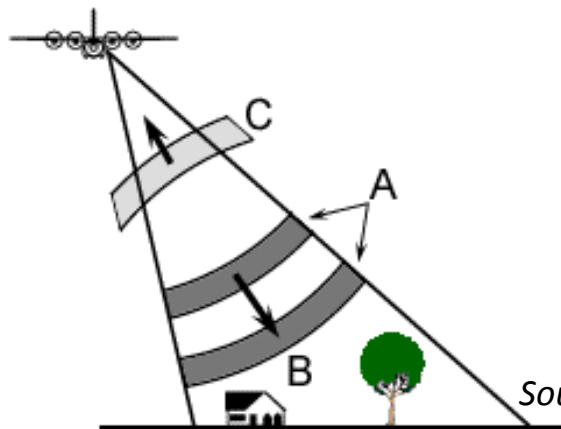
Pulse duration $= \tau_p = 1/B$

Radar remote sensing for land surfaces monitoring

Remote sensing:

Optical since 70's

Radar since 1991

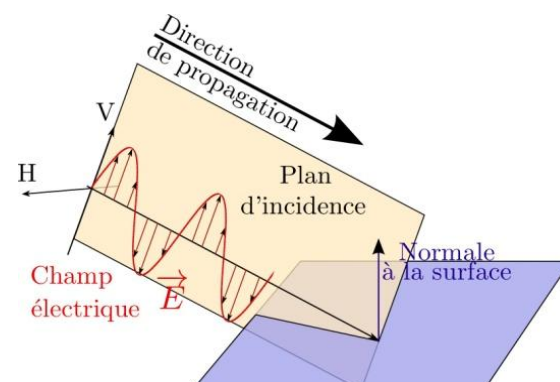


wavelength: $\lambda > 1\text{cm}$

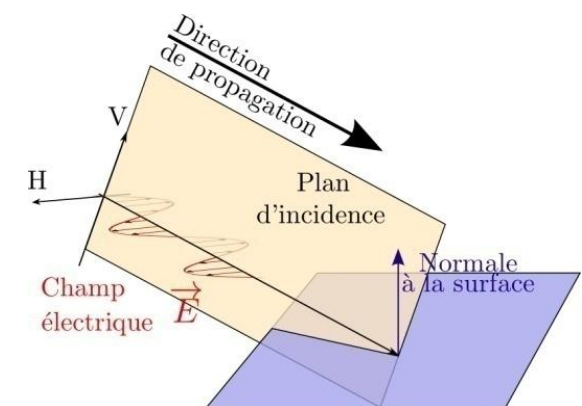
Coherent wave

Source: Centre canadien de télédétection

Polarisation diversity



Polarisation V



Polarisation H